

THERMONUCLEAR REACTIONS INVOLVING LITHIUM HYDRIDE

Andres Felipe Lopez Loaiza

Thesis supervisor
Lorenzo Fortunato

Università Degli Studi di Padova
Dipartimento di Fisica e Astronomia

“Galileo Galilei”

Corso di Laurea Magistrale in fisica

2023

Contents

Introduction	1
1 Theoretical Formalism	7
2 Jetter Cycle	17
2.1 Theoretical Approach	18
2.2 Experimental Data	21
2.2.1 ${}^6\text{Li}(n, \alpha)\text{T}$	21
2.2.2 $\text{T}(\text{D}, \alpha)n$	23
2.3 Results	25
3 Post Cycle	33
3.1 Theoretical Approach	34
3.2 Experimental Data	36
3.2.1 ${}^6\text{Li}(p, \alpha){}^3\text{He}$	36
3.2.2 ${}^3\text{He}(\text{D}, p)\alpha$	38
3.3 Results	40
4 Deuteron Knock-out reaction $\text{D}(n, 2n)p$	49
4.1 Theoretical Approach	49
4.2 Monte Carlo simulation	52
4.3 Results	57
5 Jetter + Post Cycle	61
5.1 Theoretical Approach	61
5.2 Experimental Data	66
5.2.1 $\text{D}(n, 2n)p$	66
5.3 Results	68

6 Conclusions	81
A Reaction Rates	85
B Mathematica routine	87
C C++ routine: Monte Carlo deuterium breakup.	91
Bibliography	93

Introduction

Background and wider motivations

It is evident that modern society is highly energy dependent. In fact, in different regions a quantifier related with quality of life is the energy used per capita (1). It is foreseen that energy demand will triple in the next decades. Using the current sources for electricity production, this increasing demand might be fulfilled. Nevertheless, if the present rate of fossil fuel consumption carries on, the CO₂ content in the atmosphere will reach 560 ppm and the temperature may increase by 1°C or even more via the “greenhouse” effect that this produces. The International Energy Agency proposes two possible scenarios in which the electrical demand in 2050 would produce a 6°C or 2°C increase in the global temperature if it is covered by existing technologies (2). This stresses the point that the environment cannot absorb for much longer at the present and future rate the waste of human activities in general and of energy production in particular (3).

For this, it is necessary to verify not only the internal limits of the energy system, such as the reserves or the economics, but also the external limits, which refers to the finite capacity to self-regeneration of the environment.

It is possible to summarize the criteria that an energy solution has to fulfil in order to replace the current fossil fuel alternatives, these are (3):

- ✓ **Fuel:** Supply abundant and largely available.
- ✓ **Safety:** All "internal" accidents caused either by plant failures or by operator mistakes and conceivable "external" accidents should not disrupt the life of the population.
- ✓ **Environment:** Human health and eco-system non affected. No waste or waste isolation. Minimum use of land and of fresh water.

- ✓ **Affordability:** Energy cost competitive and predictable.
- ✓ **Social acceptability.**
- ✓ **Proliferation:** No direct relation with nuclear weapons.

One of the possible solutions is the exploitation of nuclear energy, which occurs in various forms. One such form is explored in the following.

Motivations for the present thesis

After of the discover in 1920 that an α -particle has a slightly less mass than four times the hydrogen mass, Eddington suggested that this could be the method in which the stars and the Sun are producing its energy (4). From this point the humankind was aware about the possible source of energy hidden in the nucleus.

The first approach in order to use it to generate energy in a powerplant was inspired in the fission discovery by Meitner and Hahn in 1938 (5). In 1957 the first commercial electricity-generating plant powered by nuclear energy was located in Pennsylvania and from this year this kind of energy production type has continuously grown. In 1970 the nuclear energy represented the 0.9% of the shared energy supply and it scaled to be the 5% in 2020 (6). The fission based nuclear power is expected to continue increasing in the next decades despite this alternative does not fulfil several criteria previously listed. Such as, naturally fissible materials like ^{235}U are non-renewable and will get exhausted in a few hundred years, even more, if with only this alternative would try to cover a consumption of 80 TWY, which is the expected in the next decades, the reserves get exhausted in only 100 years (3). Besides, fission alternatives have faced serious troubles related with social acceptability due to concerns of proliferation, radioactive waste disposal, the potential for catastrophic Chernobyl like disasters, etc. (1). Finally, it is worth to comment that this is an active research area in order to become safer. Moreover, new ideas came up trying to achieve different fission chain reactions using Thorium (7).

In the 80's and 90's the ideas of implementing the fusion reactions for energy purposes started to be a reality, the reaction that was chosen is the fusion of the deuterium (D) and tritium (T) in which, approximately, 17.8 MeV of energy is released in the form of kinetic energy shared by the products. This idea rapidly attracted attention because the fuel supply is practically unlimited on the scale of human

civilization and quite cheap (3).

Some approaches have been considered in order to use this reaction in the electricity production, one of them is the so call Tokamak in which a plasma formed from deuterium and tritium is magnetically confined in a toroidal geometry, this confinement and external heatings produce a fully ionized gas which achieves a temperature of 20 keV, giving to nuclei the enough energy to fuse via tunneling effect producing an α -particle and a neutron. This last particle easily escapes because it has no charge and it will end up in reacting (neutron absorption) with the material in the outer region of the surrounding blanket of approximately one meter made of lithium in order to produce the tritium that will constantly feed the plasma, and also convert its kinetic energy in heat for electrical purposes (10). Also the lithium is widely available in the Earth's crust and oceans. It is worth to notice that tritium is a radioactive material with a decay time constant of only about 12 years and low toxicity. But apart from the first start up charge of tritium, no transport of radioactive fuel outside the plant is required (3).

Currently, every new technical has the aim of improving in the confinement time, the temperature achieved for the plasma and the density of particles gathered in the so call triple product (11). At this moment the project ITER is under construction and it is expected that in 2027 the first plasma will be realized. Also, the project DEMO is being planned, that will be the last step previously to a commercial power plant (8).

A second approach is the inertial confinement developed by United States in which a target made of deuterium and tritium is bombarded with high power laser beams. These beams heat the most external layer of the target and vaporize it. This causes a compression of the inner part, with a strong density increase, allowing to overcome the Coulomb barrier and make fusion reactions happen (4),(11). Recently, the researchers working at this approach have announced for first time a setup that achieves a positive balance between the energy needed to work and the energy produced (12).

Another way in which this reaction could be used is focusing a neutron beam against a solid target of ionic salt ${}^6\text{LiD}$ of such way that the neutron reacts with Lithium producing an α -particle and a tritium nucleus, where the nuclear rearrangement results in a reduction in total mass that is translated in 4.8 MeV of kinetic energy of the reaction products. Consequently, the tritium nucleus will fuse with a deuterium

nucleus producing another α -particle and a neutron, where again, a reduction of the total mass is present corresponding to 17.6 MeV of kinetic energy of the reaction products. Finally, this neutron released can again react with a nucleus of 6-Lithium closing the cycle.

The discussion about the feasibility of using this cycle for energetic purposes was kept secret for a long time during the Cold War era and then resumed by J. R. McNally in the 70's (20) proposing an external beam, either a proton beam or neutron beam, that might trigger different reactions.

Throughout the discussion, the author expressed several times the idea that the poor data set known for cross sections at that time limited the possible decisions of choosing a specific fuel and the predictions of the energy generated that might be converted in electricity (21). In the present work a modern study from a theoretical point of view of this cycle is proposed, in which a crystal of lithium deuteride (${}^6\text{LiD}$) is bombarded with a neutron beam which turns on the Jetter cycle. Several assumptions must be taken into account in order to simulate a drastically ideal system, and little by little some of them will be relaxed to get closer, in every step, to a more realistic system. In Fig. 1, a sketch of the crystal and the neutron beam is displayed.

The lithium deuteride (${}^6\text{LiD}$) is a blue or colorless crystal usually prepared by the direct high-temperature reaction of lithium and deuterium. The melting point of lithium is lower than that of lithium-deuteride. Therefore, the direct reaction at 700-730 °C can afford high-quality bulk lithium deuteride crystal (13). Stable under normal temperature and pressure. Its density will be taken as $\rho = 0.883 \text{ g/cm}^3$ (32).

In principle the reactions could be studied keeping these energies all the time, namely, assuming for example, that the α -particle with 2.1 MeV will keep this energy all the time. Of course it is well-known that a charged particle moves inside ordinary matter, by losing some of its kinetic energy in accordance with the formula of Bethe-Block, initiating a series of ionizations along its track. This will be a possible refinement to our work.

The present work is aimed to analyze the abundance dynamic of the different species in time, adding different kind of interactions like collateral reactions that can occur between the particles present in the cycle and asking us what species are proliferated, what species are depleted, what competitive reactions are relevant in the present conditions, if an ignition condition is possible with this approach and how efficient could be.

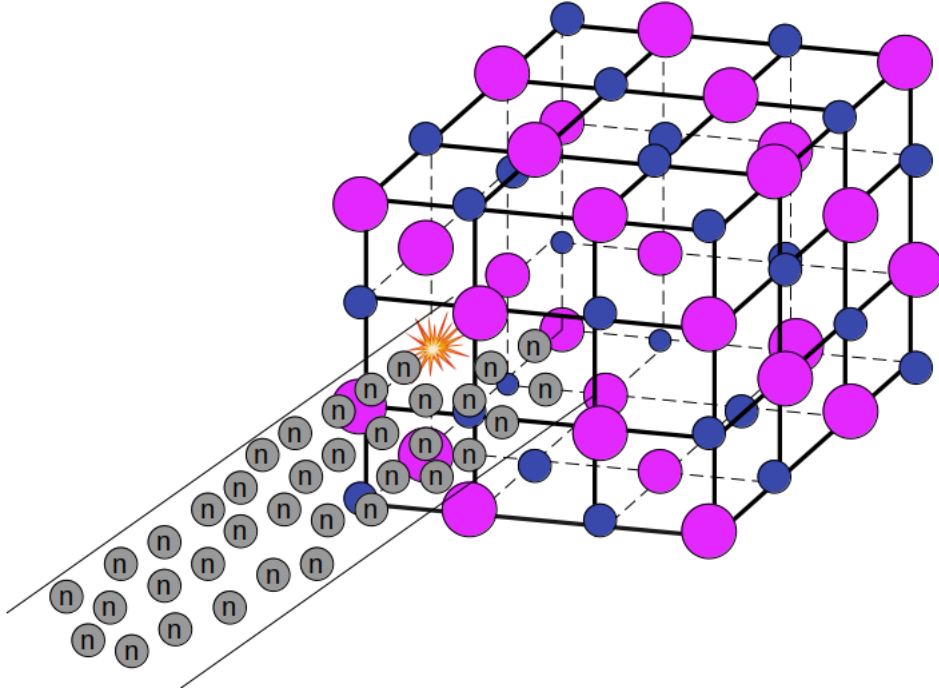
${}^6\text{LiD}$ Crystal bombarded by a neutron beam

Figure 1: ${}^6\text{LiD}$ crystal sketch being bombarded by a neutron beam. Lithium represented in magenta and deuterium represented in blue.

In the first chapter the necessary theoretical frame is displayed. The Jetter cycle simulation is explored in the second chapter. An analogous study using the Post cycle is carried out in the third chapter. A Monte Carlo simulation of the deuterium-breakup is proposed in the fourth chapter to produce a considerable proton population with a different energy distribution that would trigger the Post cycle. And finally in the fifth chapter a simulation merging the two cycles through the deuterium-breakup is done.

Chapter 1

Theoretical Formalism

A typical nuclear reaction is commonly written in two ways. We can express it like $a + X \rightarrow Y + b$ where the left side are the reactans and the right side are the products. Generally, b is a light particle that can be detected and Y will be a heavy product that stops in the target and is not directly observed. An alternative and more compact way to indicating the same reaction is $X(a, b)Y$.

One of several conserved quantities that we can find in a nuclear reaction is the kinetic energy plus the rest mass, which leads to the reaction Q -value (1.1):

$$\begin{aligned} a + X &\rightarrow Y + b \\ (m_a c^2 + T_a) + (m_X c^2 + T_X) &= (m_Y c^2 + T_Y) + (m_b c^2 + T_b) \end{aligned} \quad (1.1)$$

$$\begin{aligned} (m_a c^2 + m_X c^2 - m_Y c^2 - m_b c^2) &= (T_Y + T_b - T_X - T_a) \\ Q = (m_{ini} - m_{fin})c^2 &= T_{fin} - T_{ini} \end{aligned} \quad (1.2)$$

Therefore, the Q -value is defined as the initial mass energy minus the final mass energy or analogously, the excess kinetic energy of the final products. For instance, we are going to compute this and other quantities in detail only for one reaction of the Jetter cycle, this could be done using two analogous methods taking into account the nuclides masses. Firstly, we can directly replace the nuclear masses in the expression 1.2

$$\begin{aligned} Q &= (m_{ini} - m_{fin})c^2 = [m(^2\text{H}) + m(^3\text{H}) - m(^4\text{He}) - m(n)]c^2 \\ &= [1875.6129 + 2808.9211 - 3727.3793 - 939.5654] \frac{\text{MeV}}{c^2} c^2 \\ &= 17.5893 \text{ MeV} \end{aligned} \quad (1.3)$$

Secondly, we can take advantage of the fact that in a nuclear reaction the mass number is conserved. Therefore, we have

$$\begin{aligned}
 {}^2\text{H} \quad + \quad {}^3\text{H} \quad &\rightarrow \quad {}^4\text{He} \quad + \quad n \\
 \left[Z_{2\text{H}}(m_p + m_e) + N_{2\text{H}}m_n - \frac{(b.e)_{2\text{H}}}{c^2} \right] &+ \left[Z_{3\text{H}}(m_p + m_e) + N_{3\text{H}}m_n - \frac{(b.e)_{3\text{H}}}{c^2} \right] \\
 &= \left[Z_{4\text{He}}(m_p + m_e) + N_{4\text{He}}m_n - \frac{(b.e)_{4\text{He}}}{c^2} \right] + m_n + \frac{Q}{c^2} \quad (1.4)
 \end{aligned}$$

$$\begin{aligned}
 & \left[(Z_{2\text{H}} + Z_{3\text{H}} - Z_{4\text{He}})m({}^1\text{H}) + (N_{2\text{H}} + N_{3\text{H}} - N_{4\text{He}} - 1)m_n \right] \\
 &= - \left[\frac{(b.e)_{4\text{He}}}{c^2} - \frac{(b.e)_{2\text{H}}}{c^2} - \frac{(b.e)_{3\text{H}}}{c^2} \right] + \frac{Q}{c^2} \quad (1.5)
 \end{aligned}$$

$$\frac{Q}{c^2} = \left[\frac{(b.e)_{4\text{He}}}{c^2} - \frac{(b.e)_{2\text{H}}}{c^2} - \frac{(b.e)_{3\text{H}}}{c^2} \right] \quad (1.6)$$

$$Q = [(b.e)_{4\text{He}} - (b.e)_{2\text{H}} - (b.e)_{3\text{H}}] \quad (1.7)$$

$$= [28.2957 - 2.2246 - 8.4818] \text{ MeV}$$

$$= 17.5893 \text{ MeV}. \quad (1.8)$$

This procedure showed that the Q -value could be understood as if the energy released was equal to the difference in binding energy between the products and the reactants.

Besides, the products have to share the energy released into kinetic energy, and this division is weighted by the mass, namely:

$$Q_Y = Q \left(\frac{m(b)}{M_T} \right) \quad , \quad Q_b = Q \left(\frac{m(Y)}{M_T} \right). \quad (1.9)$$

$$M_T = 939.5654 \text{ MeV}/c^2 + 3727.3793 \text{ MeV}/c^2 = 4666.9447 \text{ MeV}/c^2 \quad (1.10)$$

$$Q_n = Q \left(\frac{m({}^4\text{He})}{M_T} \right) = 17.5893 \text{ MeV} \left(\frac{3727.3793}{4666.9447} \right) = 14.0481 \text{ MeV}, \quad (1.11)$$

$$Q_{4\text{He}} = Q \left(\frac{m_n}{M_T} \right) = 17.5893 \text{ MeV} \left(\frac{939.5654}{4666.9447} \right) = 3.5411 \text{ MeV}. \quad (1.12)$$

This process must be done with every reaction involved in the system in order to know the excess of energy of the products particles and the consequent energy at which next reactions will be accomplished.

Hence, we already know that the outgoing particles in every reaction carry a certain energy, but the quantity in which we are interested in the system is the total nuclear energy released per unit volume. This depends on two factors. First, the velocity distribution of the particles and secondly the nuclear cross section.

The last quantity is a measure of the probability that a given nuclear reaction takes place. It is symbolized with the lower-case Greek letter sigma and it depends on the relative projectile-target velocity, or alternatively on the kinetic energy, that is $\sigma = \sigma(v)$.

In order to obtain a more precise definition, let us consider again the generic reaction $X(a, b)Y$. If I_0 is the flux of incident particles of type a impinging on a target consisting of N nuclei of type X , then the number of particle of type b emitted per unit time (I) will be proportional to both I_0 and N (17).

$$I \propto I_0 N \quad (1.13)$$

The constant of proportionality that links these quantities is called the cross-section.

$$I = \sigma I_0 N \quad (1.14)$$

$$\sigma = \frac{I}{I_0 \cdot N} \quad (1.15)$$

$$= \frac{\text{(Number of interactions per time)}}{\text{(Number of incident particles per area per time)} \cdot \text{(Number of target nuclei within the beam)}}$$

σ has unit of area and in Nuclear Physics the unit of cross section is a Barn (b) $1 \text{ b} = 10^{-24} \text{ cm}^2 = 10^{-28} \text{ m}^2$. But, the submultiples are used more often: milibarn, $1 \text{ mb} = 10^{-3} \text{ b}$, microbarn, $1 \mu\text{b} = 10^{-6} \text{ b}$.

The velocity distribution and nuclear cross section are related through the reaction rate (16), which express the number of reactions per unit volume and time.

$$r_{01} = \frac{N_0 N_1 \langle \sigma v \rangle}{1 + \delta_{01}} \quad (1.16)$$

Where N_i is the number of species i per unit volume. $\langle \sigma v \rangle$ represents the expected value of cross section and velocity product. The expected value is taken over a relative velocity probability distribution $P(v)$ or its analogous energy distribution $P(E)$ which is most often used due to the fact that the cross section is usually given

as function of the energy.

$$\langle \sigma v \rangle = \int v \sigma(v) P(v) dv = \int v \sigma(E) P(E) dE \quad (1.17)$$

Indeed, $P(v)$ fulfils the properties of a probability distribution as being no negative defined function and normalized over the sample space:

$$\int_0^\infty P(v) dv = 1 \quad (1.18)$$

Of this way, $P(v)dv$ is the probability that the relative velocity of the nuclei involved in the reaction is in the range between v and dv . The specific function $P(v)$ will depend on the nature of the system and the allowed energy range.

The denominator of the expression [1.16](#) appears due to the fact that N_0 and N_1 are the total number density of pairs of different nuclei 0 and 1 in units of particles per volume. But, in the case of identical nuclei a term of the form

$$\frac{N_j^2}{2!} \quad (1.19)$$

must appear, or for a three-body interaction a term of the form

$$\frac{N_j^3}{3!} \quad (1.20)$$

is needed.

Up to now, we have all the ingredients to study of a set of nuclear reactions with time expressing the element abundance in the system. Understanding abundance as the fraction of a given sample which is in a particular form. This means that we will consider the ratio of number of this particular species to some standard. It is desirable to consider this standard to be invariant with respect to the compression or expansion that the system could undergo, so that changes in abundance reflect only nuclear processing. [\(1.8\)](#)

Therefore, let us perform some changes and include some definitions in order to modify the expression [1.16](#) to deal with matter densities and obtain a nuclear abundance.

The Avogadro number N_A is defined like the number of atoms of species i which makes W_i grams, where W_i is the atomic weight of species i .

$$N_A = \frac{W_i}{m_i} = 6.022 \times 10^{23} \text{ mol}^{-1} \quad (1.21)$$

If m_i is the mass of a nucleus of species i as measured in the lab, then for a mixture consisting only of species i , the mass density is

$$\rho_m = N_i m_i \quad (1.22)$$

And for a mixture of species

$$\rho_m = \sum_i N_i m_i = \frac{\sum_i N_i W_i}{N_A} \quad (1.23)$$

We can carry out some change in W_i in order to use the mass number instead of the mass weight. We, also know, that the mass unit M_u is

$$M_u = \frac{m(^{12}\text{C})}{12} = \frac{1}{N_A} \quad (1.24)$$

In the sense that the mass excess is $m_i - A_i M_u$

$$W_i = \frac{m_i}{M_u} = [Z_i m(\text{H}) + (A_i - Z_i)m(n) - (b.e)_i/c^2]/M_u \quad (1.25)$$

Where $m(n)$ refers to neutron mass and $m(\text{H}) = m(p) + m(e)$. Besides, using Carbon binding energy and [1.24](#), it is possible to write

$$\frac{b.e(^{12}\text{C})}{m(^{12}\text{C})c^2} = \frac{6[m(\text{H}) + m(n)] - m(^{12}\text{C})c^2}{m(^{12}\text{C})c^2} = \frac{(W_{\text{H}} + W_n)}{2} - 1 \quad (1.26)$$

Finally, the atomic weight could be written as

$$\begin{aligned} W_i &= Z_i W_{\text{H}} + (A_i - Z_i)W_n - (b.e)_i/M_u c^2 = Z_i(W_{\text{H}} - W_n) + A_i W_n - (b.e)_i/M_u c^2 \\ &= Z_i(W_{\text{H}} - W_n) + A_i W_n - \frac{(b.e)_i}{M_u c^2} + \left(\frac{A_i}{2} W_{\text{H}} - \frac{A_i}{2} W_{\text{H}} \right) \\ &= Z_i(W_{\text{H}} - W_n) - \frac{A_i}{2}(W_{\text{H}} - W_n) - \frac{(b.e)_i}{M_u c^2} + A_i \left(\frac{W_{\text{H}} + W_n}{2} \right) \\ &= A_i + A_i \frac{(b.e)_{12\text{C}}/12 - (b.e)_i/A_i}{M_u} + \left(Z_i - \frac{A_i}{2} \right) (W_{\text{H}} - W_n) \end{aligned} \quad (1.27)$$

Since $W_{\text{H}} = 1.007825$ and $W_n = 1.008664$ ([14](#)), and also Z_i is often approximately $A_i/2$, the last term might be neglected.

The second term is less meaningful than A_i . Therefore, the atomic weight could be written as

$$W_i = A_i + A_i b_i = A_i(1 + b_i) \quad (1.28)$$

And the mass density [1.23](#) will read as

$$\rho_m = \frac{\sum_i N_i W_i}{N_A} = \frac{\sum_i N_i A_i}{N_A} (1 + b_i) \quad (1.29)$$

The last quantity is not relativistically invariant and change with the composition [\(18\)](#), namely, nuclear transmutations transform a fraction of the nuclear mass into energy or leptons and vice versa. Nevertheless, the next quantity, called nucleon density, is used in order to avoid these difficulties based on the fact that the mass number in a nuclear reaction is a conserved quantity.

$$\rho \equiv \frac{\sum_i N_i A_i}{N_A} \quad (1.30)$$

It is worth to notice that both are almost equal and the distinction is usually not important numerically [\(16\)](#).

Now, the nucleon fraction X_i for the species i is defined to be

$$X_i \equiv \frac{N_i A_i}{\rho N_A} \quad (1.31)$$

Where this quantity represents the fraction of the nucleons in the sample that is in a form of particles of species i .

Combining [1.31](#) and [1.30](#), it is evident that this quantity has to fulfil the next constraint for a closed system.

$$\sum_i X_i = 1 \quad (1.32)$$

A related quantity is

$$Y_i = \frac{X_i}{A_i} = \frac{N_i}{\rho N_A} \quad (1.33)$$

Which is a ratio of the number of nuclei of species i to the total number of nucleons in the system. Besides, the total number of nucleons is related to number density as follows:

$$n = \sum_i N_i A_i \quad (1.34)$$

then

$$\sum_i Y_i = \frac{\sum_i N_i}{n} \quad (1.35)$$

Notice that Y_i is the fraction of a mole of particles in the form of species i . So, Y_i is a mole fraction and the goal of building a quantity that is invariant under expansion or contraction -a common phenomenon for gases and plasmas- is done. Notice that N_i reflects this structural effects even if a nuclear reaction has not occurred (118). Instead, Y_i depends only on nuclear reactions (119).

Notice that the constraint for a closed systems could be written also in terms of the molar fraction

$$\sum_i X_i = \sum_i Y_i A_i = 1. \quad (1.36)$$

At this moment the dynamic could be implemented. Consider the rate of change in the number density N_i of species i . This rate of change must be proportional to a positive term if particles of species i are the result of a nuclear reaction, or proportional to a negative term if particles of species i are part of the reactans. These terms are also called source or sink terms respectively (119).

$$\frac{dN_i}{dt} = +(\text{sum of creation terms}) - (\text{sum of destruction terms}) \quad (1.37)$$

Using the reaction rate (1.16), it could be written for a generic reaction

$$\left(\frac{dN_0}{dt}\right)_1 = -(1 + \delta_{01})r_{01} = -(1 + \delta_{01})\frac{N_0 N_1 \langle \sigma v \rangle}{1 + \delta_{01}} = -N_0 N_1 \langle \sigma v \rangle \quad (1.38)$$

And using the mole fraction (1.33), the differential equation could be expressed as

$$\left(\frac{dY_0}{dt}\right)_1 = -Y_0 Y_1 \rho N_A \langle \sigma v \rangle \quad (1.39)$$

Despite that the reaction considered in the last expression is a particle-induced reaction, some authors (116) define a constant decay λ , or an analogously mean lifetime τ for the reaction $0 + 1$ as

$$\left(\frac{dY_0}{dt}\right)_1 = -Y_0(Y_1 \rho N_A \langle \sigma v \rangle) = -Y_0 \lambda_1(0) = -\frac{Y_0}{\tau_1(0)} \quad (1.40)$$

And it is evident that the decay constant of a nucleus via a particle-induced reaction depends explicitly on the density of the system treated and implicitly, through the cross section, of the energy at which the reaction is accomplished.

We can also have a reaction that involves a single nucleus, which includes decays, electron and positron captures, photodisintegrations, and neutrino induced reactions that only depends on the target nucleus abundance. And, not less important, reactions involving three particles might be present, for instance the triple- α process of fundamental role in Helium burning stage (18).

Therefore, gathering all these possible processes, a set of ordinary differential equations might be defined leading the element abundance evolution in a system of this way

$$\frac{dY_i}{dt} = +Y_j Y_k (\rho N_A \langle \sigma v \rangle_{jk,i}) - Y_i Y_j (\rho N_A \langle \sigma v \rangle_{ij,n}) + Y_l \lambda_l(i) - Y_i \lambda_i(m) + \dots \quad (1.41)$$

This set of coupled, nonlinear ordinary differential equations is dubbed as nuclear reaction network.

An useful notation might be introduced intended to put the equations shorter

$$[j(k, i)] = \rho N_A \langle \sigma v \rangle_{jk,i} \quad (1.42)$$

Finally, the the nuclear reaction network holds

$$\frac{dY_i}{dt} = +Y_j Y_k [j(k, i)] - Y_i Y_j [i(j, n)] + Y_l \lambda_l(i) - Y_i \lambda_i(m) + \dots \quad (1.43)$$

Finally, let us make a recap of the units involved in the quantities of interest. Using the expression 1.39 the units of the molar fraction would be

$$\left[\frac{dY_0}{dt} \right] = -[Y_0][Y_1] [\rho_m][N_A][\langle \sigma v \rangle], \quad (1.44)$$

$$\frac{\text{mol}}{g \cdot s} = \frac{\text{mol}}{g} \frac{\text{mol}}{g} \frac{g}{\text{m}^3} \frac{1}{\text{mol}} \frac{\text{m}^3}{s} \quad (1.45)$$

being consistent.

Despite of having the dynamic equations of the species abundance, the quantity of crucial interest is the gain power. This is important because it must be understood if the system under study provides an option for power production or not.

Obtaining a single expression containing all the information related with the energy injected to the system and the energy produced for this, is not a simple task.

In the current setups every apparatus has its own criterion. For instance, the Tokamak system uses a modified version of the Lawson criterion (I0), instead the inertial confinement approach measures the injected energy according with the external compression work on the fuel (II).

What is common to both approach is the calculation of the power per unit volume produced in these reactions, also referred to as specific power. This is obtained by multiplying the reaction rate and the reaction Q -value and it is proportional to the product of the densities of the two reactants species (A)

$$P = N_i N_j \langle \sigma v \rangle Q, \quad (1.46)$$

which we can take as a theoretical maximum. Then, using the expression (1.33) and the notation (1.42), the above expression could be rewritten as

$$\begin{aligned} P(t) &= \left(1.602 \times 10^{-22} \rho N_A [i(j, k)] Q\right) Y_i(t) Y_j(t), \\ &= p_0 Y_i(t) Y_j(t) \end{aligned} \quad (1.47)$$

where in the last expression the explicit time dependence is shown. Besides, the density is given in g/m^3 , the reaction Q -value in MeV and the reactivity in $m^3 s^{-1}$. This is done in order to obtain the specific power with units of $GJ s^{-1} m^{-3}$.

Therefore, if the specific power curve as a time function is obtained, it is possible to know the energy produced in GJ by integrating it over the time and multiplying by the crystal volume.

Chapter 2

Jetter Cycle

In the present chapter we focus on the simulation of the Jetter cycle. This cycle was first proposed as a fusion chain reaction in 1950 (9) for the German physicist Ulrich Jetter, where the fuel is the ${}^6\text{LiD}$ compound and the chain centers are the neutron and tritium.

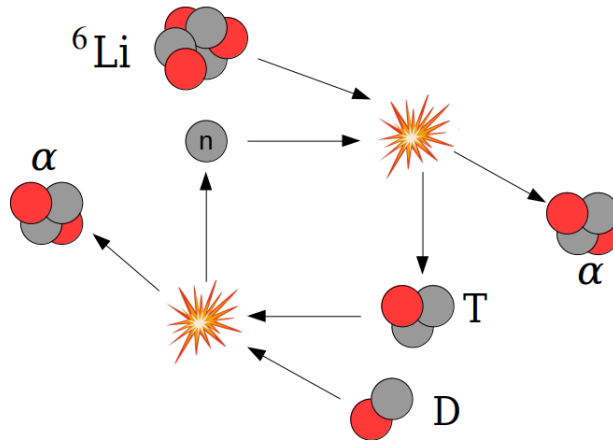
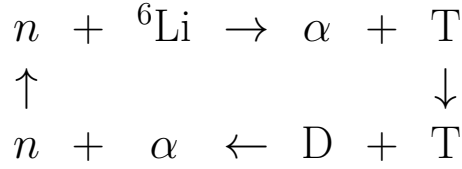


Figure 2.1: Jetter Cycle.

The lithium-deuteride is a ionic crystal at room temperature, but its state (solid, liquid or gas) does not change the picture very much, only the density is affected by the environmental temperature.

The cycle is formed by two reactions, the first one is a neutron fission induced reaction in which a neutron collides with the 6-Lithium producing a tritium and α -particle. Afterwards, the outgoing tritium nucleus will fuse with a deuterium nucleus obtaining an α -particle and another neutron that will close the cycle, which is depicted in the figure [2.1](#).

First, let us suppose that only the reactions involved in the Jetter cycle are possible, namely, no other channels are possible. Suppose no particle losses from the boundary of the crystal and no energy losses of the particle through the system. Then, the energy is just converted into mass or the mass converted into kinetic energy. Finally, like ${}^6\text{Li}$ and D nuclei are part of the crystal lattice, they are considered still and the relative energy of the reaction in the first case is the beam neutron energy or the energy shared by the product neutron of the second reaction and in the second case would be the energy of the outgoing tritium nuclei. The α -particles are an inert byproduct.

2.1 Theoretical Approach

For the Jetter cycle two reactions are involved. Using the expression [1.2](#) the Q -value of both reactions might be calculated and also the energy shared by the products using the expression [1.9](#). The relevant information is displayed in table [2.1](#) for ${}^6\text{Li}(n, \alpha)\text{T}$, whereas in table [2.2](#) the relevant information for $\text{T}(\text{D}, \alpha)n$ is displayed. All data used were taken from [\(14\)](#).

Nuclide	Mass (MeV/ c^2)	Binding Energy (b.e) (MeV)	Excess T-Energy (MeV)
${}^6\text{Li}$	5601.5184	31.9939	—
n	939.5654	—	—
α	3727.3793	28.2957	2.0557
T	2808.9211	8.4818	2.7273
			4.7830

Table 2.1: Data used to calculate the reaction Q -value for ${}^6\text{Li} + n \rightarrow \alpha + \text{T}$.

Nuclide	Mass (MeV/c ²)	Binding Energy (b.e) (MeV)	Excess T-Energy (MeV)
D	1875.6129	2.2246	—
T	2808.9211	8.4818	—
α	3727.3793	28.2957	3.5411
n	939.5654	—	14.0481
			17.5892

Table 2.2: Data used to calculate the reaction Q -value for $D + T \rightarrow \alpha + n$.

Hence, The first reaction concerning to the fission has a Q -value of 4.7834 MeV which are shared by the two products, such as the outgoing α -particle carries and excess of kinetic energy of 2.0557 MeV, whereas the tritium carries 2.7273 MeV.

Analogously for the second reaction, the fusion of a tritium nuclide with a deuterium nuclide has a Q -value of 17.5893 MeV which is shared by the two products, such as the outgoing α -particle carries and excess of kinetic energy of 3.5411 MeV, whereas the neutron carries 14.0481 MeV.

Due to the assumption of no energy losses the consequent reactions produced by the chain centers will be accomplished at this precise energy. This implies that the energy distribution is a Dirac delta function.

$$P(E) = \delta(E - E_0) \quad (2.1)$$

and the expected value of the cross section is easily computed using [1.17](#)

$$\langle \sigma v \rangle = \int \left(\frac{2E}{m} \right)^{1/2} \sigma(E) \delta(E - E_0) dE = \left(\frac{2E_0}{m} \right)^{1/2} \sigma(E_0) \quad (2.2)$$

Because the species have and keep a specific energy this acts like an additional label. Namely, particles of the same element but different energy are dealt as a different species. For instance, the two α -particles released in the complete cycle will have its own differential equation and its abundance will be stored separately.

The neutrons coming from the beam are labeled as n_1 whereas the resulting neutron from $T(D, \alpha)n$ is labeled as n_2 . Analogously, the resulting α -particle of ${}^6\text{Li}(n, \alpha)T$ is labeled as α_1 , whereas the resulting α -particle of $T(D, \alpha)n$ is labeled as α_2 .

Therefore, the set of ordinary differential equations that describes the abundance behaviour of the Jetter cycle reads

$$\frac{dY_{n_1}}{dt} = i - Y_{n_1}(t) \cdot Y_{6\text{Li}}(t) \left[{}^6\text{Li}(n_1, \alpha) \right] \quad (2.3)$$

$$\frac{dY_{n_2}}{dt} = + Y_{\text{D}}(t) \cdot Y_{\text{T}}(t) [\text{D}(\text{T}, n_2)] - Y_{n_2}(t) \cdot Y_{6\text{Li}}(t) \left[{}^6\text{Li}(n_2, \alpha) \right] \quad (2.4)$$

$$\frac{dY_{\text{D}}}{dt} = - Y_{\text{D}}(t) \cdot Y_{\text{T}}(t) [\text{D}(\text{T}, n_2)] \quad (2.5)$$

$$\begin{aligned} \frac{dY_{\text{T}}}{dt} = & + Y_{n_1}(t) \cdot Y_{6\text{Li}}(t) \left[{}^6\text{Li}(n_1, \alpha) \right] + Y_{n_2}(t) \cdot Y_{6\text{Li}}(t) \left[{}^6\text{Li}(n_2, \alpha) \right] \\ & - Y_{\text{D}}(t) \cdot Y_{\text{T}}(t) [\text{D}(\text{T}, n_2)] \end{aligned} \quad (2.6)$$

$$\frac{dY_{\alpha_1}}{dt} = + Y_{n_1}(t) \cdot Y_{6\text{Li}}(t) \left[{}^6\text{Li}(n_1, \alpha_1) \right] + Y_{n_2}(t) \cdot Y_{6\text{Li}}(t) \left[{}^6\text{Li}(n_2, \alpha_1) \right] \quad (2.7)$$

$$\frac{dY_{\alpha_2}}{dt} = + Y_{\text{D}}(t) \cdot Y_{\text{T}}(t) [\text{D}(\text{T}, \alpha_2)] \quad (2.8)$$

$$\frac{dY_{6\text{Li}}}{dt} = - Y_{6\text{Li}} \cdot Y_{n_1}(t) \left[{}^6\text{Li}(n_1, \alpha_1) \right] - Y_{6\text{Li}} \cdot Y_{n_2}(t) \left[{}^6\text{Li}(n_2, \alpha_1) \right] \quad (2.9)$$

The i in the equation [2.3](#) is the neutron injection rate [\(20\)](#) provided by the external beam. This injection rate has to be suitable set according to the current neutron beam facilities in order to achieve a more realistic system.

Neutrons can be produced using a variety of techniques, including linear electron or proton accelerators, electrostatic accelerators and also via reactors.

At linear electron accelerator, neutrons are produced via (γ, n) reactions by bombarding heavy metal targets. The outgoing neutrons have energies ranging from the subthermal region up to 50 MeV. Instead, for proton accelerator, the neutrons are produced via spallation reactions [\(16\)](#).

Fluxes of the order of $\approx 10^6$ neutron/cm²s, spanning an energy range of 1-300 keV, are typically achieved at both kind of facilities [\(29\)](#). It will be shown soon that is in this precise range where the maximum of the reaction rate is achieved for the fission reaction with ⁶Li.

Besides, charged-beams might be implemented in order to produce neutrons via nuclear reactions. For instance, a very frequently employed reaction is ⁷Li(p, n)⁷Be. In this case integrated neutron yields of $\approx 10^8 - 10^9$ neutron/s are achieved [\(30\)](#).

However, the energy distribution of the emitted neutrons closely follows a Maxwell-Boltzmann distribution, which adds some difficulties in order to compute the reaction rate. Despite of this, there are other facilities that implement filtered neutron-beams (FNBT) (31) to extract a quasi-monoenergetic neutron line from a continuous neutron spectrum with high intensity. This extraction is achieved by means of two nuclear physics processes. The first one employs Bragg reflection of neutrons in single crystals. The second one is based on the transmission of neutrons through large quantities of materials, which show deep interference minima in their total neutron cross sections. This technique allows the selection of quasi-monoenergetic neutron lines with energies 2, 3.5, 7.5, 13, 24, 54, 59, 133, 148 and 275 keV with intensities ranging from $5 \times 10^4 \text{ cm}^{-2}\text{s}^{-1}$ to $5 \times 10^7 \text{ cm}^{-2}\text{s}^{-1}$ (31). The injection rate was established to be

$$i = 1.1016 \times 10^6 \text{ mol/g} \cdot \text{s} \quad (2.10)$$

2.2 Experimental Data

In order to obtain the expected value of the energy distribution and cross section 2.2, the cross section has to be known for several specific energies which implies that an interpolation has to be performed on the experimental data for each reaction over the energy range of interest.

Different data set were used to collect the data, such as Joint Evaluated Fission and Fusion (JEFF) (22), Japanese Evaluated Nuclear Data Library (JENDL) (23)-(24) and the Evaluated Nuclear reaction Data File (ENDF/B-VIII.0) (25). All of these data set were consulted using the software versions Experimental Nuclear Reaction Data (EXFOR) (26) and specially Evaluated Nuclear Data File (ENDF) (27) in which the interpolation data of the majority of the reactions of interest of the current work were found and used directly.

2.2.1 ${}^6\text{Li}(n, \alpha)\text{T}$

The data for this reaction were extracted from ENDF (27) in which the interpolation was already performed following the library ENDF/B-VIII.0 and its held by Ref. (28), which allows to choose the energy range for displaying a list of points that will guide the interpolation. For instance, choosing the energy range from 0.1 MeV to 20 MeV, 411 points are shown in order to make the interpolation.

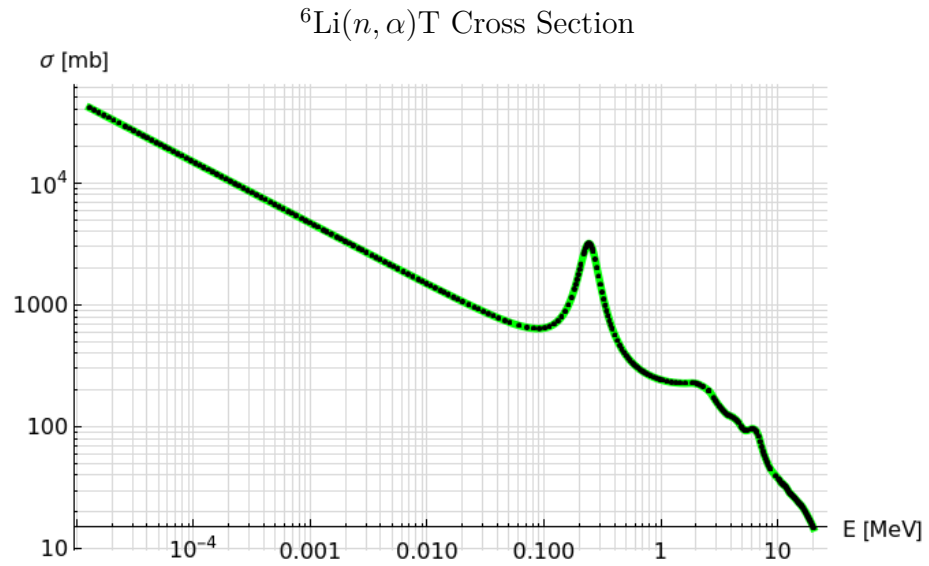


Figure 2.2: Cross Section for ${}^6\text{Li}(n, \alpha)\text{T}$. Black-points: Data taken from (25) in which the interpolation was already performed. Green-line: Interpolation using Mathematica.

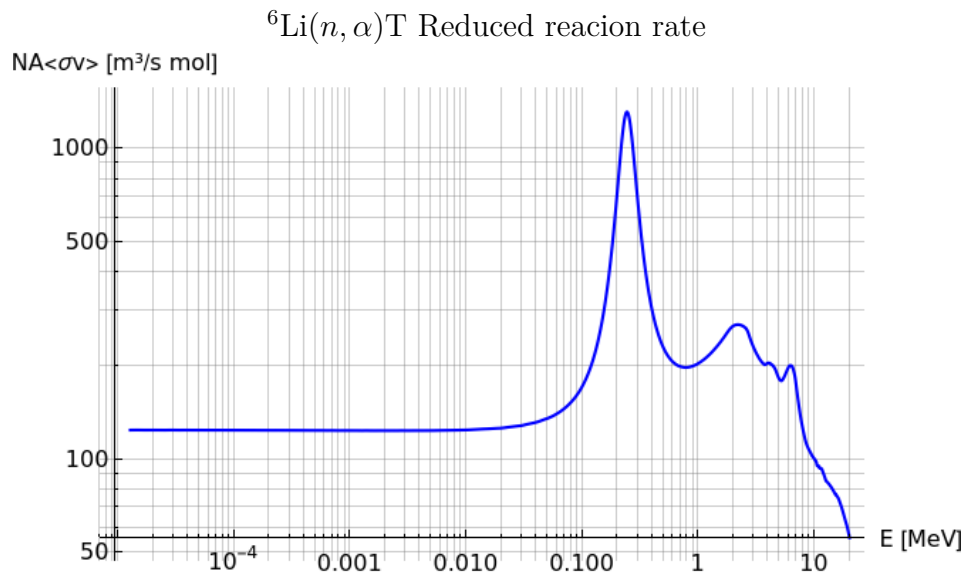


Figure 2.3: Reduced reaction rate $N_A \langle \sigma v \rangle$ for ${}^6\text{Li}(n, \alpha)\text{T}$ using the expression 2.2.

The figure [2.2](#) shows the cross section for the fission reaction. The black dots are the data given by the ENDF/B-VIII.0 whereas the green line is the interpolation made using Mathematica in order to obtain a function that might be evaluated at whatever energy, as required in order to numerically solve the set of ordinary equations.

As the cross section and the energy distribution probability of the reactans are known, the expected value of the product of velocity and energy [2.2](#) is easily calculated. More often, the reduced reaction rate $N_A \langle \sigma v \rangle$ is plotted. The result is shown in the figure [2.3](#).

It is worth to notice how the reduced reaction rate for the fission reaction ${}^6\text{Li}(n, \alpha)\text{T}$ achieves its maximum when the coming neutrons have an energy of 0.24 MeV. And these neutrons energy, in principle, is set by hand, because these are the particles coming from the beam.

2.2.2 $\text{T}(\text{D}, \alpha)n$

The data for this reaction were extracted from ENDF [\(27\)](#) in which the interpolation was already performed following the library ENDF/B-VI and its held by Ref.[\(35\)](#), which allows to choose the energy range for displaying a list of points that will guide the interpolation. For instance, choosing the energy range from 0.1 MeV to 10 MeV, 89 points are shown in order to make the interpolation.

The figure [2.4](#) shows the cross section for the fusion reaction. The black dots are the data given by the ENDF/B-VI whereas the green line is the interpolation made using Mathematica in order to obtain a function that might be evaluated at whatever energy, as required in order to numerically solve the set of ordinary equations.

Again, as the cross section and also the energy distribution probability of the reactans are known, the expected value of the product of velocity and energy [2.2](#) is easily calculated. The reduced reaction rate $N_A \langle \sigma v \rangle$ for the fusion reaction is showed in figure [2.5](#).

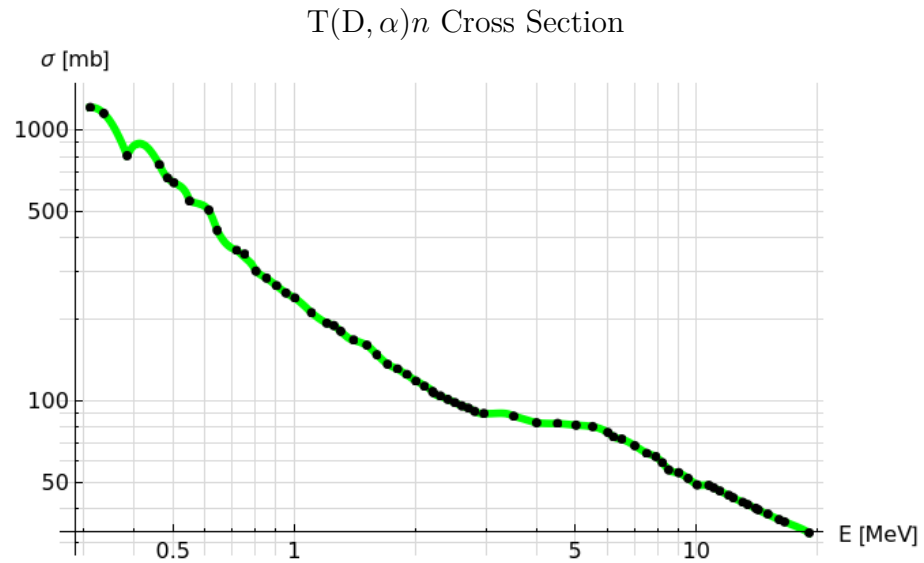


Figure 2.4: Cross Section for $T(D, \alpha)n$. Black-points: Data taken from (35) in which the interpolation was already performed. Green-line: Interpolation using Mathematica.

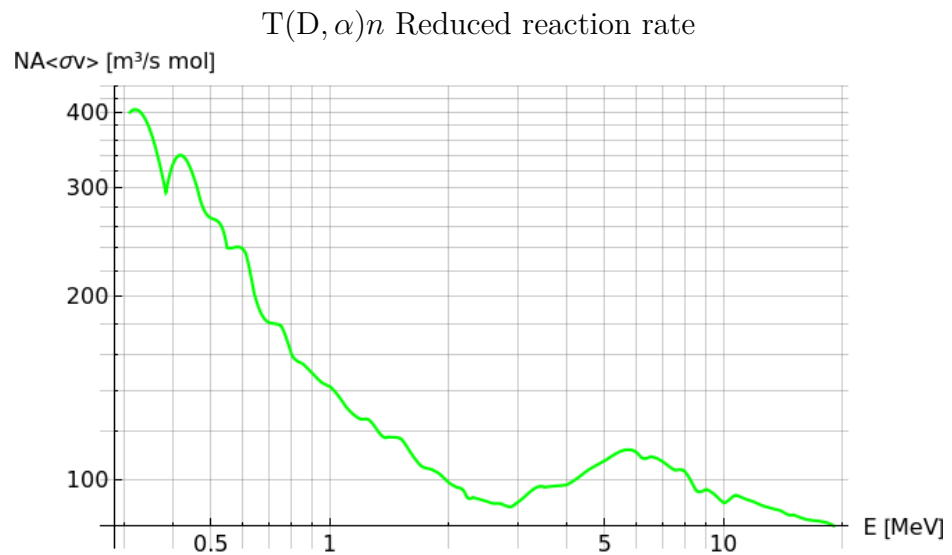


Figure 2.5: Reduced reaction rate $N_A \langle \sigma v \rangle$ for reaction $T(D, \alpha)n$ using the expression 2.2

2.3 Results

After obtaining the expected values between the cross section interpolation and the energy distribution of the reactions involved. The set of ordinary differential equations might be numerically solved. For that, initial conditions have to be set.

These initial conditions refer to the initial abundance in the system. Then, at the beginning the deuterium and 6-Lithium are present at equal proportion due to chemical stoichiometry. The neutrons present are only from the external beam which at $t = 0$ is turned on and therefore their total number is a (almost) linearly growing function. Besides, the energy of these particles is set to 0.24 MeV because at this precise energy the maximum of the reduced reaction rate is found, like it is shown in the figure [2.3](#). This choice is made in order to considerably increase the fission probability between ${}^6\text{Li}$ and n .

We propose to simulate 1 mol of ${}^6\text{LiD}$, this means that the initial molar fraction can be calculated using the expression [1.33](#)

$$Y_{6\text{Li}} = \frac{N_{6\text{Li}}}{\rho N_A} = \frac{N_A}{V \rho N_A} = \frac{1}{V \rho} = \frac{1}{8} \frac{g}{\text{mol}} = 0.125 \frac{\text{mol}}{g}. \quad (2.11)$$

Following the same procedure the initial molar fraction for the deuterium can be calculated and how is to expected, it is the same.

Since there is an external source of nucleons, just at the starting point the constraint over the nucleon fraction is fulfilled [1.36](#).

$$X_{6\text{Li}} = Y_{6\text{Li}} A_{6\text{Li}} = 0.75 \quad X_{\text{D}} = Y_{\text{D}} A_{\text{D}} = 0.25, \quad (2.12)$$

and evidently, the sum is 1 and the conditions is satisfied.

The initial conditions for solving the set of ordinary equations are listed in the table [2.3](#).

Finally the system of coupled first order differential equation is solved, using the built-in routine in Mathematica [B](#). The results are shown in the figures [2.6](#), [2.7](#) and [2.8](#), where the abundance evolution of each species is separately displayed. Several intuitive behaviour is present.

Molar Fraction	Value (mol/g)
$Y_{n_1}(0)$	0.0
$Y_{n_2}(0)$	0.0
$Y_{\alpha_1}(0)$	0.0
$Y_{\alpha_2}(0)$	0.0
$Y_D(0)$	1.25×10^{-1}
$Y_T(0)$	0.0
$Y_{6Li}(0)$	1.25×10^{-1}

Table 2.3: *Initial conditions to solve the set of ordinary differential equations for the Jetter cycle.*

The figure [2.6](#) in the panel (a) the continuous growing in the neutron abundance of the neutrons coming from the beam is shown. Also, the neutron abundance coming from the fusion between deuterium and tritium continuously increases as is shown in the panel (b).

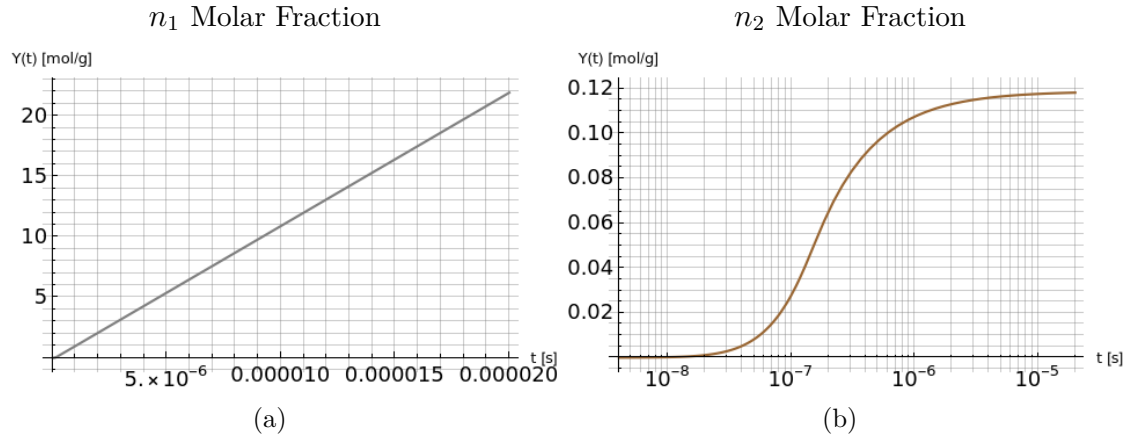


Figure 2.6: Solution of the set of ordinary differential equations describing the Jetter cycle.

The abundance evolution for the two species of α -particles is shown in the figure [2.7](#). As it is guessed from equation [2.7](#) and equation [2.8](#), both are only produced, achieving a steady point.

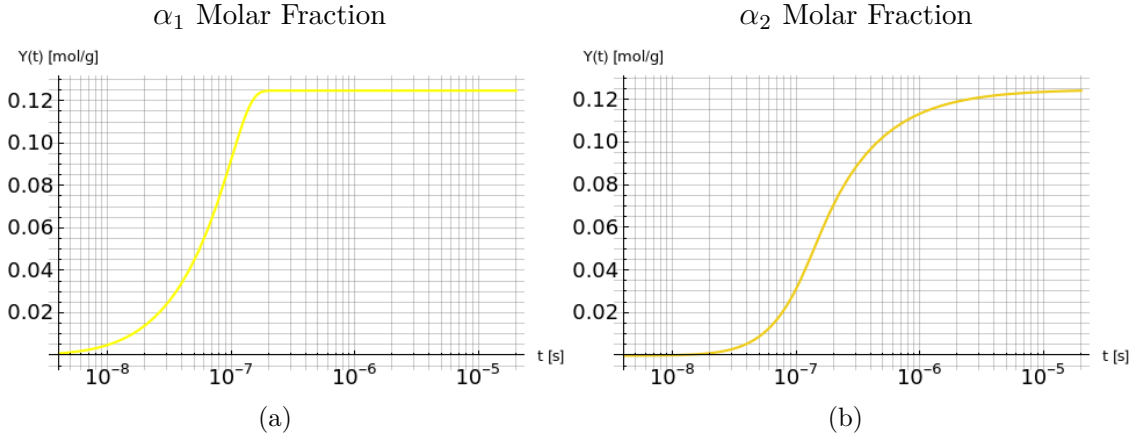


Figure 2.7: Solution for the α -particles in the Jetter cycle.

In the figure [2.8](#), from equation [2.5](#) and equation [2.9](#) we can see that the deuterium and lithium is only consumed and with a very different ratio because the system is more populated with neutrons than the tritium. Therefore, the panels (a) and (b) show the monotonically decrease of these species until the point where both are depleted.

Finally, the tritium has a more interesting dynamic, which is displayed in panel (c). At the beginning is produced via the fission reaction reaching a point in which its abundance is enough to start the deuterium consumption, this continues until the tritium is completely depleted. Hence, the radioactive tritium is not present at the end, it just was produced and consumed during the process.

In the figure [2.9](#) all the abundances curves at the same time (except the neutrons coming from the beam) are shown. Here, it is easier to appreciate the tritium cycle, it starts to be produced at the same point when the lithium starts to be consumed and the peak of tritium is achieved exactly at the same point when the lithium is exhausted and then, no more tritium is produced. Moreover, the minimum of tritium abundance also coincides with the steady point of α_2 -particle abundance. The minimum of lithium abundance also coincides with the steady point of α_1 -particle abundance. Besides, despite of the production of n_2 particles, lithium is not longer present in the system and this neutrons also achieve a steady value.

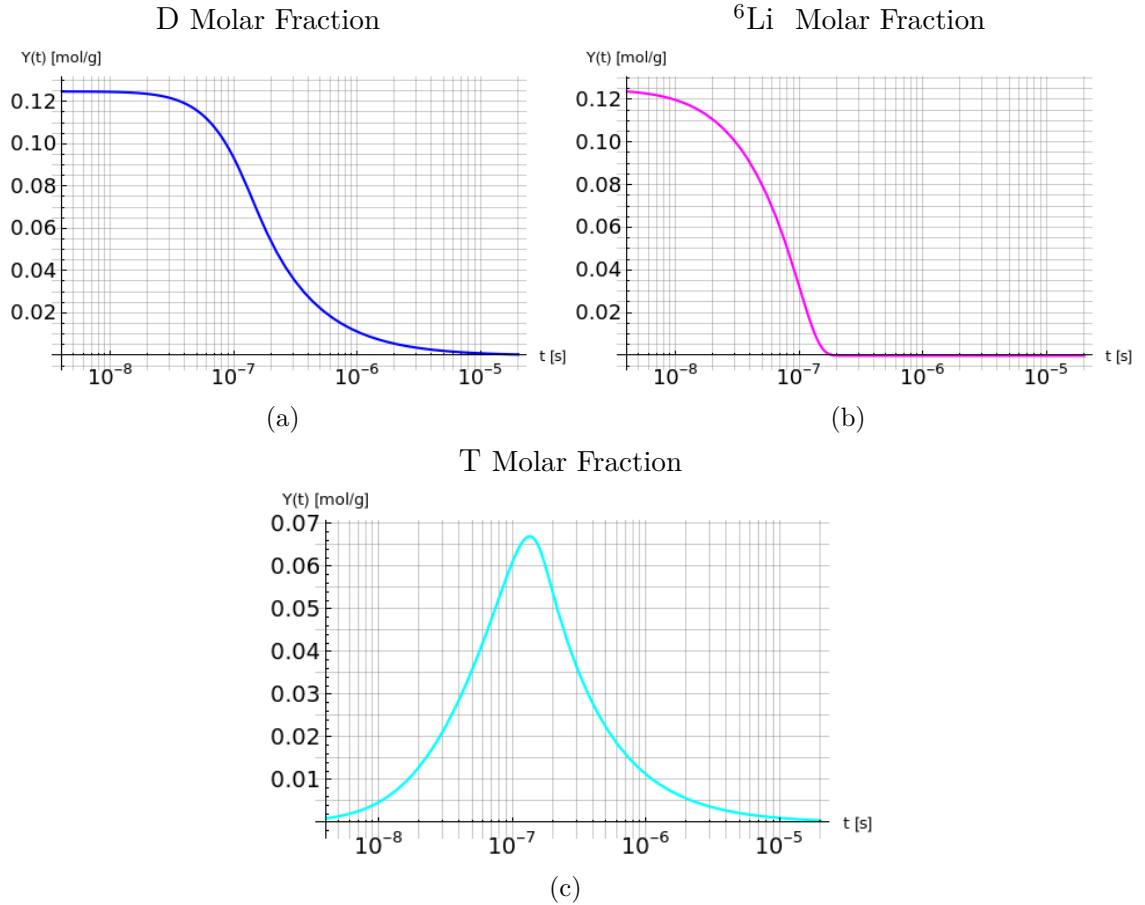


Figure 2.8: Solution of the set of ordinary differential equations describing the Jetter cycle.

It is worth to notice the time scale in which the system achieves the steady solution. This is of the order of ten micro-seconds. Moreover, due to the fact that the neutrons coming from the beam only react with the lithium, then the neutron beam might be turn off at the time when the lithium is exhausted, namely, more or less 0.2 micro-seconds. This for energetic purposes in order to obtain a real energy gain.

Notice that using the expression [1.33](#) the result expressed in terms of the molar fraction Y_i may be written in terms of the nucleon fraction X_i multiplying every species by its mass number. The results written in terms of nucleon fraction is usually given in the literature. The result is shown in the figure [2.10](#).

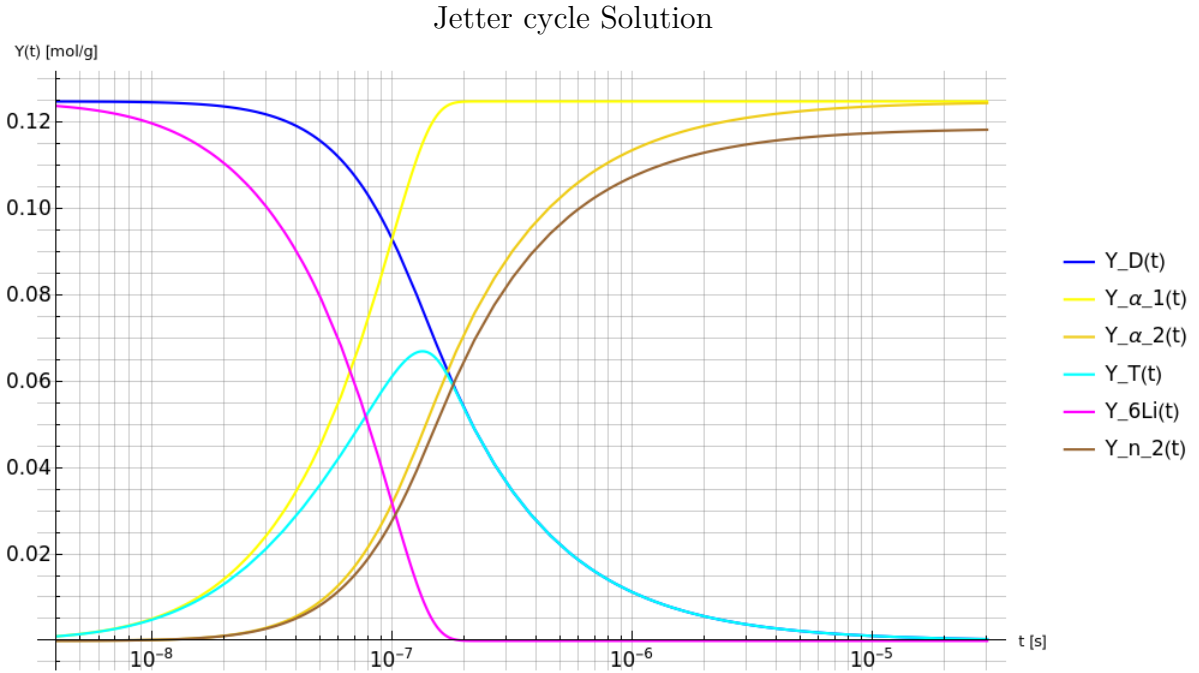


Figure 2.9: Curves of abundance evolution in terms of the molar fraction of the Jetter cycle using the initial conditions [2.3](#).

At the end, the differential equations converge to a steady point in which the system is only populated with α -particles and neutrons. This is expressed in the table [2.4](#) and depicted in the barchart [2.11](#) where is easier to appreciate the initial and final abundances. There, t_{fin} refers to the time at which the system has achieved the steady solution.

Finally, due to the fact that the curves of abundance evolution are known, the fusion yield might be calculated using the expression [1.47](#) and multiplying by the volume of the simulated system. Since we are interested in the simulation of 1 mol of the crystal ${}^6\text{LiD}$, this has a mass of 8 g and also the density is known ($\rho = 0.883 \text{ g/cm}^3$ [\(32\)](#)) then the volume is calculated in order to obtain the power as a function of the time and no the specific power like is expressed in the equation [1.47](#).

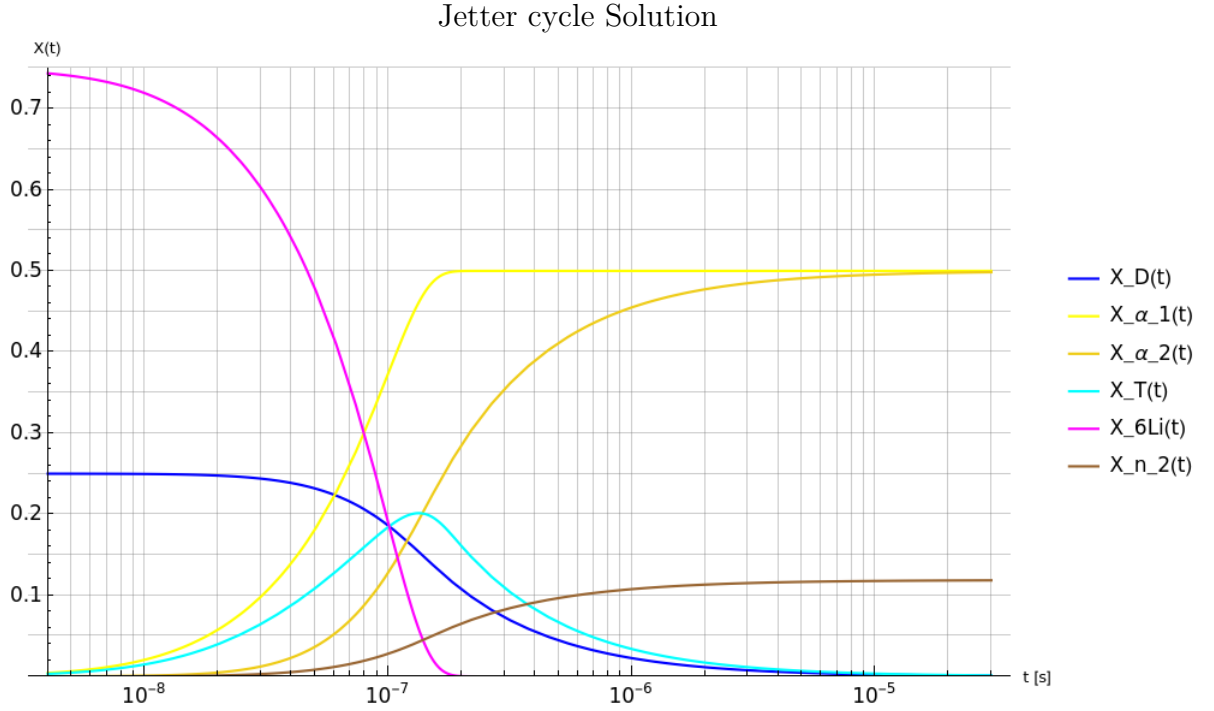


Figure 2.10: Curves of abundance evolution in terms of the nucleon fraction of the Jetter cycle using the initial conditions [2.3](#).

Molar Fraction	Value (mol/g)
$Y_{n_1}(t_{fin})$	32.92
$Y_{n_2}(t_{fin})$	1.18×10^{-1}
$Y_{\alpha_1}(t_{fin})$	1.25×10^{-1}
$Y_{\alpha_2}(t_{fin})$	1.25×10^{-1}
$Y_D(t_{fin})$	0.0
$Y_T(t_{fin})$	0.0
$Y_{6Li}(t_{fin})$	0.0

Table 2.4: Final molar fraction for the species involved in the Jetter cycle.

The curves of the power as a function of time for every reaction involved in the Jetter cycle are displayed in the figure [2.12](#). In black the curves related with fission reactions are shown, instead in red the curve related with the fusion reaction is shown.

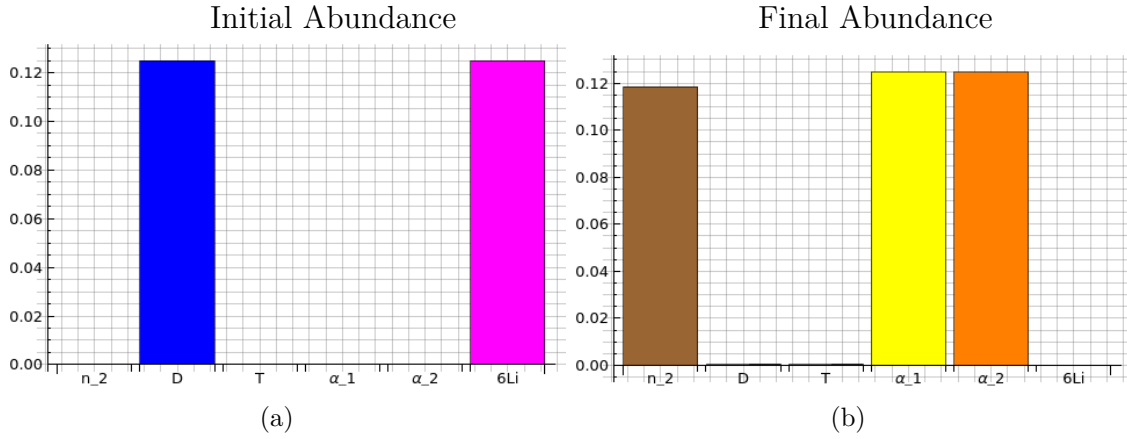


Figure 2.11: Abundance in terms of molar fraction Y expressed in units of mol/g. (a) Initial abundance according to the initial conditions [2.3](#). (b) Final abundance after the system integration.

The integration of power curves would give us the energy released in GJ and this is the reason why the graph shows the shade under the curves. The results are expressed in the table [2.5](#).

Reaction	Fusion Yield (GJ)
${}^6\text{Li}(n_1, \text{T})\alpha$	465.135
${}^6\text{Li}(n_2, \text{T})\alpha$	24.204
$\text{D}(\text{T}, n_2)\alpha$	1793.500
Total	2282.840

Table 2.5: Energy released for every reaction in the Jetter cycle.

It is worth to point out the high energy that is released by the fusion reaction compared with the fission reactions, showing that the fission reaction serves more like a mediator to the fusion reactions.

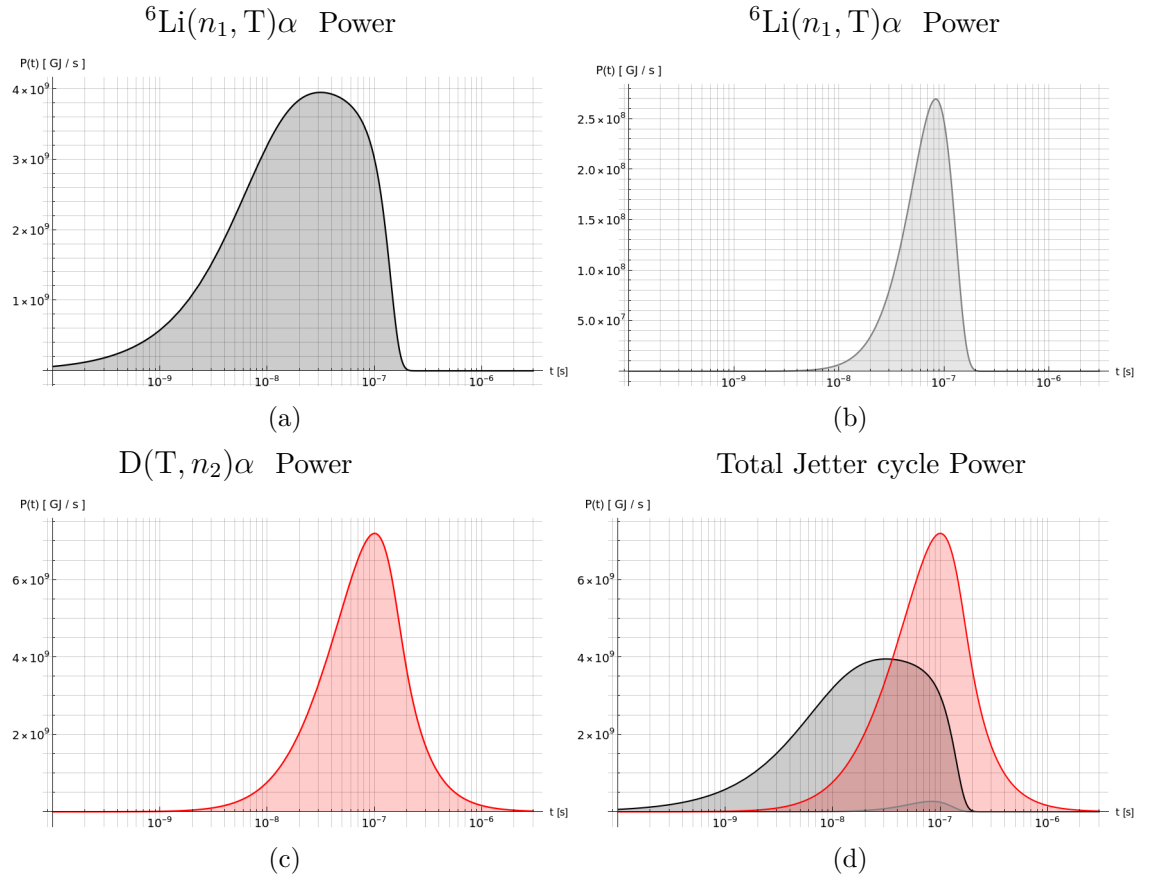


Figure 2.12: Power released in the Jetter cycle. (a) Power released by the ${}^6\text{Li}(n_1, \text{T})\alpha$ reaction. (b) Power released by the ${}^6\text{Li}(n_2, \text{T})\alpha$ reaction. (c) Power released by the $\text{D}(\text{T}, n_2)\alpha$ reaction. (d) All curves overlapped. The time integration of the curves would be the energy released.

Chapter 3

Post Cycle

The present chapter is focused on the the Post cycle simulation, which takes its name from the scientist Richard Post. This cycle is also present in the ${}^6\text{LiD}$ system, representing new channels available more than the only considered in the Jetter cycle.

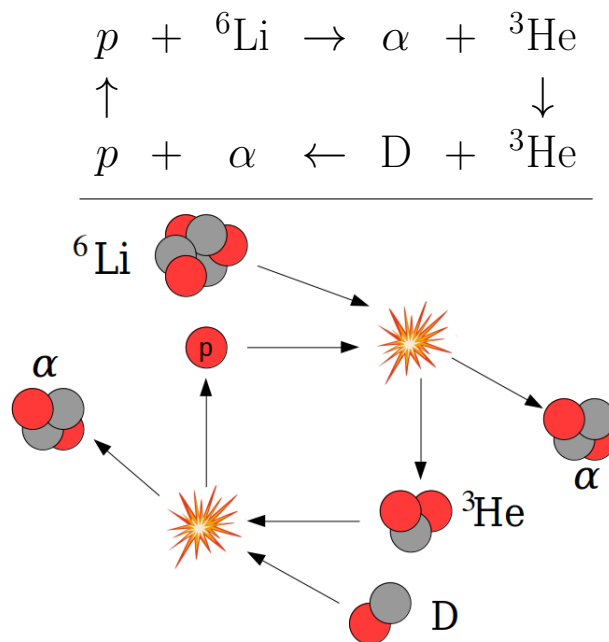


Figure 3.1: Post Cycle.

The cycle is formed by two reactions, the first one is a proton fission induced reaction in which a proton collides with the 6-Lithium producing a 3-Helium and α -particle. Afterwards, the outgoing 3-Helium nuclei will fuse with a deuterium nucleus obtaining an α -particle and another proton that will close the cycle, which is depicted in the figure 3.1. As it is shown, now the chain centers are the proton and ^3He . Besides, again the α -particles are an inert byproduct.

The Post cycle might dramatically change the final abundance displayed only by the Jetter cycle and for this, it is implemented in order to go closer to a real system. For this reason, it is kept in mind that the neutron beam is used for triggering the Jetter cycle and a population of proton is present at certain point that will trigger the Post cycle. The origin of this proton abundance will be made clear in the next chapter.

3.1 Theoretical Approach

For the Post cycle two reactions are involved. Again, using the expression 1.2 the Q -value of both reactions might be calculated and also the energy shared by the products using the expression 1.9. The relevant information is displayed in table 3.1 for $^6\text{Li}(p, ^3\text{He})\alpha$, whereas in table 3.2 the relevant information for $^3\text{He}(\text{D}, p)\alpha$ is displayed. All data used were taken from Ref. (14).

Nuclide	Mass (MeV/ c^2)	Binding Energy (b.e) (MeV)	Excess T-Energy (MeV)
^6Li	5601.5184	31.9939	—
p	938.2720	—	—
α	3727.3793	28.2957	1.7272
^3He	2808.3916	7.7180	2.2924
			4.0197

Table 3.1: Data used to calculate the reaction Q -value for $^6\text{Li} + p \rightarrow \alpha + ^3\text{He}$.

Hence, the first reaction concerning to the fission has a Q -value of 4.0197 MeV which is shared by the two products, such that the outgoing α -particle carries an excess of kinetic energy of 1.7272 MeV, whereas the ^3He carries 2.2924 MeV.

Analogously for the second reaction, the fusion of a ^3He nuclide with a deuterium nuclide has a Q -value of 18.3530 MeV which is shared by the two products, such as the outgoing α -particle carries and excess of kinetic energy of 3.6908 MeV, whereas

Nuclide	Mass (MeV/c ²)	Binding Energy (b.e) (MeV)	Excess T-Energy (MeV)
D	1875.6129	2.2246	—
³ He	2808.3916	7.7180	—
α	3727.3793	28.2957	3.6908
p	938.2720	—	14.6622
			18.3530

Table 3.2: Data used to calculate the reaction Q -value for $D + {}^3\text{He} \rightarrow \alpha + p$.

the proton carries 14.6622 MeV.

In this case, again, the assumption of no energy losses implies that the consequent reactions produced by the chain centers will be accomplished at this precise energy. Namely, the energy distribution probability function is a Dirac delta function and the expected value between the energy distribution function and cross section is calculated using [2.2](#).

Again, the two α -particles released in the complete cycle will be described by its own differential equation and its abundance will be stored separately. Then, the resulting α -particle of ${}^6\text{Li}(p, {}^3\text{He})\alpha$ is labeled as α_3 , whereas the resulting α -particle of ${}^3\text{He}(D, p)\alpha$ is labeled as α_4 .

Therefore, the set of ordinary differential equations that describes the abundance behaviour of the Post cycle reads

$$\frac{dY_p}{dt} = + Y_D(t) \cdot Y_{{}^3\text{He}}(t) [{}^3\text{He}(D, p)] - Y_p(t) \cdot Y_{{}^6\text{Li}}(t) [{}^6\text{Li}(p, {}^3\text{He})] \quad (3.1)$$

$$\frac{dY_{{}^3\text{He}}}{dt} = + Y_p(t) \cdot Y_{{}^6\text{Li}}(t) [{}^6\text{Li}(p, {}^3\text{He})] - Y_{{}^3\text{He}}(t) \cdot Y_D(t) [{}^3\text{He}(D, p)] \quad (3.2)$$

$$\frac{dY_D}{dt} = - Y_D(t) \cdot Y_{{}^3\text{He}}(t) [{}^3\text{He}(D, p)] \quad (3.3)$$

$$\frac{dY_{\alpha_3}}{dt} = + Y_p(t) \cdot Y_{{}^6\text{Li}}(t) [{}^6\text{Li}(p, {}^3\text{He})] \quad (3.4)$$

$$\frac{dY_{\alpha_4}}{dt} = + Y_D(t) \cdot Y_{{}^3\text{He}}(t) [{}^3\text{He}(D, p)] \quad (3.5)$$

$$\frac{dY_{{}^6\text{Li}}}{dt} = - Y_p(t) \cdot Y_{{}^6\text{Li}}(t) [{}^6\text{Li}(p, {}^3\text{He})] \quad (3.6)$$

3.2 Experimental Data

The same procedure was followed in order to solve the set of ordinary differential equations as for the Jetter cycle. The data of the cross section are searched for the specific reaction in the energy range of interest. The interpolation of this data is performed. Combining this interpolation with the energy distribution probability the expected value between the energy distribution function and the cross section is calculated.

3.2.1 ${}^6\text{Li}(p, \alpha){}^3\text{He}$

Unlike the previous cases, for this reaction data are not available in ENDF (27) and then no interpolation was already performed. Therefore, the data were taken from EXFOR (26) in which 13 experiments are reported for a total of 192 data points. The plot of the cross section data points in the energy range of interest, taking in account also the errors is shown in figure 3.2.

It is evident that the interpolation might not be done using all these data. Firstly, because for a specific energy (x -axis) there might be two different experimental values, which produces an error in the interpolation function in Mathematica. Besides, although this previous case will not be present, if two very close points in energy have a very different experimental value, this would produce a high oscillating function due to the fact that the interpolation always tries to cross every single point, with a polynomial of a certain order.

The criteria chosen to perform the interpolation was to remove the data for which no errors were reported in (26) and remove the overlapping data by selecting minor errors. The result is plotted in figure 3.3. The green line represents the interpolation made using Mathematica.

After having the interpolation function of the cross section, the reduced reaction rate for the outgoing protons of 14.6622 MeV of kinetic energy could be computed using 2.2. The result is depicted in the figure 3.4.

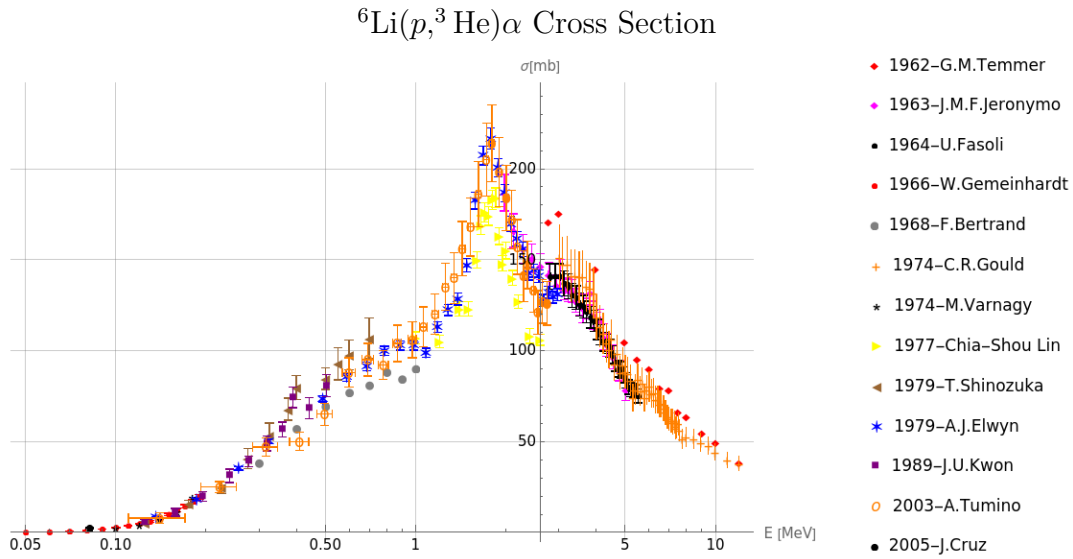


Figure 3.2: Cross Section data for ${}^6\text{Li}(p, {}^3\text{He})\alpha$ taken from (26). Energy axis in logarithmic scale.

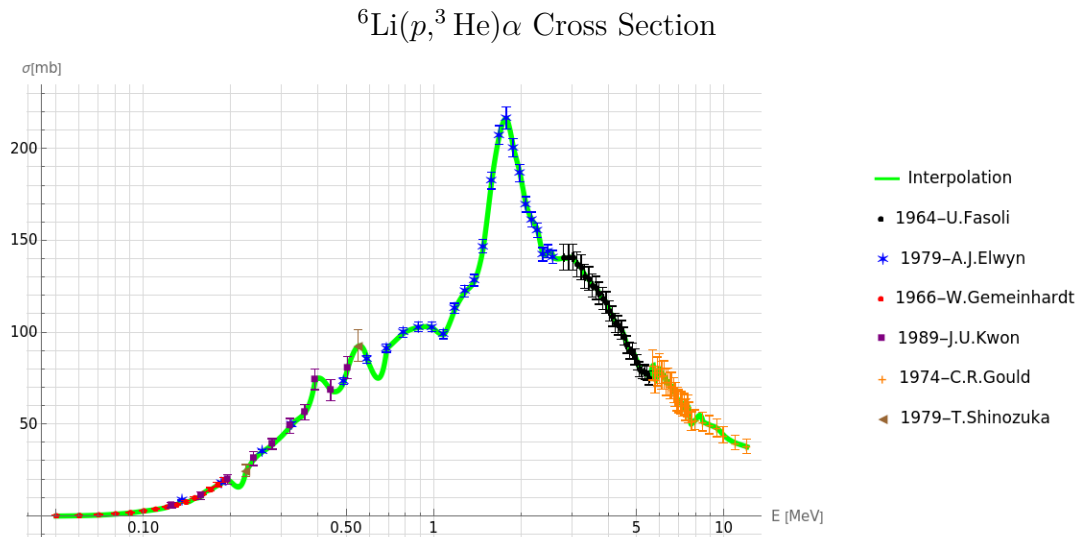


Figure 3.3: Cross Section for ${}^6\text{Li}(p, \alpha){}^3\text{He}$ using the data taken from (26). Interpolation made using Mathematica.

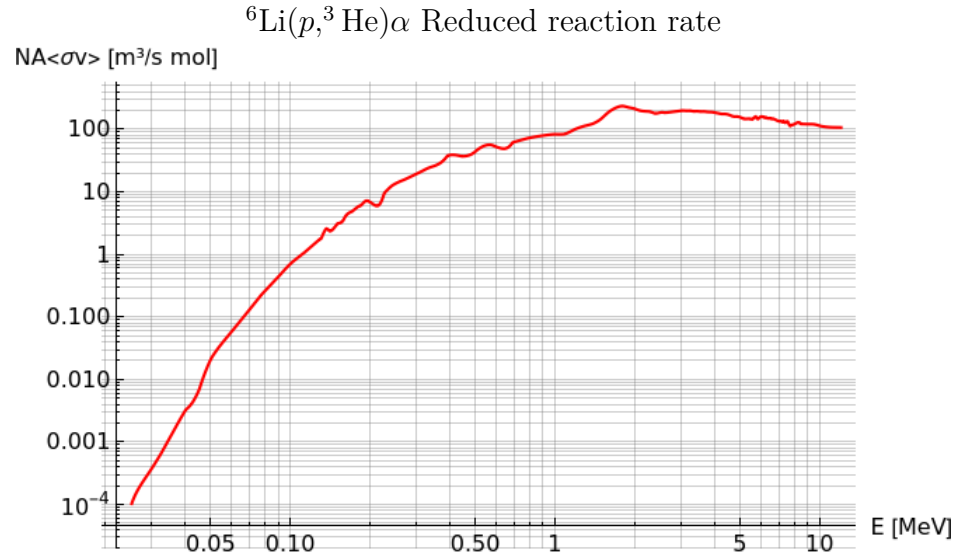


Figure 3.4: Reduced reaction rate $N_A \langle \sigma v \rangle$ for the reaction ${}^6\text{Li}(p, {}^3\text{He})\alpha$ calculated using the expression [2.2](#).

3.2.2 ${}^3\text{He}(\text{D}, p)\alpha$

The data for this reaction were extracted from ENDF ([27](#)) in which the interpolation was already performed following the library ENDF/B-VI and its held by ([33](#)), ([34](#)), which taking the data in the energy range from 0.1 MeV to 9.6 MeV displays a list of 88 points that will guide the interpolation. The result is plotted in [fig 3.5](#), the black dots are the data given by the ENDF/B-VI, whereas the green line is the interpolation made using Mathematica.

Again, as the cross section and also the energy distribution probability of the reactants are known, the expected value of the product of velocity and energy [2.2](#) is easily computed. The reduced reaction rate $N_A \langle \sigma v \rangle$ for the current reaction is showed in [figure 3.6](#).

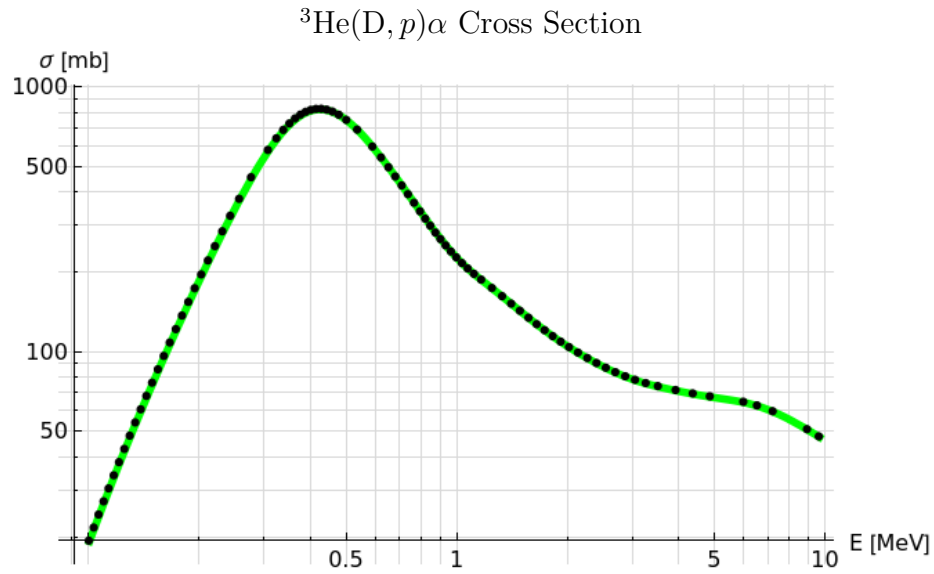


Figure 3.5: Cross Section for ${}^3\text{He}(\text{D}, p)\alpha$ using the data taken from (33) interpolated using Mathematica.

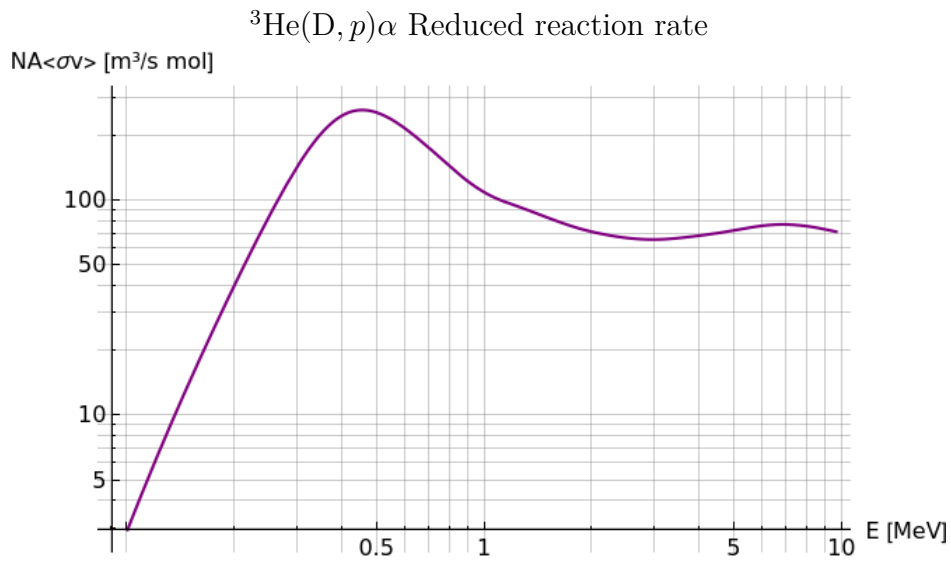


Figure 3.6: Reduced reaction rate $N_A \langle \sigma v \rangle$ for ${}^3\text{He}(\text{D}, p)\alpha$ using the expression 2.2.

3.3 Results

After obtaining the expected values between the cross section interpolation and the energy distribution of the reactions involved, the set of ordinary differential equations might be numerically solved. For that, initial conditions have to be set in sufficient number.

These initial conditions refer to the initial abundance of the various species in the system. Then, at the beginning it is assumed that the deuterium and 6-Lithium are present at equal proportion and a considerably quantity of protons also is present, this due to the fact that if no protons are present the complete cycle is off. Then, we are assuming that there is an unknown source of protons until the point that the Post cycle is triggered. Again, this source of protons will be explored in the next chapter.

Moreover, due to the fact that there is not an external source of nucleons, the constraint over the nucleon fraction is totally fulfilled [1.32](#)

Again, we propose to simulate 1 mol of ${}^6\text{LiD}$, this means that the initial molar fraction can be calculated using the expression [1.33](#)

$$Y_{6\text{Li}} = \frac{N_{6\text{Li}}}{\rho N_A} = \frac{N_A}{V \rho N_A} = \frac{1}{V \rho} = \frac{1}{8} \frac{g}{\text{mol}} = 0.125 \frac{\text{mol}}{g} \quad (3.7)$$

Following the same procedure the initial molar fraction for the deuterium can be calculated and how is to expected, it is the same.

The initial conditions for solving the set of ordinary equations are listed in the table [3.3](#).

Finally the system of coupled first order differential equation is solved, using the built-in routine in Mathematica [B](#). The results are shown in the figure [3.7](#).

In this figure the abundance evolution of every species is displayed. Some behaviour is similar to the Jetter cycle. For instance, from equation [3.3](#) and equation [3.6](#), it is possible to see that deuterium and lithium are only consumed and with a different ratio. Therefore, the panels (e) and (f) show the monotonically decrease of these species until the point where both are completely depleted.

The two species of α -particles (a) and (b) are only produced like it is guessed from

Molar Fraction	Value (mol/g)
$Y_{^3\text{He}}(0)$	0.0
$Y_p(0)$	10^{-2}
$Y_{\alpha_3}(0)$	0.0
$Y_{\alpha_4}(0)$	0.0
$Y_{\text{D}}(0)$	1.25×10^{-1}
$Y_{^6\text{Li}}(0)$	1.25×10^{-1}

Table 3.3: *Initial conditions to solve the set of ordinary differential equations for the Post cycle.*

equation [3.4](#) and equation [3.5](#) achieving at the end a steady point.

The proton and ^3He have a more interested dynamic. The initial population of proton is consumed through the first reaction producing ^3He nuclei. After, when a significant abundance of ^3He is reached, the second reaction starts to produce more protons, increasing the abundance of this species at the same time that the abundance of ^3He is decreased again. This continues until the point in which the 6-lithium is depleted and the first reaction stops. The ^3He remnant is finally consumed through the fusion with the deuterium.

In figure [3.8](#) all the abundance curves are shown. Here, it is easier to appreciate how the protons achieves the steady-point when the deuterium is completely depleted and also previously the lithium was exhausted. The same occurs for the α -particles. α_3 achieves the steady point when the lithium is totally consumed, whereas the steady point for α_4 coincides when the deuterium is completely consumed. On the other hand, the ^3He nuclei appear at certain point like the product of the first reaction, but are rapidly consumed again for the second reaction until the point that is not present at the end. A very similar dynamic like the tritium in the Jetter cycle.

It is worth to notice the time scale in which the system achieves the steady solution. This is of the order of 0.1 milli-seconds, one order of magnitude slower than the Jetter cycle. It is clear that this time depends on the initial proton population. The two close time scales at which these two cycles occur is a sign that when they will be merged an overlap of the two dynamics will be seen.

Notice that using the expression [1.33](#) the result expressed in terms of the molar

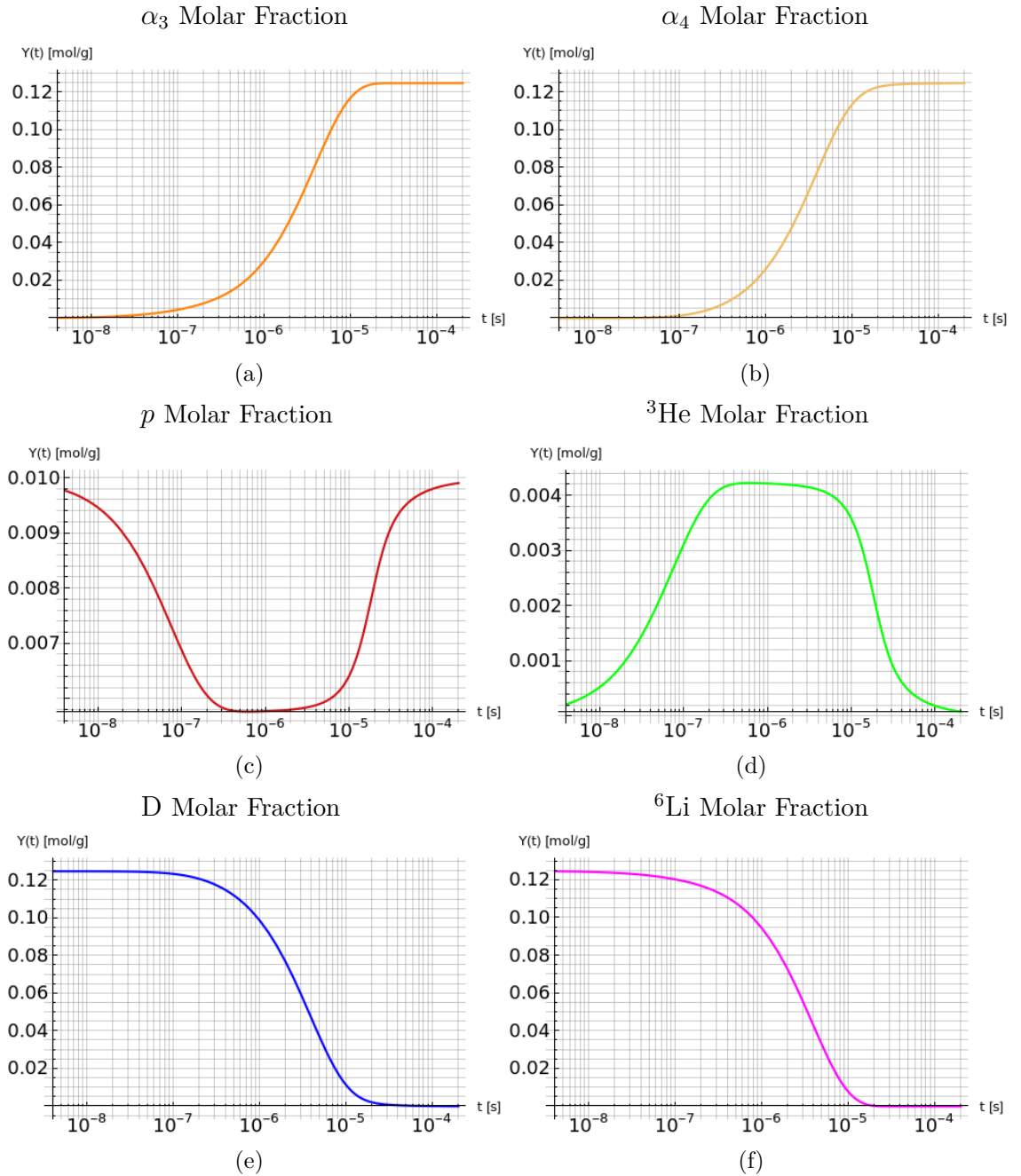
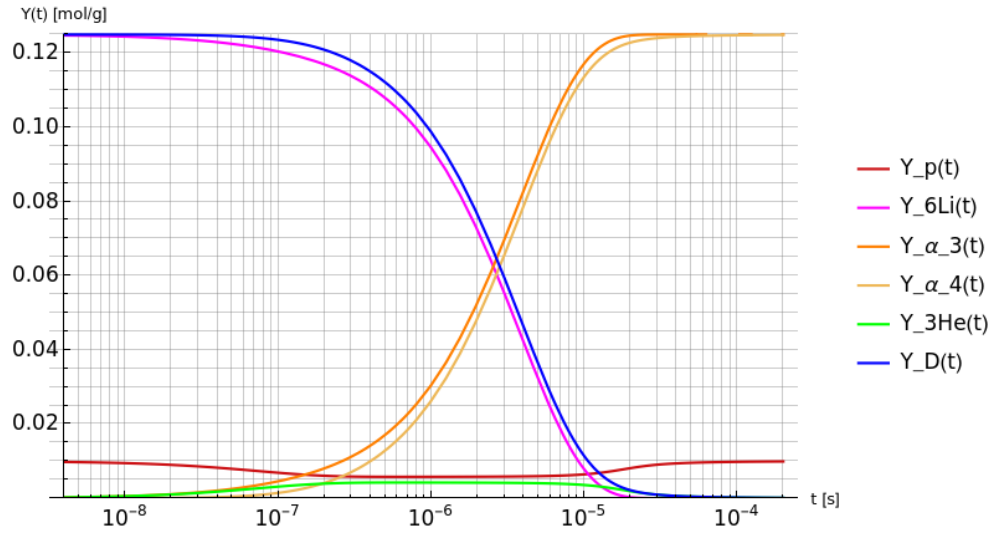
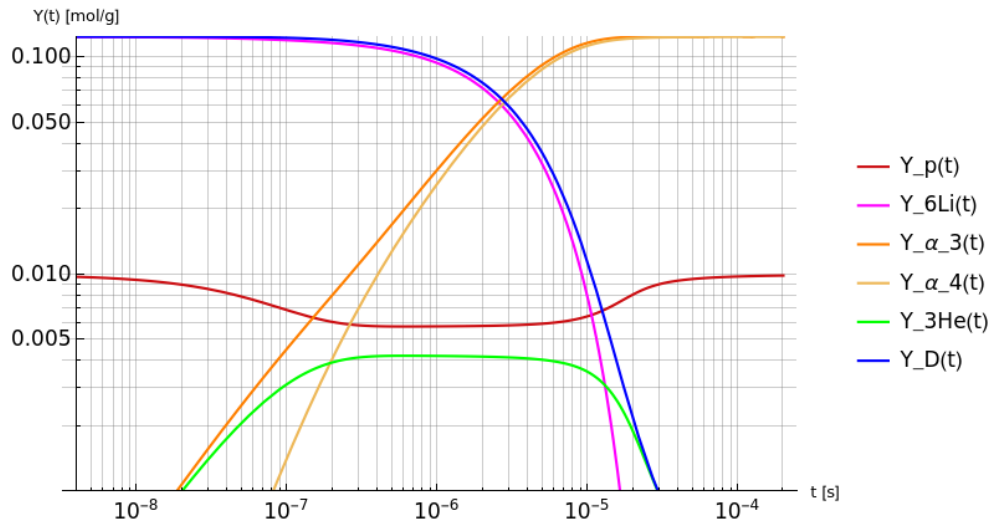


Figure 3.7: Solution of the set of ordinary differential equations describing the Post cycle in terms of molar fraction Y_i .

Post cycle Solution



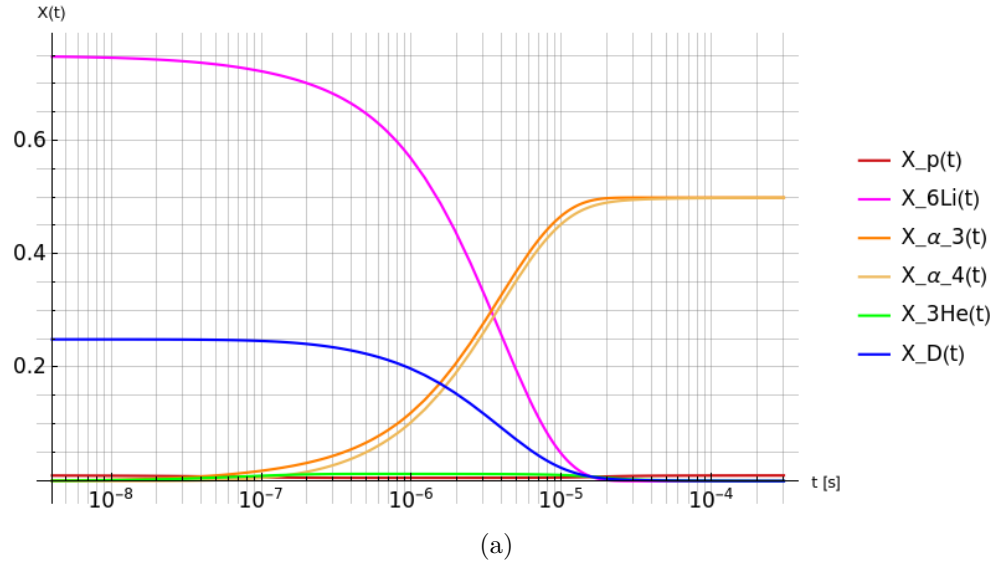
(a)



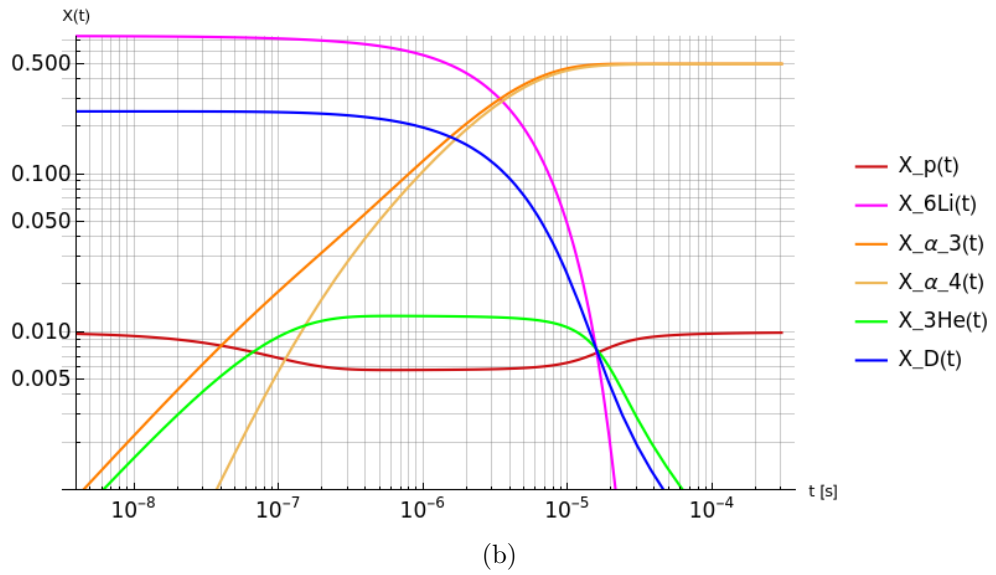
(b)

Figure 3.8: Curves of abundance evolution in the Post cycle using the initial conditions [3.3](#). (a) Linear scale in the y -axis. (b) logarithmic scale in the y -axis to better visualization of the p and ^3He species.

Post cycle Solution



(a)



(b)

Figure 3.9: Curves of abundance evolution in terms of nucleon fraction of the Post cycle using the initial conditions [3.3](#). (a) Linear scale in the y -axis. (b) logarithmic scale in the y -axis to better visualization of the p and ^3He species.

fraction Y_i may be written in terms of the nucleon fraction X_i , multiplying every species by its mass number. Results written in terms of nucleon fraction are usually given in the literature. The result is shown in the figure [3.9](#).

At the end, the differential equations converge to a steady point in which the system is only populated with α -particles and protons. This is expressed in the table [3.4](#) and depicted in the barchart [3.10](#), where it is easier to appreciate the initial and final abundances. There, t_{fin} refers to the time at which the system has achieved the steady solution.

Molar Fraction	Value (mol/g)
$Y_{3\text{He}}(t_{fin})$	0.0
$Y_p(t_{fin})$	10^{-2}
$Y_{\alpha_3}(t_{fin})$	1.25×10^{-1}
$Y_{\alpha_4}(t_{fin})$	1.25×10^{-1}
$Y_D(t_{fin})$	0.0
$Y_{6\text{Li}}(t_{fin})$	0.0

Table 3.4: Final molar fraction for the species involved in the Post cycle.

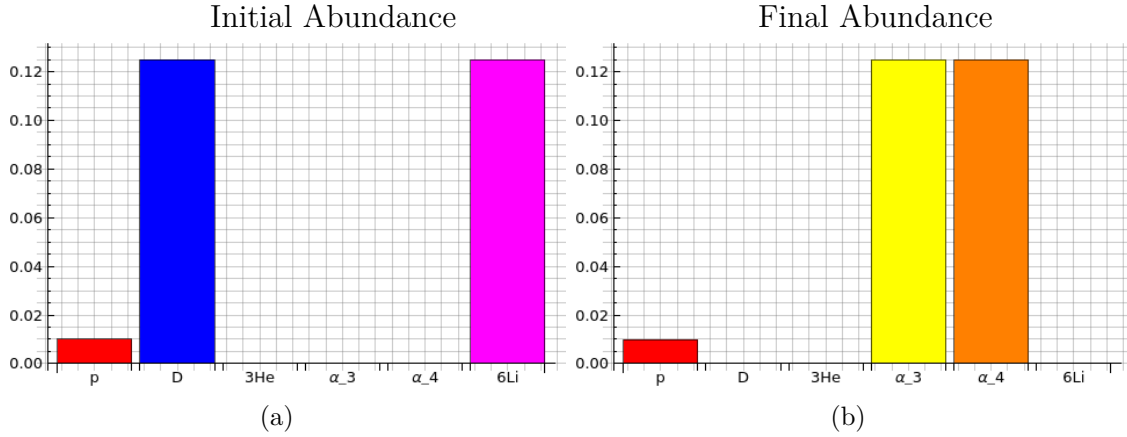


Figure 3.10: (a) Initial abundance according to the initial conditions [3.3](#). (b) Final abundance after system integration.

From the barchart is easy to see how in this case the condition over the nucleon

fraction is conserved [1.32](#). This is due to the fact that the system under consideration is totally closed, namely, there is no nucleon injection or losses. Therefore, the population of protons at the end is exactly as much as at the beginning and the α -particles achieve also the same value as the deuterium and lithium because the mass number of lithium plus the mass number of deuterium is the same as the mass number of 2 α species.

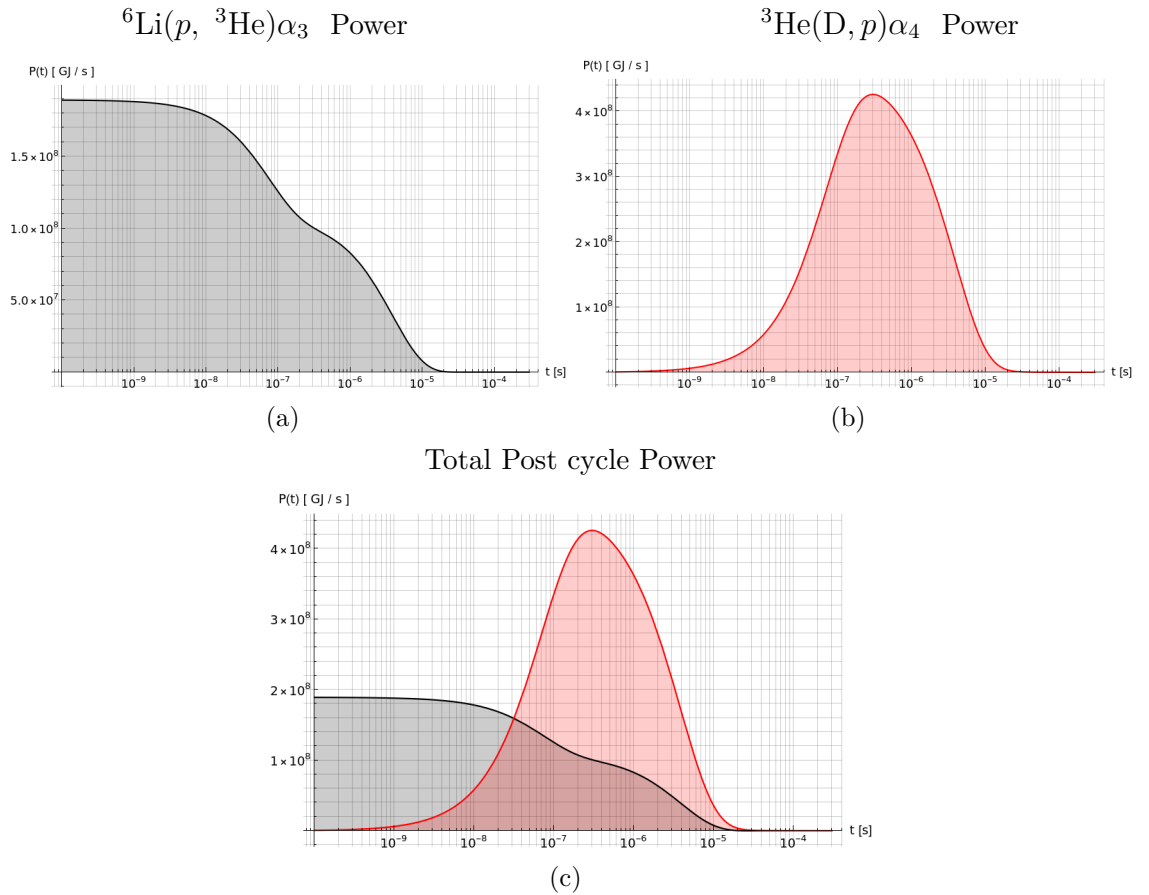


Figure 3.11: Power released in the Post cycle. (a) Power released by the ${}^6\text{Li}(p, {}^3\text{He})\alpha_3$ reaction. (b) Power released by the ${}^3\text{He}(\text{D}, p)\alpha_4$ reaction. (c) All curves overlapped. The time integration of the curves would be the energy released.

Finally, due to the fact that the curves of abundance evolution are known, the fusion yield might be calculated using the expression [1.47](#) and multiplying the specific

power by the volume of the simulated system, that it is the same like in the Jetter cycle chapter, finding the power as a function of the time.

The curves of the power as a function of time for every reaction involved in the Post cycle are displayed in the figure [3.11](#). In black, the curve related with fission reaction is shown, instead in red the curve related with the fusion reaction is shown.

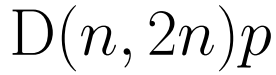
The integration of power curves would give us the energy released in GJ and this is the reason why the graph shows the shade under the curves. The results are expressed in the table [3.5](#).

Reaction	Fusion Yield (GJ)
${}^6\text{Li}(p, {}^3\text{He})\alpha_3$	411.12
${}^3\text{He}(\text{D}, p)\alpha_4$	1798.14
Total	2209.26

Table 3.5: *Energy released for every reaction in the Post cycle.*

Chapter 4

Deuteron Knock-out reaction



At this point the Jetter cycle and the Post cycle have been separately studied. Both are present when a neutron beam is focused on the solid target ${}^6\text{LiD}$. Nevertheless, the Post cycle is triggered by an initial population of protons in the system. This means that at the beginning only the Jetter cycle is working. It is found that there is one reaction that might produce enough population of protons to ignite the Post cycle. This reaction is the deuterium breakup $D(n, 2n)p$. In which, a sufficiently energetic neutron impinges the deuterium nucleus and break it up releasing a neutron and a proton. Where, in principle, the incoming neutron might be the one from the beam or from the fusion product between D and T in the Jetter cycle.

The objective of this chapter is to explore through a Monte Carlo simulation the energy distribution of the protons in the exit channel.

4.1 Theoretical Approach

As before, the first step is compute the Q -reaction value for the deuteron breakup. For this, the values of the masses are directly replaced into [1.2](#)

$$\begin{aligned} Q &= (m_{ini} - m_{fin})c^2 = [m(n) + m(D) - 2 m(n) - m(p)]c^2 \\ &= (b.e)_D = -2.2245 \text{ MeV} \end{aligned} \tag{4.1}$$

Then, the reaction Q -value is negative, in which case, a threshold energy appears, namely, a minimum of energy required to perform the reaction [\(15\)](#). Besides, as

there are three particles in the final state, energy can be shared in a number of ways (I7). Therefore, the energy distribution for the products is not anymore a peaked one in a specific energy but a distribution over a wide range.

In order to obtain an expression for the threshold energy and energy distribution of the products let us review the kinematics of the system expressed in the graph 4.1. And again, for a generic reaction $X(a, b)Y$.

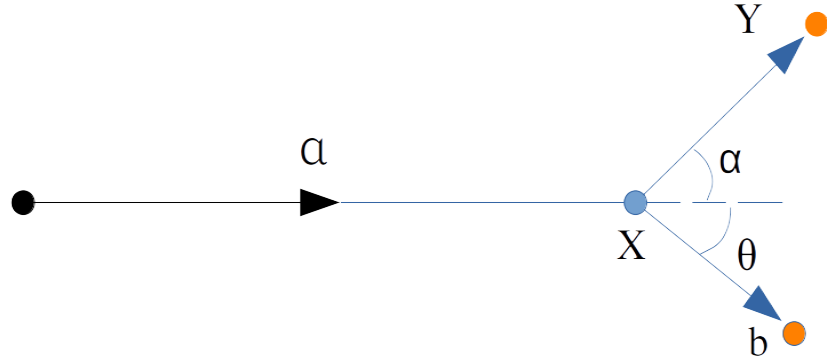


Figure 4.1: Generic nuclear reaction $X(a, b)Y$ described in the laboratory reference frame.

In the Fig 4.1 the reaction in the laboratory reference frame is shown, where the target X is considered at rest and the unique initial kinetic energy is due to the projectile labeled with a .

From momentum and energy conservation we have:

$$P_a = P_Y \cos(\alpha) + P_b \cos(\theta) \quad (4.2)$$

$$0 = P_Y \sin(\alpha) - P_b \sin(\theta) \quad (4.3)$$

$$Q = T_Y + T_b - T_a \quad (4.4)$$

Where the angles are indicated in the figure above. Considering Q as a known quantity and T_a (and therefore P_a) as a parameter that might be controlled, it is possible to eliminate the quantities related with Y . This due to the fact that Y is usually not measurable.

To achieve this, equations 4.2 and 4.3 can be squared and added each other.

$$P_a^2 - 2P_a P_b \cos(\theta) + P_b^2 = P_Y^2 \quad (4.5)$$

and using the connection between the classical linear momentum and the kinetic energy, i.e.:

$$T = \frac{1}{2}mv^2 \Rightarrow P^2 = 2mT \quad (4.6)$$

replacing into [4.5](#)

$$\left(\frac{m_a}{m_Y}\right) T_a - \frac{2}{m_Y} \sqrt{m_a T_a} \sqrt{m_b T_b} \cos(\theta) + \left(\frac{m_b}{m_Y}\right) T_b = T_Y \quad (4.7)$$

adding to both sides $T_b - T_a$ and using the expression [1.2](#) for the Q -value is possible to isolate T_b .

$$T_b = \frac{T_a(m_Y - m_a) + Q m_Y}{m_b + m_Y} + \frac{2\sqrt{m_a m_b T_a} \cos(\theta)}{m_b + m_Y} \sqrt{T_b} \quad (4.8)$$

The idea is study the variation of T_b with respect a fixed Q . Then, following [1.7](#), the next change of variables is performed:

$$D = \frac{T_a(m_Y - m_a) + Q m_Y}{m_b + m_Y} \quad (4.9)$$

$$C = \frac{2\sqrt{m_a m_b T_a} \cos(\theta)}{m_b + m_Y} \quad (4.10)$$

$$\therefore T_b = D + 2C\sqrt{T_b} \implies T_b - 2C\sqrt{T_b} - D = 0 \quad (4.11)$$

Besides, let x be equal to $\sqrt{T_b}$:

$$x^2 - 2Cx - D = 0 \implies x = C \pm \sqrt{C^2 + D} \quad (4.12)$$

Now, T_b must always be real and positive

$$\sqrt{T_b} = \frac{\sqrt{m_a m_b T_a}}{m_Y + m_b} \cos(\theta) \pm \sqrt{\frac{m_a m_b T_a \cos^2(\theta)}{(m_b + m_Y)^2} + \frac{T_a(m_Y - m_a) + Q m_Y}{(m_b + m_Y)}} \quad (4.13)$$

Until here, this expression is totally general and it is valid whatever sign takes the reaction Q -value. Nevertheless, if Q is negative there is a value for T_a , from which the square root starts to be real, rather than imaginary.

Imposing the condition that the square root must be zero and changing T_a for T_{th} and Q for $-|Q|$, it is obtained

$$E_{th}(\theta) = \frac{|Q|(m_b + m_Y)m_Y}{m_a m_b \cos^2(\theta) + (m_b + m_Y)(m_Y - m_a)} \quad (4.14)$$

The smallest value of $E_{th}(\theta)$ occurs for $\theta = 0^\circ$, and it is the absolute threshold of the reaction, namely, the smallest value of the incident energy T_a for which the reaction can occur.

$$E_{th}(0) = \frac{|Q|(m_b + m_Y)}{(m_b + m_Y - m_a)} \quad (4.15)$$

This is an important point because this imposes a condition over the possible incoming neutrons that might produce the deuteron breakup.

Then, using the Q -value [4.1](#) and the masses involved, the threshold energy is:


$$E_{th} = 3.3396 \text{ MeV} \quad (4.16)$$

Hence, for the deuterium breakup exists a threshold, below which the reaction cannot proceed. This means that the minimum kinetic energy that the neutron must have in order to produce in the exit channel one proton and two neutrons should be 3.3396 MeV. This totally discards the possibility that the incoming neutron from the beam can produce this reaction, because, like it was argued in the Jetter cycle chapter, these neutrons have an energy of 240 keV in order to maximize the yield of the ${}^6\text{Li}(n, \alpha)\text{T}$ reaction.

Now, the goal is finding the energy distribution of the proton that emerges from the deuterium breakup, and for this a Monte Carlo simulation is implemented.

4.2 Monte Carlo simulation

The proposal for the simulation of this reaction is to consider it as a two-step reaction in which, first an inelastic scattering between the incoming neutron and the deuterium occurs. The outgoing deuterium obtains an excitation energy that overpasses its binding energy. Secondly, the breakup occurs sharing the extra energy between the products. In every step a uniform distribution is proposed for the angles because, in principle, the system is isotropic and the reaction takes place at whatever possible angle in the space.

A code in C++ (39)  was implemented to run a high number of events and collect the proton energy in a histogram that permits to know the energy probability distribution.

At the beginning, the kinetic energy in the laboratory reference frame of the incoming neutron is known. This is 14.0481 MeV, because this neutron is the product of the fusion reaction in the Jetter cycle. Then, the initial energy and momentum is known and must be conserved for the two reactions. This is the major constraint that must always be fulfilled.

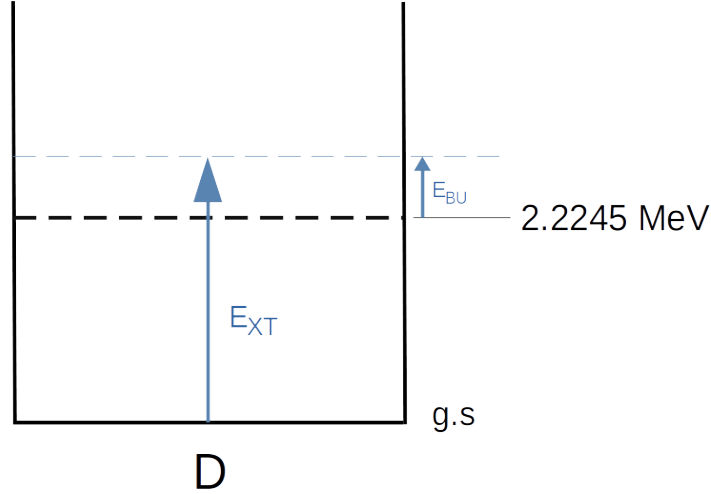


Figure 4.2: Excitation energy absorbed by the deuterium.

The conservation of the energy reads

$$E_T^{\text{lab}} = E_{\text{rel}}^{\text{CM}} + E_{XT} + E_{\text{CM}}, \quad (4.17)$$

where E_T^{lab} is the initial kinetic energy in the laboratory frame. $E_{\text{rel}}^{\text{CM}}$ is the relative energy in the center of mass, namely, this will be the energy available to be shared in the deuteron-neutron scattering and its computed using the next expression:

$$E_{\text{rel}}^{\text{CM}} = \left(\frac{m(D)}{m(D) + m(n)} \right) E_T^{\text{lab}} - E_{XT}, \quad (4.18)$$

where E_{XT} is established to be 0.1 MeV over the Q -value.

Besides, E_{CM} is the energy due to the motion of the CM system itself with velocity

v_{CM} along the incident direction (z -axis).

$$E_{\text{CM}} = \frac{1}{2} [m(\text{D}) + m(n)] v_{\text{CM}}^2 = \frac{1}{2} [m(\text{D}) + m(n)] \left(\frac{m(n)}{m(\text{D}) + m(n)} u_n^{\text{lab}} \right)^2 \quad (4.19)$$

Therefore, the energy conservation is fulfilled

$$\begin{aligned} E_T^{\text{lab}} &= E_{\text{rel}}^{\text{CM}} + E_{\text{XT}} + E_{\text{CM}} \\ &= 7.0358 \text{ MeV} + 2.3245 \text{ MeV} + 4.6877 \text{ MeV} = 14.0481 \text{ MeV} \end{aligned} \quad (4.20)$$

The relation between these two reference frames is depicted in the figure [4.3](#), where the letter u is used for the velocities before the collisions and the letter v for the ones after the collision. The direction of the collision coincides with z -axis in the laboratory reference frame.

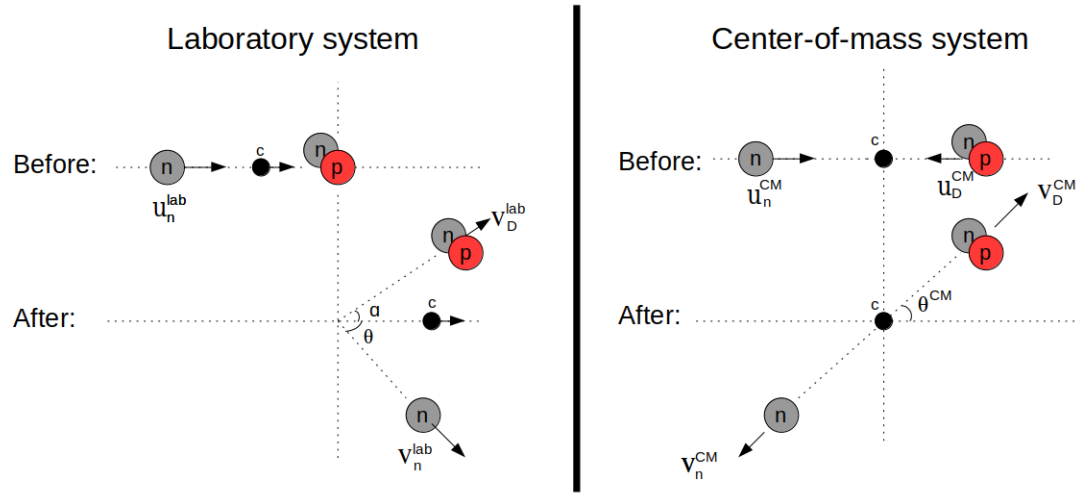


Figure 4.3: Left. Laboratory reference frame before and after of deuterium-neutron scattering. Right. Center of mass reference frame before and after of deuterium-neutron collision.

The next step is computing the resulting velocities of the deuterium and the incoming neutron after the collision in the center of mass reference frame. The resulting velocities were computed using the following expressions

$$V_n^{\text{CM}} = \sqrt{2 \frac{m(\text{D})}{m(n)} \frac{E_{\text{rel}}^{\text{CM}}}{(m(\text{D}) + m(n))}} \quad (4.21)$$

$$V_D^{\text{CM}} = \sqrt{2 \frac{m(n)}{m(\text{D})} \frac{E_{\text{rel}}^{\text{CM}}}{(m(\text{D}) + m(n))}} \quad (4.22)$$

Until this point the magnitude of the resulting velocities are known and also the momentum that the deuterium carries. This is a key point, because this momentum must be conserved when the fragments momenta are added in every component.

Notice that the deuterium momentum components depend of the angles $(\theta^{\text{CM}}, \phi^{\text{CM}})$, which are the azimuthal and polar angles respectively. These angles are randomly generated via a uniform probability distribution for every event considered.

After the scattering, the deuterium suddenly breaks-up in its constituents sharing the energy above the binding energy (E_{BU}). The velocities calculation for these fragments is carried out in the rest frame of the deuterium using the following expressions:

$$V_n^{\text{Rest}} = \sqrt{2 \frac{m(p)}{m(n)} \frac{E_{\text{BU}}}{(m(p) + m(n))}} \quad (4.23)$$

$$V_p^{\text{Rest}} = \sqrt{2 \frac{m(n)}{m(p)} \frac{E_{\text{BU}}}{(m(p) + m(n))}} \quad (4.24)$$

The relation between the frame where the deuterium has kinetic energy and the rest frame is depicted in the figure [4.4](#).

Again, notice that neutron and proton momentum components in the rest frame depend of the angles $(\theta^{\text{Rest}}, \phi^{\text{Rest}})$, which are the azimuthal and polar angles respectively. These angles are randomly generated via a uniform probability distribution for every event considered.

The calculations at every step must be performed respecting the energy and momentum conservation, this is the most faithful statement that guided the code. For instance, it was verified that the total momentum in the center of mass reference frame is always zero, and also that the sum of momentum in the rest frame for the fragments must vanish. Besides, the energy and momentum of the scattering particles in the center of mass must be equal before and after the collision. The same must be valid for the deuterium breakup, the energy and momentum before the breakup and after the breakup must be equal. Finally, when the reconstruction of the outgoing particles quantities is performed in the laboratory reference frame,

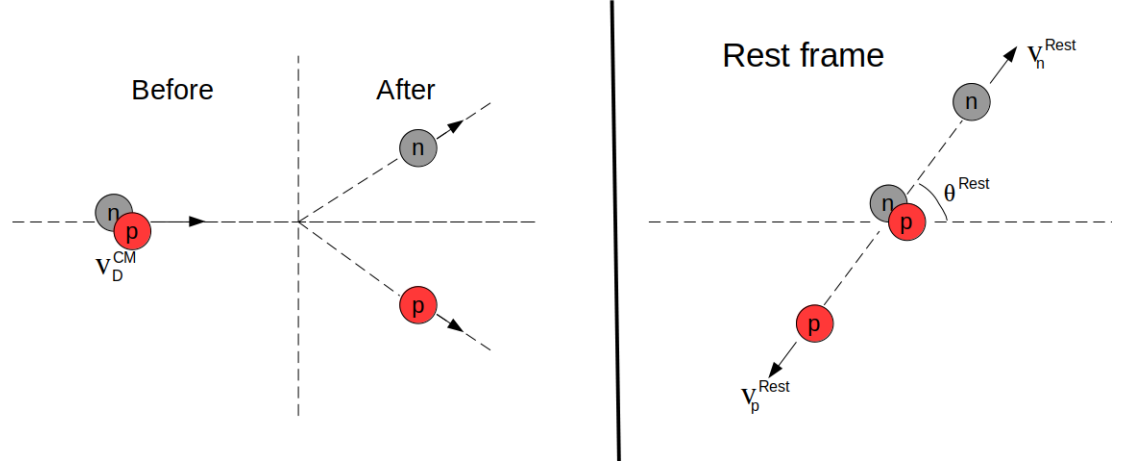


Figure 4.4: Left. Reference frame where deuterium has kinetic energy before and after of deuterium break-up. Right. Rest reference frame before and after of deuterium break-up.

the energy and momentum must be coherent with the energy and momentum of the incoming neutron.

Therefore, until this point all the kinematic quantities are known and the two pairs of angles were randomly generated. Namely, in the rest frame the three velocity components for every fragment are known, the same for the three velocity components of the deuterium and the neutron in the center of mass frame, and the last task to do is carefully to make the composition of these velocities to obtain them in the laboratory frame for the three fragments.

The reconstruction of the velocity components starts from the rest frame of the deuterium, where the breakup occurs. The situation is that before going to the rest frame, the deuterium has a definite velocity. Hence, it is necessary to boost the fragments to the moving frame of the deuterium (36). For this, the following composition is proposed.

$$M_n = \frac{m(D)^2 + m(n)^2 - m(p)^2}{2m(D)^2} \quad (4.25)$$

$$M_p = \frac{m(\text{D})^2 + m(p)^2 - m(n)^2}{2m(\text{D})^2} \quad (4.26)$$

And the momentum in every direction, for instance, for the proton in the frame where the deuterium has velocity reads.

$$P_x(p) = P_x^{\text{Rest}}(p) + M_p V_x^{\text{CM}}(\text{D}) \quad (4.27)$$

$$P_y(p) = P_y^{\text{Rest}}(p) + M_p V_y^{\text{CM}}(\text{D}) \quad (4.28)$$

$$P_z(p) = P_z^{\text{Rest}}(p) + M_p V_z^{\text{CM}}(\text{D}) \quad (4.29)$$

The momentum for the neutron fragment is computed following the analogous expressions than for the proton fragment.

Again, the momentum conservation holds, in the sense that the sum of the neutron and proton momentum in every component must be equal to that carried by the deuterium before to the breakup.

Finally, the magnitude of the momentum vector in the laboratory reference frame might be written in the following way

$$|\vec{\mathbf{P}}(p)| = \sqrt{(P_x(p))^2 + (P_y(p))^2 + (P_z(p) + M_p V_{\text{CM}})^2}. \quad (4.30)$$

Analogously, for the two neutrons this composition is performed taking into account that the velocity of the center of mass has to be added for the z -component because this axis coincides with collision direction for the scattering process.

It is evident that having the magnitude of the momentum vector for the three products, the kinetic energy of each particle is completely known according to the non-relativistic formula:

$$E_p = \frac{(|\vec{\mathbf{P}}(p)|)^2}{2M_p}. \quad (4.31)$$

4.3 Results

The program was run using 10^7 events and the energy of the three products was stored for every event in order to obtain the energy distribution.

In the first step of the reaction the distributions for the neutron and deuterium that are obtained are shown in the figures [4.5](#) and [4.6](#).

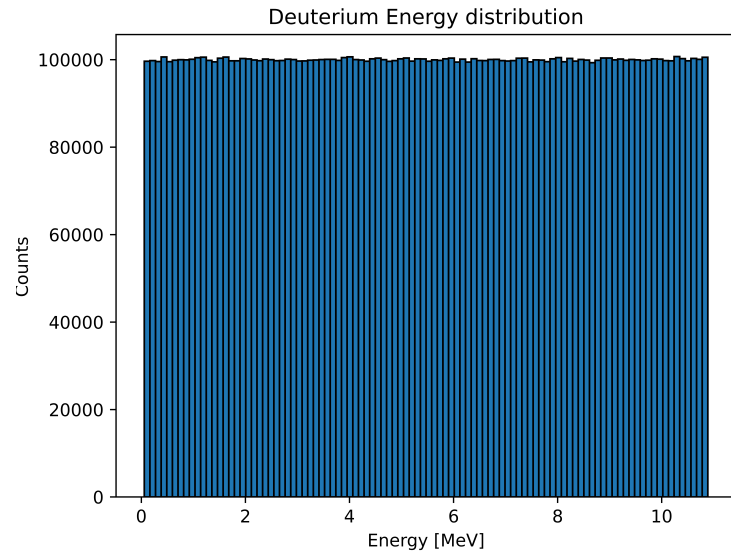


Figure 4.5: Deuterium energy distribution after the inelastic scattering. Data obtained from simulation of 10^7 events with the Monte Carlo code [C](#).

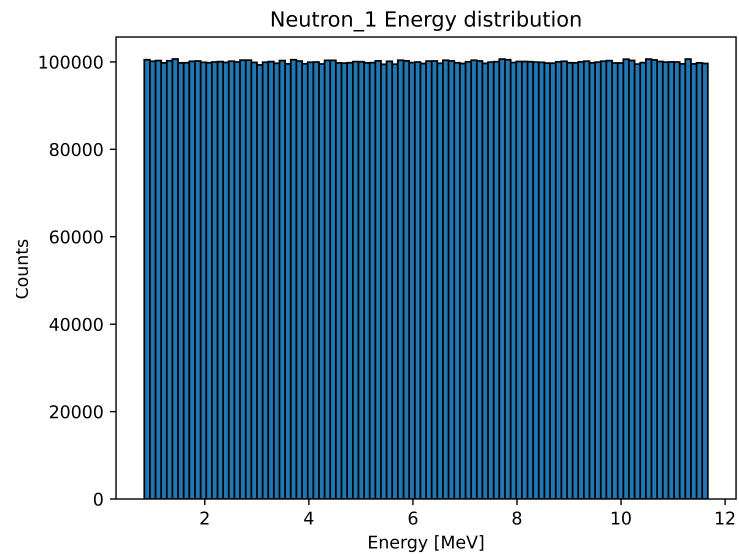


Figure 4.6: Neutron energy distribution after the inelastic scattering. Data obtained from simulation of 10^7 events with the Monte Carlo code [C](#).

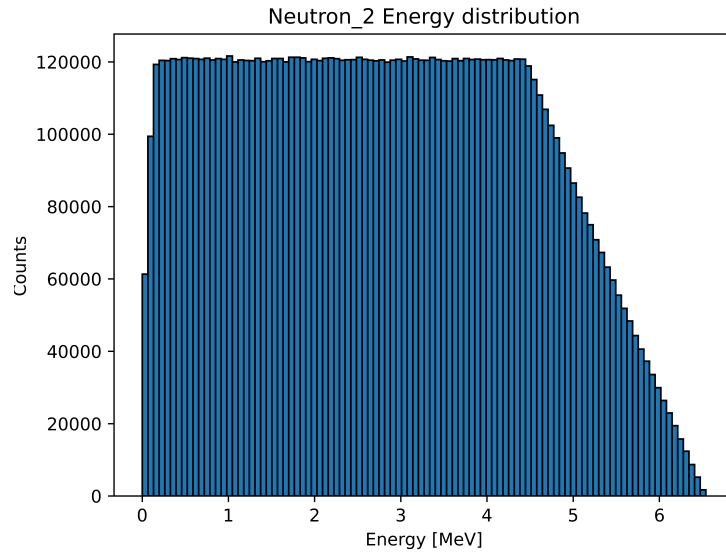


Figure 4.7: Neutron energy distribution after the inelastic scattering and deuterium breakup. Data obtained from simulation of 10^7 events with the Monte Carlo code [C](#).

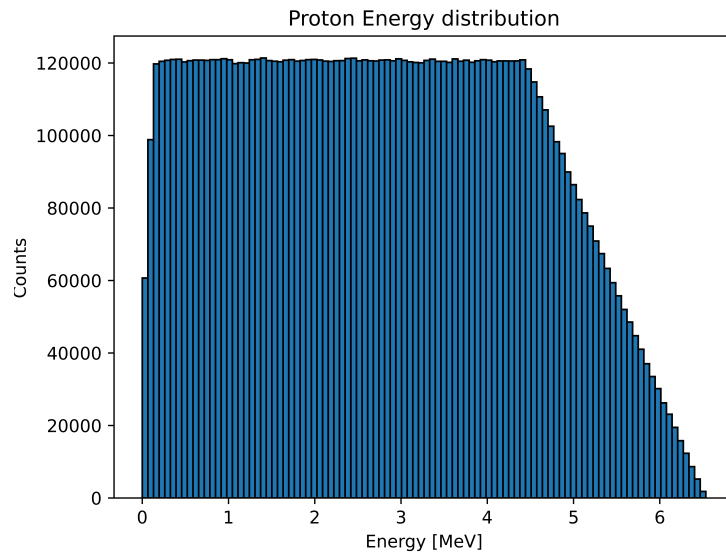


Figure 4.8: Proton energy distribution after the inelastic scattering and the deuterium breakup. Data obtained from simulation of 10^7 events with the Monte Carlo code [C](#).

Finally, the proton and the second neutron energy distributions from the breakup reaction are shown in the figures [4.7](#) and [4.8](#).

At the end, the code prints the data showed in the table [4.1](#) which are the relevant data in the two-step reaction.

Quantity	Magnitude
E_T^{lab}	14.0481 MeV
E_{XT}	2.3245 MeV
E_{CM}	4.6877 MeV
$E_{\text{rel}}^{\text{CM}}$	7.0358 MeV
E_{D}^{CM}	2.3478 MeV
$E_{n_1}^{\text{CM}}$	4.6880 MeV
E_{BU}	0.1 MeV
$E_{n_2}^{\text{Rest}}$	0.0499 MeV
E_p^{Rest}	0.0500 MeV
E_p^{Rest}	0.0500 MeV
M_p	937.670 MeV/ c^2
M_n	938.453 MeV/ c^2

Table 4.1: *Relevant data printed by the code in the deuterium breakup reaction.*

Chapter 5

Jetter + Post Cycle

After knowing the proton energy distribution that results of the deuterium breakup, it is time to combine the Jetter and Post cycle and compare the result abundances against those of the individual cycles.

Notice that the only change is just the opening an additional channel with the species already present at the beginning.

The reaction network is depicted in the figure [5.1](#). In the upper part the Jetter cycle is shown, while in the middle and in blue color the deuterium breakup reaction is shown. Finally, at the bottom the Post cycle is shown. It is worth to notice the indexes in the diagram, for the first reaction indexes 1 and 2 appear representing the neutrons coming from the beam (1) or the neutrons coming from fusion reaction between the deuterium and tritium (2). As it was proved the deuterium breakup is achieved only with the neutrons coming from the fusion process (2). Finally, the α -particles are labeled as before.

5.1 Theoretical Approach

In order to combine the cycles, two reduced reaction rate have to be computed. The first is the one in which the neutron and the deuterium react consuming both species. In this case, again, the assumption of no energy losses implies that the consequent reactions produced by the neutron will be accomplished at the precise energy that is produced in the fusion between the tritium and deuterium. Namely,

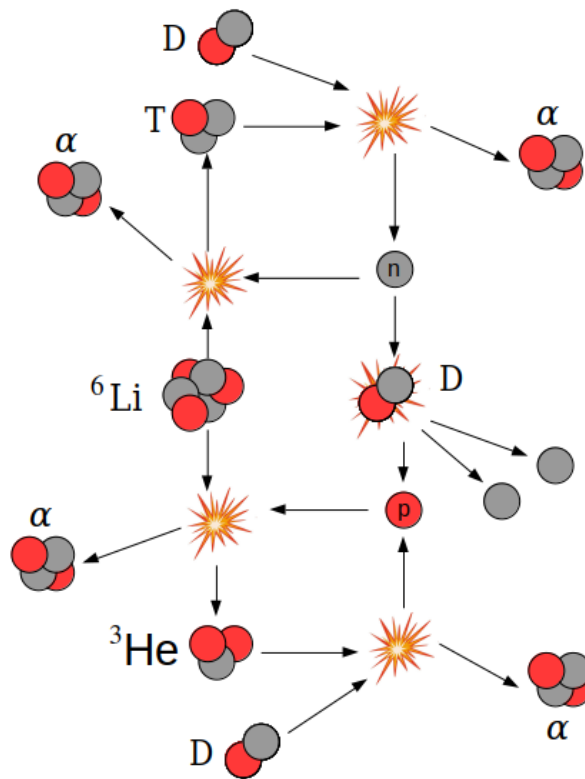
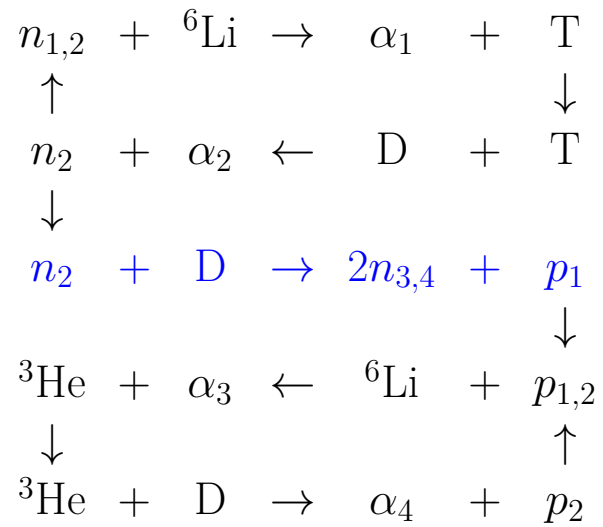


Figure 5.1: Jetter Cycle + Post cycle joined by deuterium breakup reaction.

the energy distribution probability function is a Dirac delta function.

$$P(E) = \delta(E - E_0) \quad (5.1)$$

[5.2](#) and the expected value between the energy distribution function and cross section is easily calculated using [1.17](#).

$$\langle \sigma v \rangle = \int \left(\frac{2E}{m} \right)^{1/2} \sigma(E) \delta(E - E_0) dE = \left(\frac{2E_0}{m} \right)^{1/2} \sigma(E_0) \quad (5.2)$$

The cross section and the reduced reaction rate is depicted in the figures [5.3](#) and [5.4](#) in the experimental data section.

The second reaction rate that has to be evaluated is related with the protons that emerge from the deuterium breakup and will react with lithium. Like it was pointed out in the previous chapter, the probability energy function for the protons is no more a Dirac delta function. Instead, it is a function ranging from 0 to, approximately, 6.5 MeV as it is shown at the top of the figure [5.2](#). This probability function was extracted from the histogram found in the deuterium breakup simulation [4.8](#) after carefully performing a suitable normalization in order to fulfill the requirement that the integral over the sample space amounts to unity [1.18](#).

Therefore, the reduced reaction rate has to be evaluated using the following expression

$$N_A \langle \sigma v \rangle = \int_{E_{\min}}^{E_{\max}} N_A \left(\frac{2E}{m} \right)^{1/2} \sigma(E) P(E) dE = \int_{E_{\min}}^{E_{\max}} \mu(E) dE \quad (5.3)$$

At the middle of the figure [5.2](#) the cross section of the fission reaction ${}^6\text{Li}(p, \alpha){}^3\text{He}$ is chopped exactly at the energy range in which the probability function is different from zero is shown.

At the bottom of the figure [5.2](#) the product of all the terms inside the integral gathered in the auxiliary function $\mu(E)$ is shown. Notice that the reduced reaction rate is the area under this curve. The integration was numerically performed, the results are resumed in the table [5.1](#).

Finally, the set of ordinary differential equations that describes the abundance behaviour of the system schematized in [5.1](#) reads

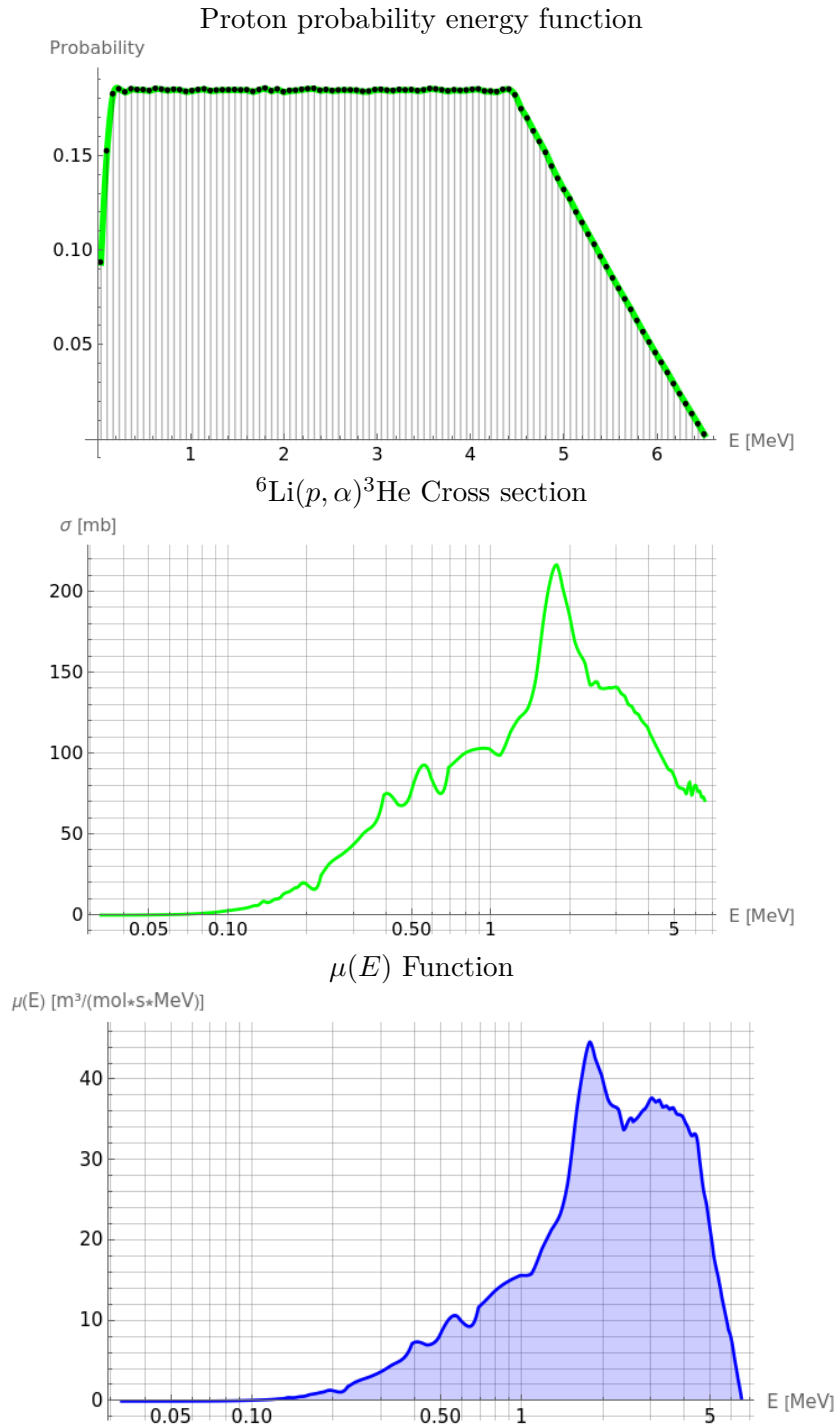


Figure 5.2: **Top.** Proton probability energy function resulted from the deuterium breakup. Black dots. Histogram values after the normalization. Green line. Interpolation made using Mathematica. **Mid.** Cross section chopped in the possible energy range. **Bottom.** $N_A \langle \sigma v \rangle$ is the area under the curve of $\mu(E)$ (5.3).

Quantity	Magnitude
E_{\min}	0.0327 MeV
E_{\max}	6.5011 MeV
$N_A \langle \sigma v \rangle$	155.5510 m ³ /mol · s

Table 5.1: *Relevant data for the calculation of the reduced reaction rate and the numerical integration of the μ function.*

$$\frac{dY_{n_1}}{dt} = i - Y_{n_1}(t) \cdot Y_{6\text{Li}}(t) [{}^6\text{Li}(n_1, \alpha)] \quad (5.4)$$

$$\begin{aligned} \frac{dY_{n_2}}{dt} = & + Y_{\text{D}}(t) \cdot Y_{\text{T}}(t) [\text{D}(\text{T}, n_2)] - Y_{n_2}(t) \cdot Y_{6\text{Li}}(t) [{}^6\text{Li}(n_2, \alpha)] \\ & - Y_{n_2}(t) \cdot Y_{\text{D}}(t) [n_2(\text{D}, 2n)] \end{aligned} \quad (5.5)$$

$$\frac{dY_{n_3}}{dt} = + Y_{\text{D}}(t) \cdot Y_{n_2}(t) [n_2(\text{D}, 2n)] \quad (5.6)$$

$$\frac{dY_{n_4}}{dt} = + Y_{\text{D}}(t) \cdot Y_{n_2}(t) [n_2(\text{D}, 2n)] \quad (5.7)$$

$$\frac{dY_{\alpha_1}}{dt} = + Y_{n_1}(t) \cdot Y_{6\text{Li}}(t) [{}^6\text{Li}(n_1, \alpha_1)] + Y_{n_2}(t) \cdot Y_{6\text{Li}}(t) [{}^6\text{Li}(n_2, \alpha_1)] \quad (5.8)$$

$$\frac{dY_{\alpha_2}}{dt} = + Y_{\text{D}}(t) \cdot Y_{\text{T}}(t) [\text{D}(\text{T}, \alpha_2)] \quad (5.9)$$

$$\frac{dY_{\alpha_3}}{dt} = + Y_{p_1}(t) \cdot Y_{6\text{Li}}(t) [{}^6\text{Li}(p_1, {}^3\text{He})] + Y_{p_2}(t) \cdot Y_{6\text{Li}}(t) [{}^6\text{Li}(p_2, {}^3\text{He})] \quad (5.10)$$

$$\frac{dY_{\alpha_4}}{dt} = + Y_{\text{D}}(t) \cdot Y_{3\text{He}}(t) [{}^3\text{He}(\text{D}, p)] \quad (5.11)$$

$$\begin{aligned} \frac{dY_{\text{D}}}{dt} = & - Y_{\text{D}}(t) \cdot Y_{\text{T}}(t) [\text{D}(\text{T}, n_2)] - Y_{\text{D}}(t) \cdot Y_{3\text{He}}(t) [{}^3\text{He}(\text{D}, p)] \\ & - Y_{\text{D}}(t) \cdot Y_{n_2}(t) [n_2(\text{D}, 2n)] \end{aligned} \quad (5.12)$$

$$\begin{aligned} \frac{dY_{\text{T}}}{dt} = & + Y_{n_1}(t) \cdot Y_{6\text{Li}}(t) [{}^6\text{Li}(n_1, \alpha)] + Y_{n_2}(t) \cdot Y_{6\text{Li}}(t) [{}^6\text{Li}(n_2, \alpha)] \\ & - Y_{\text{D}}(t) \cdot Y_{\text{T}}(t) [\text{D}(\text{T}, n_2)] \end{aligned} \quad (5.13)$$

$$\begin{aligned} \frac{dY_{3\text{He}}}{dt} = & + Y_{p_1}(t) \cdot Y_{6\text{Li}}(t) [{}^6\text{Li}(p_1, {}^3\text{He})] + Y_{p_2}(t) \cdot Y_{6\text{Li}}(t) [{}^6\text{Li}(p_2, {}^3\text{He})] \\ & - Y_{3\text{He}}(t) \cdot Y_{\text{D}}(t) [{}^3\text{He}(\text{D}, p_2)] \end{aligned} \quad (5.14)$$

$$\frac{dY_{p_1}}{dt} = + Y_D(t) \cdot Y_{n_2}(t) [n_2(D, 2n)] - Y_{p_1}(t) \cdot Y_{6\text{Li}}(t) [{}^6\text{Li}(p_1, {}^3\text{He})] \quad (5.15)$$

$$\frac{dY_{p_2}}{dt} = + Y_D(t) \cdot Y_{3\text{He}}(t) [{}^3\text{He}(D, p_2)] - Y_{p_2}(t) \cdot Y_{6\text{Li}}(t) [{}^6\text{Li}(p_2, {}^3\text{He})] \quad (5.16)$$

$$\begin{aligned} \frac{dY_{6\text{Li}}}{dt} = & - Y_{6\text{Li}} \cdot Y_{n_1}(t) [{}^6\text{Li}(n_1, \alpha_1)] - Y_{6\text{Li}} \cdot Y_{n_2}(t) [{}^6\text{Li}(n_2, \alpha_1)] \\ & - Y_{p_1}(t) \cdot Y_{6\text{Li}}(t) [{}^6\text{Li}(p_1, {}^3\text{He})] - Y_{p_2}(t) \cdot Y_{6\text{Li}}(t) [{}^6\text{Li}(p_2, {}^3\text{He})] \end{aligned} \quad (5.17)$$

The interaction of the n_3 and n_4 is missing.

5.2 Experimental Data

Unlike to the previous cases, this time just one reaction was added. This was the deuterium breakup. Then, the cross section has to be searched and the reduced reaction rate calculated.

In order to obtain the expected value of the energy distribution and cross section [2.2](#), the cross section has to be known for several specific energies which implies that an interpolation has to be performed to the experimental data for the reaction over the energy range of interest. Combining this interpolation with the energy distribution probability the expected value between the energy distribution function and the cross section is calculated.

5.2.1 $D(n, 2n)p$

The data for this reaction were extracted from ENDF [\(27\)](#) in which the interpolation was already performed following the library ENDF/B-VIII.0 and it is held by Ref. [\(37\)](#), which allows to choose the energy range for displaying a list of points that will guide the interpolation. For instance, choosing the energy range from 3.339 MeV to 30 MeV, 37 points are shown in order to make the interpolation.

The figure [5.3](#) shows the cross section for the breakup reaction. the black dots are the data given by the ENDF/B-VIII.0 whereas the green line is the interpolation made using Mathematica in order to obtain a function that might be evaluated at whatever energy, as it is required to solve numerically the set of ordinary equations.

After having the interpolation function of the cross section, the reduced reaction rate could be computed using [5.2](#). The result is depicted in the figure [5.4](#).

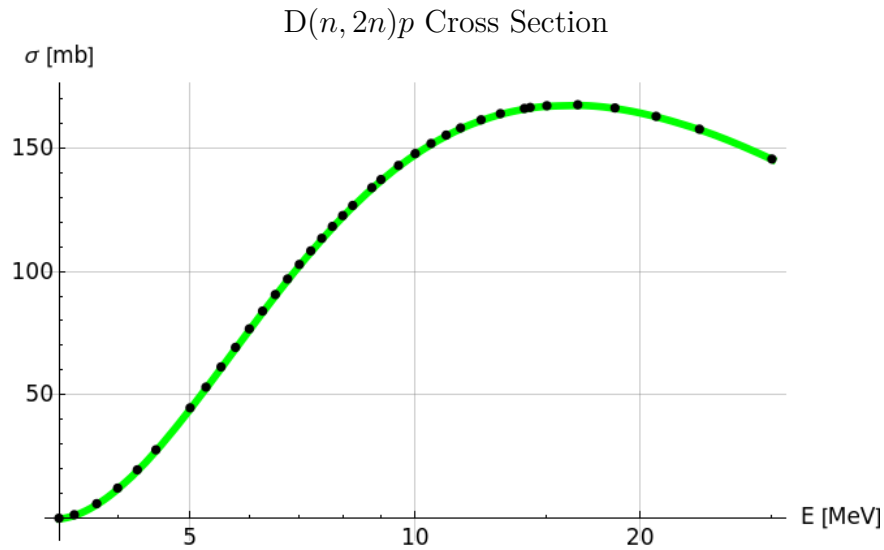


Figure 5.3: Cross Section for $D(n, 2n)p$ using the data taken from Ref. (37) and interpolated using Mathematica.



Figure 5.4: Reduced reaction rate $N_A \langle \sigma v \rangle$ for the reaction $D(n, 2n)p$ using the expression 2.2

As it was pointed out in the previous sub-section, the outgoing neutrons from the deuterium breakup will not react again in the current open channels.

5.3 Results

After obtaining the expected values between the cross section interpolation and the probability energy distribution of the reactions involved, the set of ordinary differential equations might be numerically solved using the built-in routine in Mathematica [\[B\]](#). For that, initial conditions have to be set in sufficient number.

These initial conditions refer to the initial abundance in the system. Then, at the beginning the deuterium and lithium are present at equal proportion due to chemical stoichiometry. The neutrons present are only from the external beam which at $t = 0$ is turned on and therefore their total number is a (almost) linearly growing function. Besides, the energy of these particles is set to 0.24 MeV because, as it was pointed out in the second chapter, at this precise energy the maximum of the reduced reaction rate is found in the figure [2.3](#). This choice is made in order to considerably increase the fission probability between ${}^6\text{Li}$ and n .

Moreover, due to the fact that there is not an external source of nucleons, the constraint over the nucleon fraction is totally fulfilled [1.32](#).

Again, we propose to simulate 1 mol of ${}^6\text{LiD}$, this means that the initial molar fraction can be calculated using the expression [1.33](#)

$$Y_{6\text{Li}} = \frac{N_{6\text{Li}}}{\rho N_A} = \frac{N_A}{V \rho N_A} = \frac{1}{V \rho} = \frac{1}{8} \frac{g}{\text{mol}} = 0.125 \frac{\text{mol}}{g}. \quad (5.18)$$

Following the same procedure the initial molar fraction for the deuterium can be calculated and how is to expected, it is the same.

The initial conditions for solving the set of ordinary equations are listed in the table [5.2](#), where at the beginning only deuterium and lithium are present at equal amounts.

Molar Fraction	Value (mol/g)
$Y_{n_1}(0)$	0.0
$Y_{n_2}(0)$	0.0
$Y_{n_3}(0)$	0.0
$Y_{n_4}(0)$	0.0
$Y_{p_1}(0)$	0.0
$Y_{p_2}(0)$	0.0
$Y_{\alpha_1}(0)$	0.0
$Y_{\alpha_2}(0)$	0.0
$Y_{\alpha_3}(0)$	0.0
$Y_{\alpha_4}(0)$	0.0
$Y_D(0)$	1.25×10^{-1}
$Y_T(0)$	0.0
$Y_{6Li}(0)$	1.25×10^{-1}
$Y_{3He}(0)$	0.0

Table 5.2: *Initial conditions to solve the set of ordinary differential equations for the Jetter cycle + Post cycle.*

The abundance curves for all the species involved in the system are displayed in the figures [5.5](#), [5.6](#) and [5.7](#).

In the figure [5.5](#) the abundance evolution for all neutron species is shown. In the panel (a), the continuous growing in the neutron abundance of the neutrons coming from the beam is shown. The panel (b) shows how the neutrons coming from T and D fusion increase until the point where the deuterium breakup starts to be important, this follows until the point in which no more deuterium is present. Finally in (c) and (d), the fragments from the deuterium breakup appear, due to the fact that these two species have different energy distributions they are considered different species, but since the only source is the breakup then the abundance curve is the same for both and the expected final abundance will be also the same.

The abundance evolution for the four species of α -particles is shown in the figure [5.6](#). As it is guessed from equations [5.8](#),[5.9](#),[5.10](#) and [5.11](#), they are formed only by source terms, namely, all of them are only produced until they achieve a steady

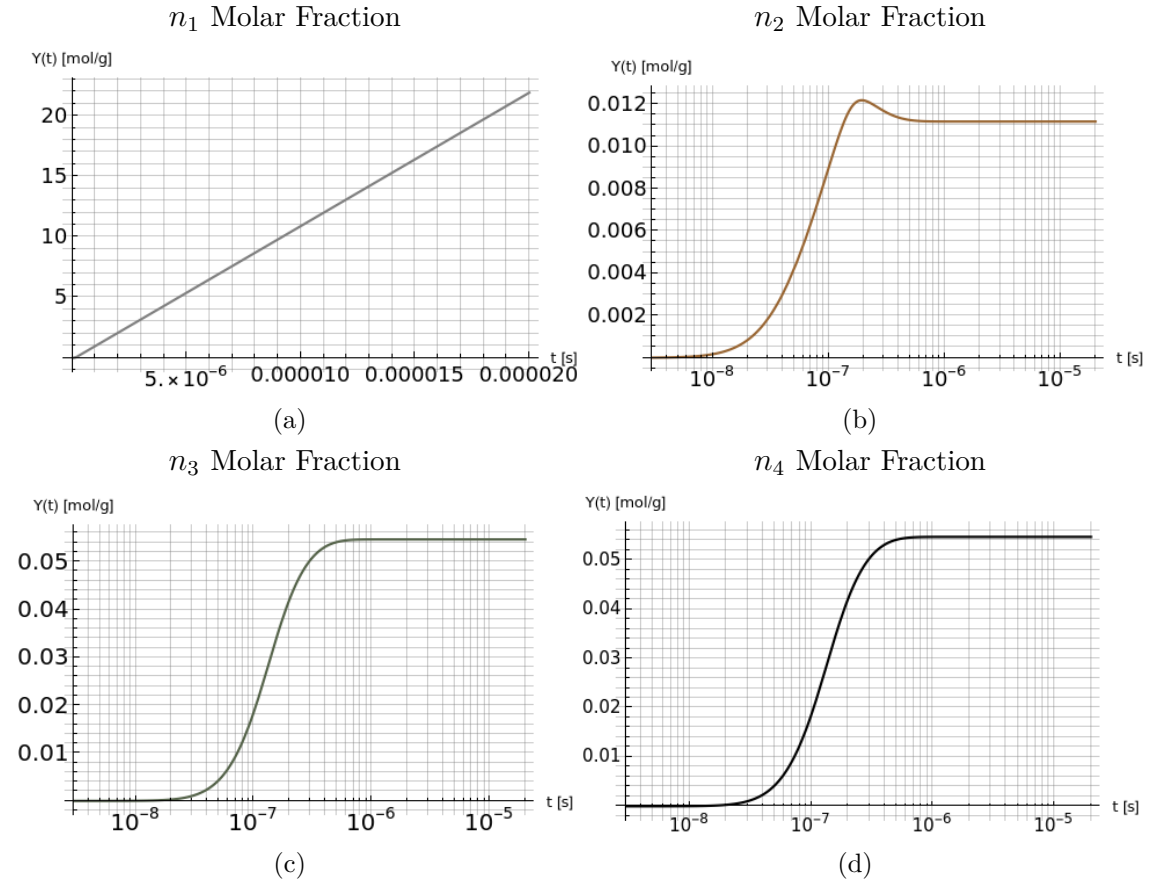


Figure 5.5: Solution of the set of ordinary differential equations describing the Jetter and Post cycle for the neutrons species.

point. They are always considered as an inert byproduct.

In the figure [5.7](#), the abundance evolution for deuterium, lithium and protons are shown. In the panel (a) and (b) we can see the monotonically decrease of deuterium and lithium due to the fact that they only have sink terms and are consumed with a very different ratio. This dynamic continues until the point in which both are completely exhausted.

In the panels (c) and (d) the protons abundance evolution are shown. The abundance of both species of protons is increased, the fact that the second species has increased is a sign that Post cycle was ignited at certain point as it was hypoth-

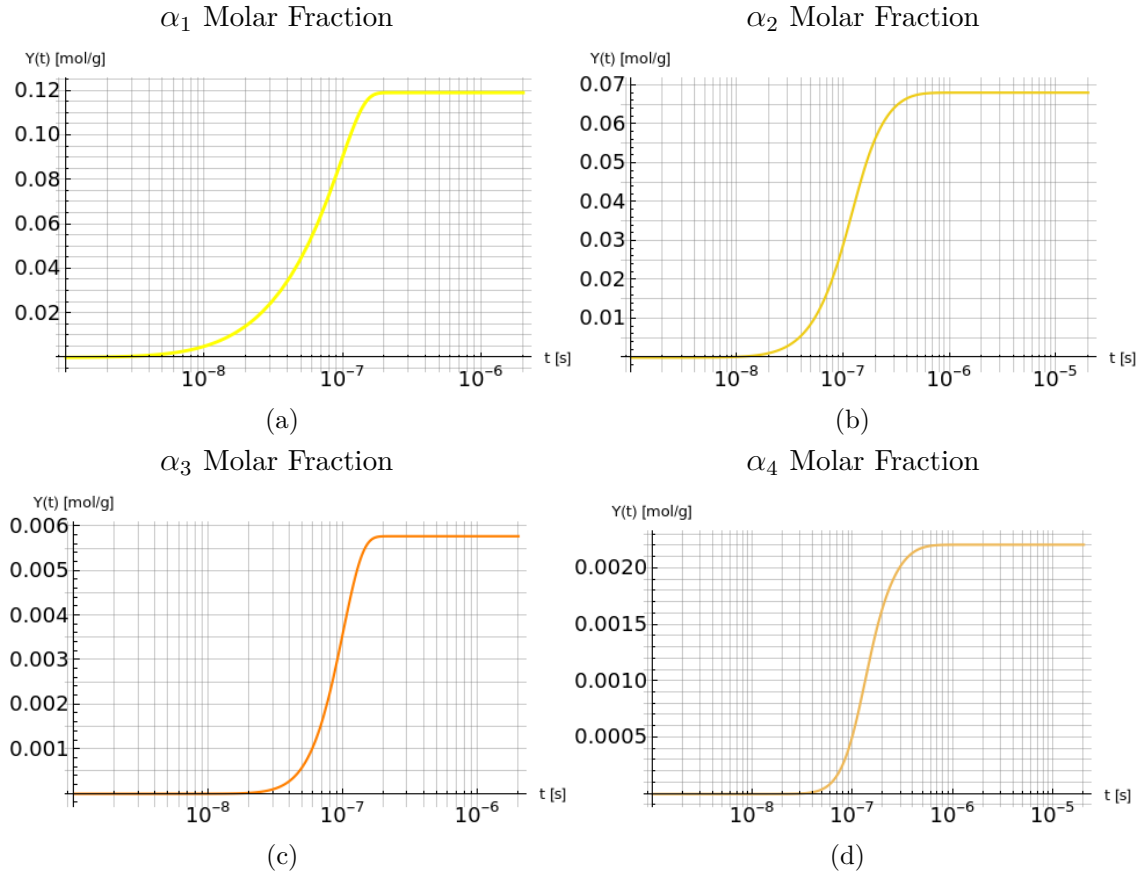


Figure 5.6: Solution of the set of ordinary differential equations describing the Jetter and Post cycle for the α -species.

esized. Namely, starting from the crystal ${}^6\text{LiD}$ and focusing a neutron beam, at certain point the reactions of the Post cycle are ignited, producing more α -particles that will increase the energy released.

Finally in the figure [5.8](#) the abundance evolution for the tritium and 3-helium is shown. Both species have similar dynamics, namely, they play a common role in both cycles. First, they are produced for the fission reactions in each cycle until the point in which they have achieved a considerable abundance to trigger the fusion reaction in each cycle and they start to be consumed until the point that deuterium is consumed, namely, the steady point of the tritium and 3-helium coincide with the point when the deuterium is totally exhausted. Due to the fact that the deuterium

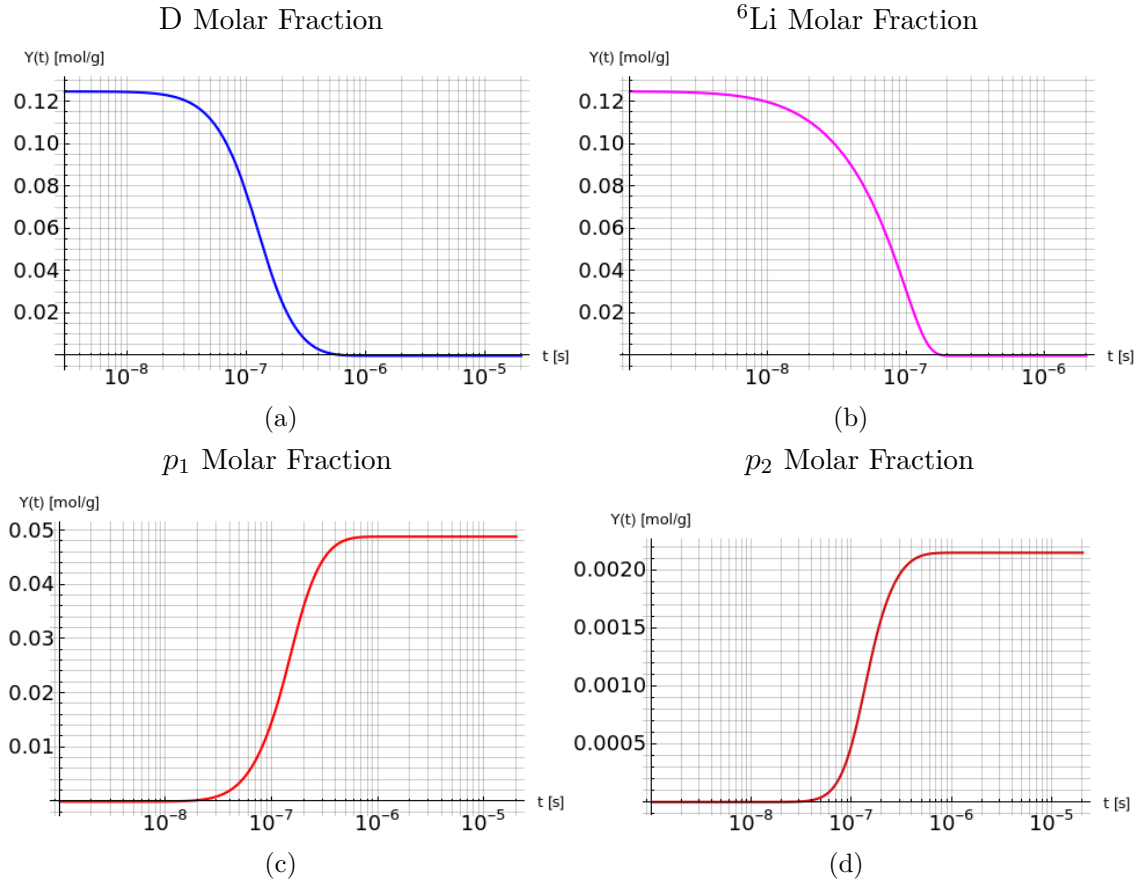


Figure 5.7: Solution of the set of ordinary differential equations describing the Jetter and Post cycle for the D, ${}^6\text{Li}$ and p -species.

is totally consumed when still tritium and 3-helium have a considerable abundance, these elements are present at the end.

In the figure [5.9](#) all the abundance evolution curves are shown (except for the neutrons coming from the beam). In this, it is possible to appreciate the real scale of the abundance of every element. It is evident that the Jetter cycle is the dominant dynamic, more than the Post cycle dynamic in the system simulated. It is worth to notice that deuterium breakup reaction is playing a fundamental role producing a considerably quantity of energetic neutrons and protons than might open new channels and triggering the Post cycle.

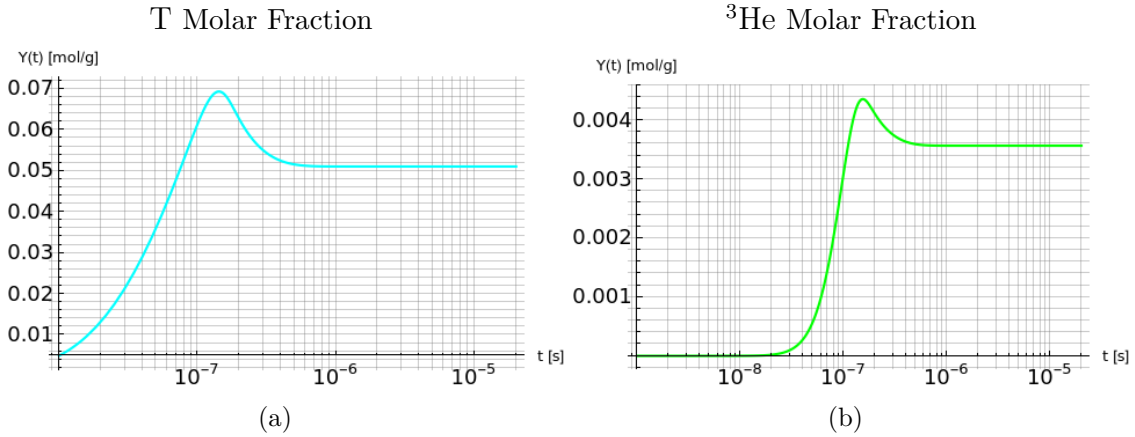


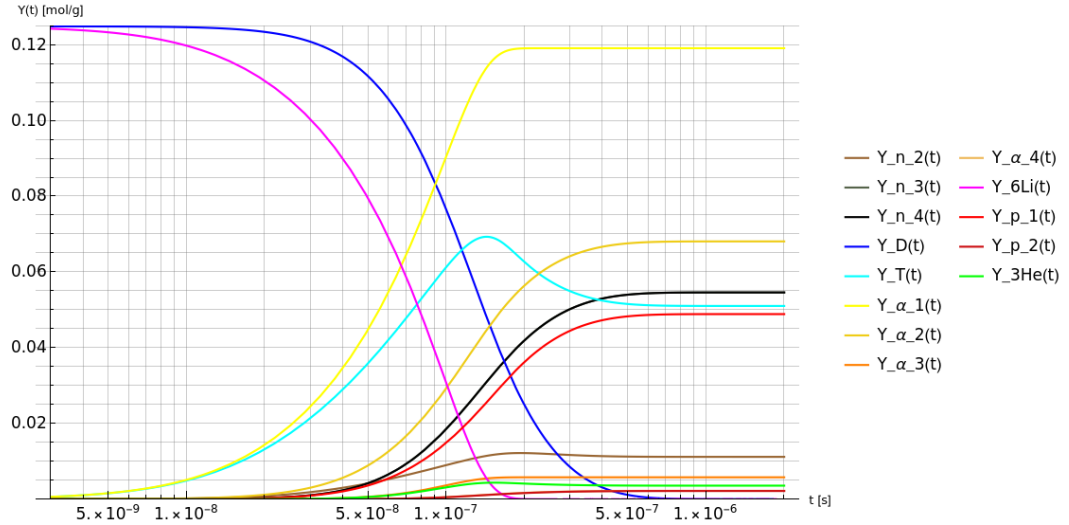
Figure 5.8: Solution of the set of ordinary differential equations describing the Jetter and Post cycle for the ^3He and T species.

Moreover, it is easy to see how the tritium and 3-helium achieve the steady point when the deuterium is depleted. Also how α_1 and α_3 particles reached their maximum at the same time that the lithium is depleted. Analogously, how α_2 and α_4 particles achieved their maximum at the same time that deuterium is depleted.

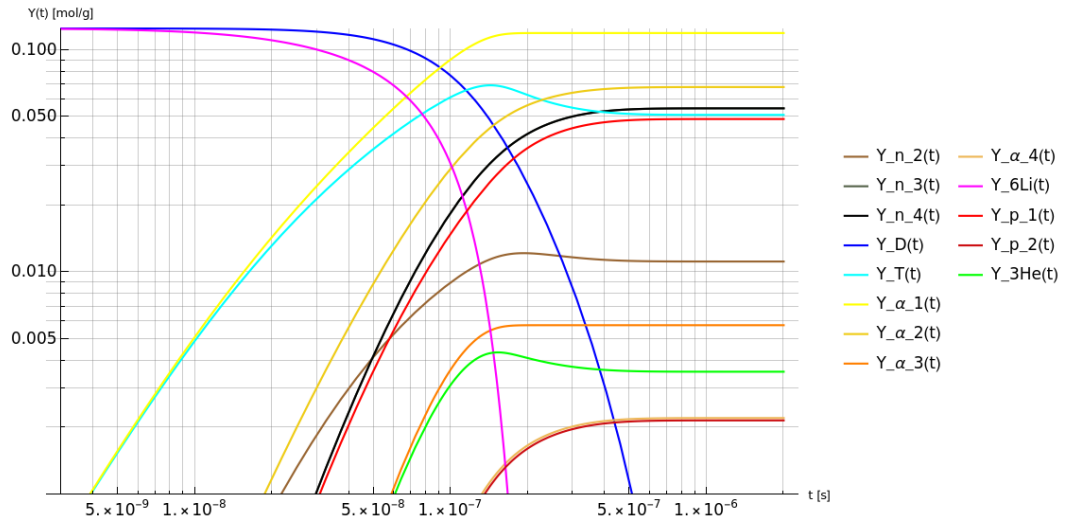
The fact that in this case the deuterium breakup channel is open produced huge changes compared with the simulation of Jetter cycle alone. This reaction increased the deuterium consumption implying that the tritium and 3-helium were not totally consumed through the fusion with deuterium. The main outcome is that the Jetter cycle and the Post cycle, where these intermediate elements are produced during the evolution, yield zero abundance at the end. Besides, there is a considerably population of protons and neutrons coming from the deuterium breakup when the system achieves the steady solution.

It is worth to notice the time scale in which the system achieves the steady regime. This is around $1 \mu\text{s}$, instead the Jetter cycle alone took around $14 \mu\text{s}$ to achieve the steady solution. Therefore, the presence of deuterium breakup and the Post cycle decreases the time that the system spends to reach the steady solution. Again, due to the fact that the neutrons coming from the beam only react with lithium, the neutron beam might be turned off at the time when the lithium is exhausted, namely, more or less $0.3 \mu\text{s}$. This for saving injection energy.

Jetter cycle + Post cycle Solution



(a)



(b)

Figure 5.9: Curves of abundance evolution for the Jetter cycle + Post cycle using the initial conditions [3.3](#) in terms of molar fraction Y_i . (a) Linear scale in the y -axis. (b) logarithmic scale in the y -axis for better visualization.

Jetter cycle + Post cycle Solution

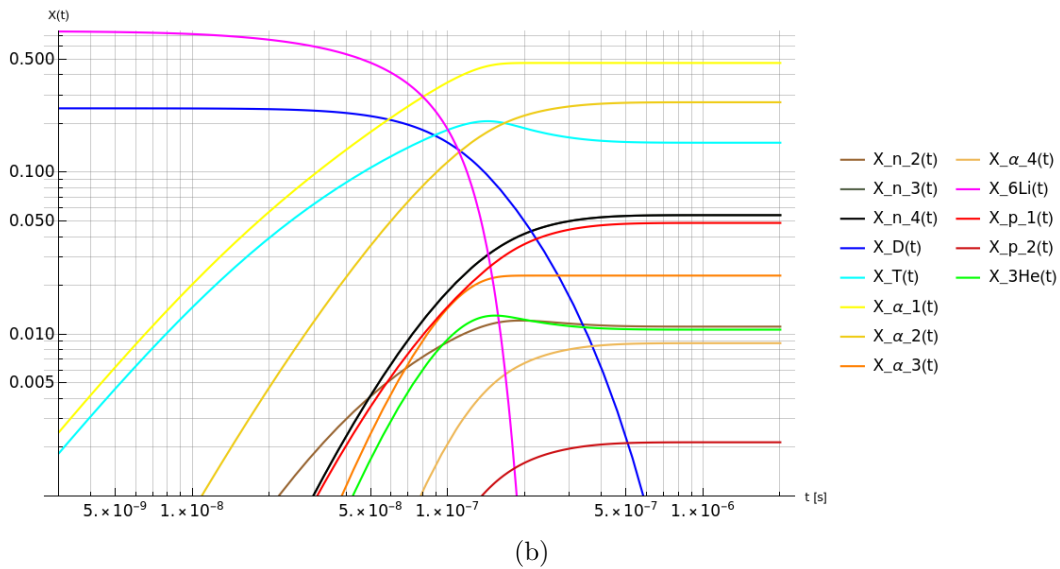
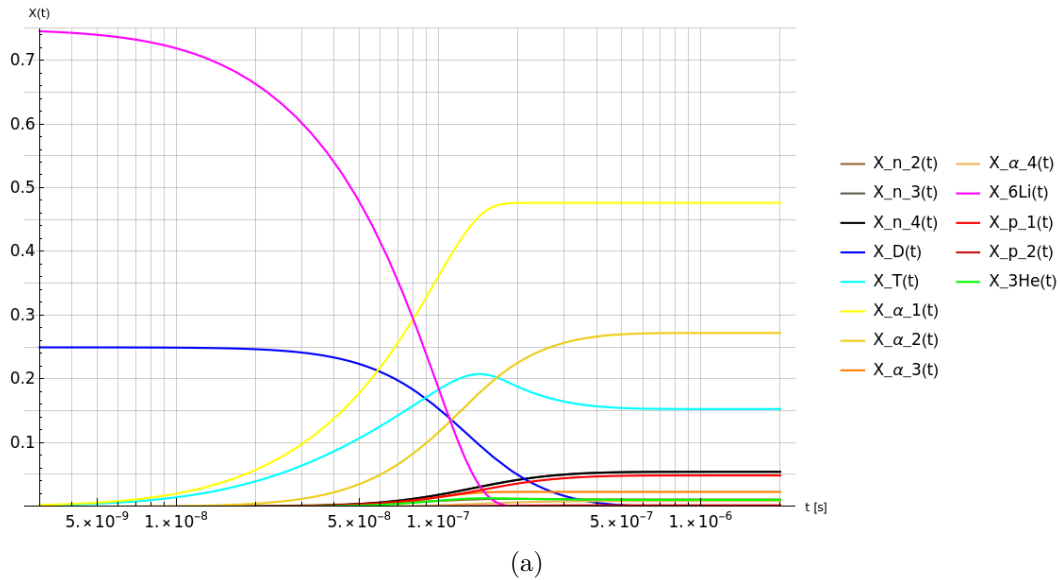


Figure 5.10: Curves of abundance evolution for the Jetter cycle + Post cycle using the initial conditions [3.3](#) in terms of nucleon fraction X_i . (a) Linear scale in the y -axis. (b) logarithmic scale in the y -axis for better visualization.

Notice that, by using the expression [1.33](#) the result expressed in terms of the molar fraction Y_i may be written in terms of the nucleon fraction X_i multiplying every species by its mass number. The result is shown in the figure [5.10](#).

At the end, the differential equations converge to a steady point in which the system is only populated with α -particles, neutrons, protons and 3-helium. This is expressed in the table [5.3](#) and depicted in the barchart [5.11](#), where it is easier to appreciate the initial and final abundances. There, t_{fin} refers to the time at which the system has achieved the steady solution.

Molar Fraction	Value (mol/g)
$Y_{n_1}(t_{fin})$	21.9
$Y_{n_2}(t_{fin})$	0.011
$Y_{p_1}(t_{fin})$	0.049
$Y_{p_2}(t_{fin})$	0.002
$Y_{n_3}(t_{fin})$	0.055
$Y_{n_4}(t_{fin})$	0.055
$Y_{\alpha_1}(t_{fin})$	0.119
$Y_{\alpha_2}(t_{fin})$	0.068
$Y_{\alpha_3}(t_{fin})$	0.006
$Y_{\alpha_4}(t_{fin})$	0.002
$Y_D(t_{fin})$	0.0
$Y_T(t_{fin})$	0.051
$Y_{6Li}(t_{fin})$	0.0
$Y_{3He}(t_{fin})$	0.0036

Table 5.3: *Final abundances in terms of molar fraction and expressed in units of mol/g for the species involved in the Jetter cycle + Post cycle.*

The barchart [5.11](#) shows the evident change in the final abundance when the deuterium breakup reaction and the Post cycle are added to the Jetter cycle. The final abundance of tritium and 3-helium differs from the abundance found at the end of the Jetter cycle [2.11](#) and of the Post cycle [3.10](#), respectively.

Finally, due to the fact that the curves of abundance evolution are known, the

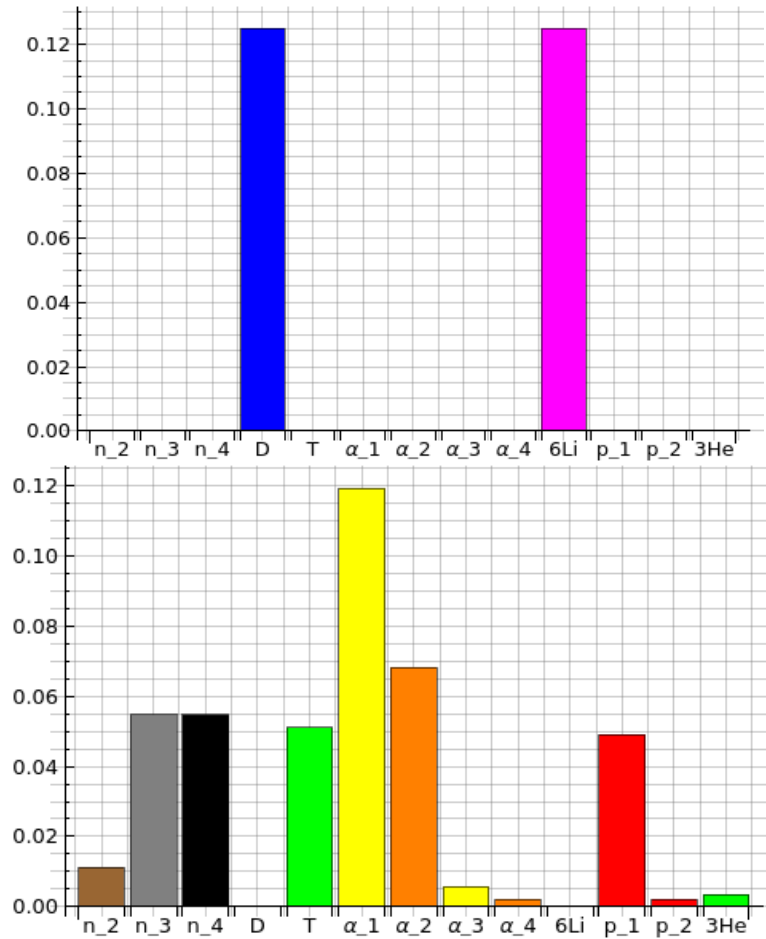


Figure 5.11: Abundance in terms of molar fraction Y expressed in units of mol/g. **Top.** Initial abundance according to the initial conditions [2.3](#). **Bottom.** Final abundance after Jetter cycle + Post cycle integration.

fusion yield might be calculated using the expression [1.47](#) and upon multiplying the specific power by the volume of the simulated system, that it is the same as in the Jetter cycle chapter, the resulting the power as a function of time can be calculated.

The curves of the power as a function of time for every reaction involved in the Jetter cycle + Post cycle are displayed in the figures [5.12](#) and [5.14](#). In black the curves related with fission reaction are shown, instead in red the curves related with

fusion reaction are shown. All these reactions are exothermic, then they correspond to energy released. Conversely, the deuterium breakup is an endothermic reaction and this implies that this energy was spent in order to produce the proton and neutrons in the exit channel. This is the reason why in the figure [5.14](#) the curve appears on the negative side.

The results for the combine cycles are expressed in the table [5.4](#).

Reaction	Fusion Yield (GJ)
${}^6\text{Li}(n_1, \text{T})\alpha_1$	457.517
${}^6\text{Li}(n_2, \text{T})\alpha_1$	9.070
$\text{D}(\text{T}, n_2)\alpha_2$	980.726
${}^6\text{Li}(p_1, {}^3\text{He})\alpha_3$	18.829
${}^6\text{Li}(p_2, {}^3\text{He})\alpha_3$	0.177
${}^3\text{He}(\text{D}, p)\alpha_2$	31.794
$\text{D}(n_2, 2n)p_1$	-99.462
Total	1398.650

Table 5.4: *Energy released for every reaction in the Jetter cycle + Post cycle.*

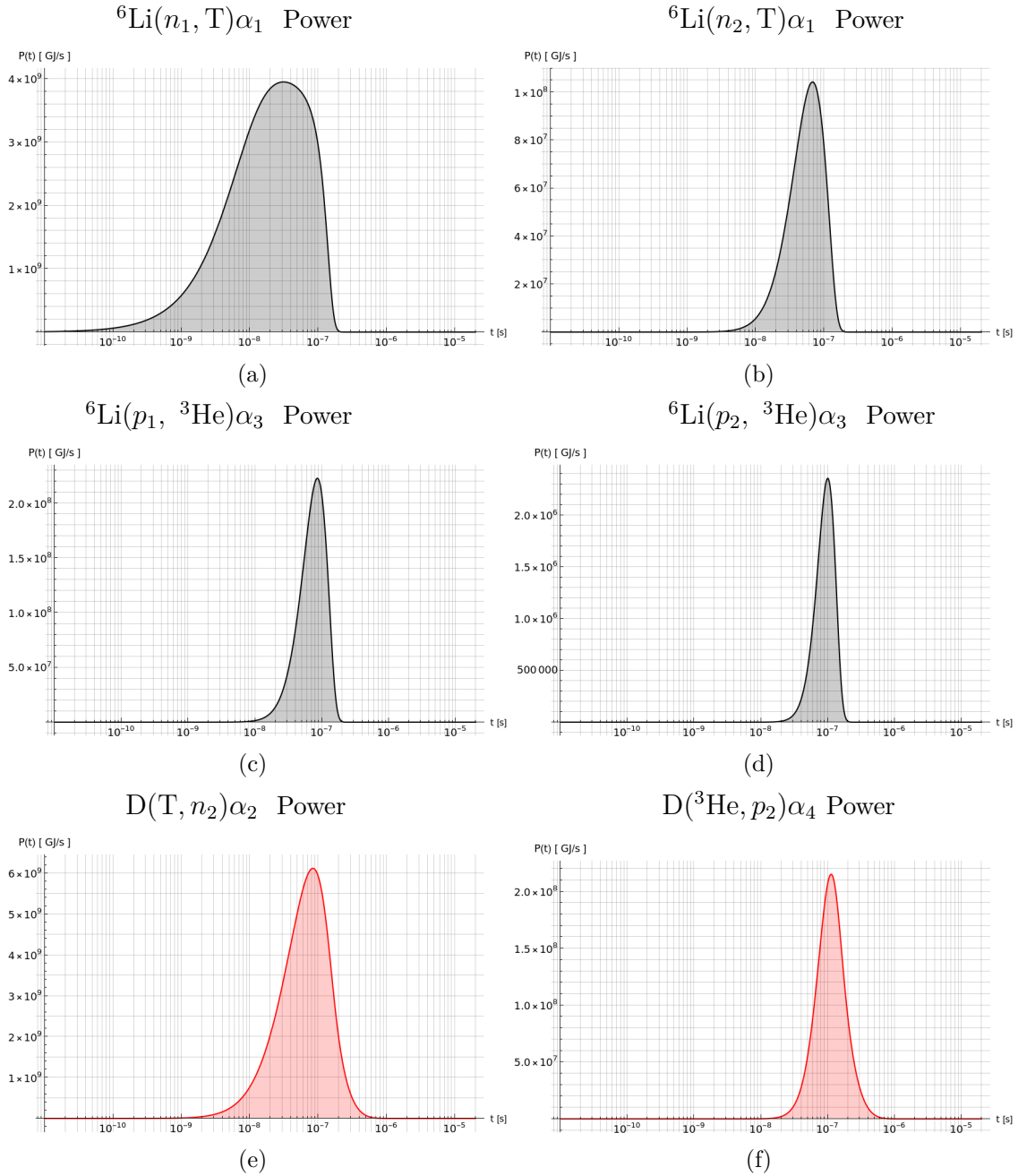


Figure 5.12: Power released in the Jetter cycle + Post cycle. (a) Power released by the ${}^6\text{Li}(n_1, \text{T})\alpha_1$ reaction. (b) Power released by the ${}^6\text{Li}(n_2, \text{T})\alpha_1$ reaction. (c) Power released by the ${}^6\text{Li}(p_1, {}^3\text{He})\alpha_3$ reaction. (d) Power released by the ${}^6\text{Li}(p_2, {}^3\text{He})\alpha_3$ reaction. (d) Power released by the $\text{D}({}^3\text{He}, n_2)\alpha_2$ reaction. (e) Power released by the $\text{D}(\text{T}, n_2)\alpha_2$ reaction. (f) Power released by the $\text{D}({}^3\text{He}, p_2)\alpha_4$ reaction.

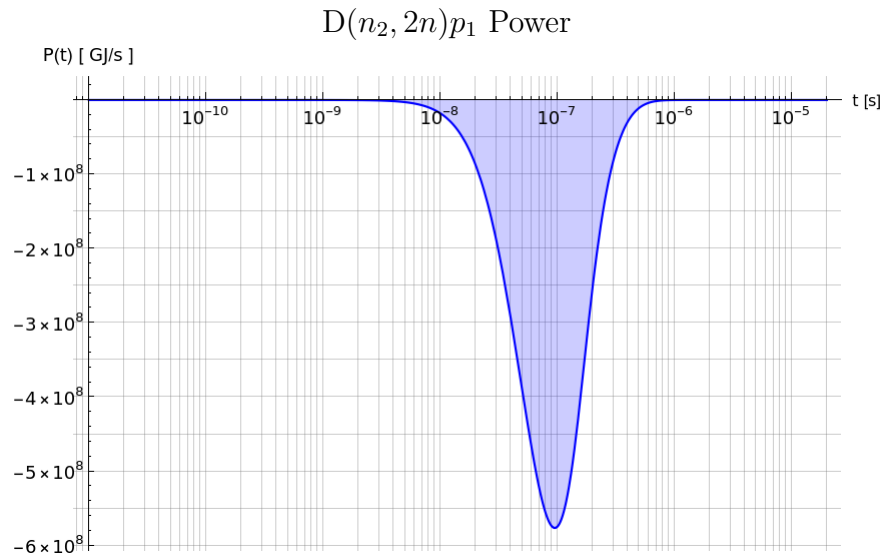


Figure 5.13: Power consumed in the deuterium breakup reaction.

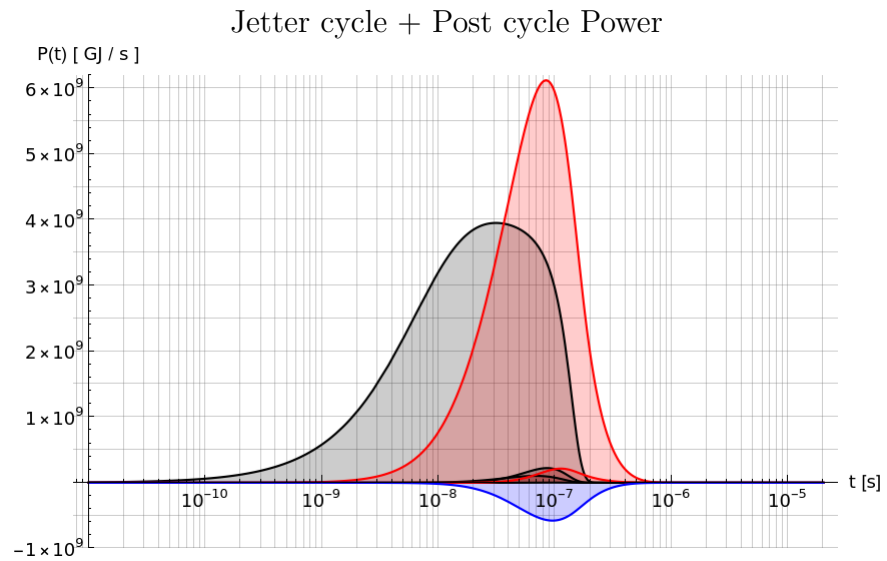


Figure 5.14: Power released and consumed in Jetter cycle + Post cycle.

Chapter 6

Conclusions

From the present study considering a neutron beam focused on a ${}^6\text{LiD}$ crystal, the chapter two showed that the Jetter cycle was successfully simulated. The results showed the abundance evolution of the elements involved and a huge quantity of nuclear energy released during the nucleosynthesis. Besides, it is desirable to compare the nuclear energy released with the entering energy in the system. For this, a rough estimate is proposed by calculating the kinetic energy of the neutrons coming from the beam that entered to the system

$$E_i = i \cdot \Delta t \cdot E_{n_1}. \quad (6.1)$$

We refer to this quantity as the injection energy. Considering only the energetic balance of the nuclear reactions and forgetting about technical implementation, device efficiency and power consumption, we can define a reaction gain factor as the fraction between the above quantity and the fusion yield Y ,

$$Q = \frac{Y}{E_i}. \quad (6.2)$$

Taking the rate used in the simulation for the incoming neutrons (2.10), the kinetic energy for these neutrons (0.24 MeV) and the time when the lithium is completely exhausted, the injection energy might be calculated. A net energy gain would require fusion yields greater than the beam energy, 40.82 GJ. The fusion yield in the Jetter cycle that we found was 2282.840 GJ (2.5) and this implies a gain factor of

$$Q = \frac{2282.840 \text{ GJ}}{40.82 \text{ GJ}} = 55.90. \quad (6.3)$$

Where this clearly results in an overestimation. Because, not all the energy produced is susceptible to be extracted from the system. In this field, a common statement on the power is to divide the gain factor by 5, due to the fact that α -particles carry 1/5 of the total fusion energy per D+T reaction. Despite this, the gain factor continues to be greater than 1 expressing a net gain in the system.

With respect to the Post cycle, the initial conditions defined in the chapter three showed that an initial small population of protons, compared with the abundance of the crystal elements, is enough to ignite the cycle and produces the total consumption of lithium and deuterium. Besides, the energy released in the Post cycle was comparable with the energy released in the Jetter cycle, with the common peculiar dynamic that the tritium and 3-helium were created and depleted during the process, respectively. Another important information from this simulation concerns the time scale at which the solution achieved the steady regime, that is found to be of the same order of the Jetter cycle, a fact that motivated to merge them in order to see an overlap of the two dynamics.

From the deuterium breakup cross section and from the final abundance of high energetic neutrons in the Jetter cycle, we could hypothesize this reaction as a candidate to link the Jetter cycle and the Post cycle and the Monte Carlo simulation, from the chapter four, successfully permitted to obtain an energy distribution for the outgoing protons.

The last simulation in the chapter five showed that, effectively, at a certain point the Post cycle is ignited. Nevertheless, the dominant reactions for this setup are those belonging to the Jetter cycle, whereas the reaction belonging to the Post cycle play a secondary role. The deuterium breakup also has an important role, a fact that is evident from the high quantity of neutrons and protons at the end. Besides, the final abundances showed sizeable changes compared with the simulation of the Jetter cycle alone. For instance, the tritium that was totally consumed in the first simulation, now it is present in a considerable amount at the end. Analogous behaviour for the 3-helium, but in less proportion, is also found.

In terms of the energy produced, the presence of the endothermic reaction of deuterium breakup led to a reduction of almost the half part of the fusion yield of the Jetter cycle alone (5.3). The gain factor reads

$$Q = \frac{1398.65 \text{ GJ}}{40.82 \text{ GJ}} = 34.26. \quad (6.4)$$

Clearly, this is a rough estimation and must be considered as an upper bound for the net gain. Facts such as particle losses or elastic scattering are factors that, eventually, will decrease the fusion yield and they have to be added in the simulation in future works. Additionally, as it was said before, not all the energy produced is susceptible to be extracted to the system.

It was noticed that the dynamic was always trying to consume the elements present in the crystal and populate the system with energetic α -particles. Therefore, the final abundances of the simulated merged system suggest that other collateral reactions have to be added. Namely, new channels has to be opened.

The present study must be considered as a preliminar scenario, where the nuclear physics involved was explored without delving into the technical feasibility.

Appendix A

Reaction Rates

In the table [A.1](#) the reduced reaction rates used for the simulations are reported. Where the notation proposed in [1.42](#) is used.

Reduced Reaction Rate	$\frac{g}{\text{mol} \cdot s}$
$[{}^6\text{Li}(n_1, \alpha)]$	1.1614×10^9
$[{}^6\text{Li}(n_2, \alpha)]$	7.1395×10^7
$[\text{D}(\text{T}, n_2)]$	8.7637×10^7
$[\text{D}(n_2, 2n)]$	4.5775×10^8
$[{}^6\text{Li}(p_1, {}^3\text{He})]$	1.3732×10^8
$[{}^6\text{Li}(p_2, {}^3\text{He})]$	4.6048×10^7
$[{}^3\text{He}(\text{D}, p)]$	6.0392×10^7

Table A.1: *Reduced reaction data for all reactions involved.*

Appendix B

Mathematica routine: Nuclear Reaction Network solver.

The solution of a nuclear reaction network could be a challenging task. As the rate at which reactions occur is proportional to products of the densities of reactants, these equations are a set of coupled and nonlinear differential equations. Such equations also are called stiff (18). As the number of species grow, or the energy is changed, the growing number of first order differential equations must be taken into account and this complicated the bookkeeping of all the abundances and the number of coupled equations, as it is evident from equations 2.3, 3.1 and 5.4.

Here, we present a nuclear reaction network code, which has been entirely written in Mathematica and has been used in the present work.

The code starts by reading a set of user-defined file in the initialization step. These files contain the cross section data for every reaction involved in the reaction network and the corresponding interpolation. After this, the user has to define a list with the nuclear species involved in the simulation, where the index chosen for the user has to be maintained until the end, because this index will serve as a label that identifies the species.

For instance, in the present work the nuclear species list that was used is displayed in table (B.1) with their arbitrary index.

Index	1	2	3	4	5	6	7
Species	n	D	T	α	${}^6\text{Li}$	p	${}^3\text{He}$

Table B.1: Nuclear species list read by the Mathematica routine.

Besides, a list with the reaction involved has to be set, again, the index given will serve as a label to identify the reaction. The list used in the present work is displayed in table [B.2](#).

Index	1	2	3	4	5
Reaction	${}^6\text{Li}(n, \text{T})\alpha$	$\text{D}(\text{T}, n)\alpha$	$n(\text{D}, 2n)p$	${}^6\text{Li}(p, {}^3\text{He})\alpha$	${}^3\text{He}(\text{D}, p)\alpha$

Table B.2: Nuclear reaction list read by the Mathematica routine.

With the knowledge of the species, the code extracts the masses involved using the Mathematica function *IsotopeData*. With all this information the code calculates the reaction Q -value of every reaction and depending on velocity distributions of the particles of every species, the reduced reaction rates are calculated at the specific energy required. The results for the present work are listed in the table [A.1](#).

Finally, the set of coupled and non-linear differential equations, the initial conditions, the final time and the step are defined by the user. With this information the code performs the numerical integration using the Mathematica function *NDSolve* which gives results in terms of interpolating function objects and uses different methods like “Adams”, “BDF”, “explicit Runge-Kutta”, “implicit Runge-Kutta”, “explicit Euler”. See ref. [\(38\)](#) for more details.

The code outputs are the abundance evolution (dependent variables) as a function of time (independent variable) for every species configured. The flow diagram that summarizes all these steps is depicted in the figure [B.1](#). There, in orange color are expressed the information that the user has to establish, whereas in blue color the tasks that the code performs.

The present version of the Reaction Network Calculator code is called RNC 2.2 [\(40\)](#) and it has been developed as a general purpose that we intend to publish in future. In this version, the set of coupled differential equations have been rewritten

in terms of molar fractions. The cross section for the deuterium breakup and the reactions involved in the Post cycle were added. The reaction network for the Jetter cycle and the Post cycle were separately simulated and a new visualization of the final abundance using a barchart was also added. Afterward, reading the energy distribution of the protons coming from the deuterium breakup (see the appendix [C](#)) the complete set of differential equations involving Jetter cycle + Post cycle were written and simulated. Finally, in every reaction network simulated the curves of power as a function of time were performed and the numerical integration using the Mathematica function *NIntegrate* was used in order to obtain the energy balance.

Flow Diagram

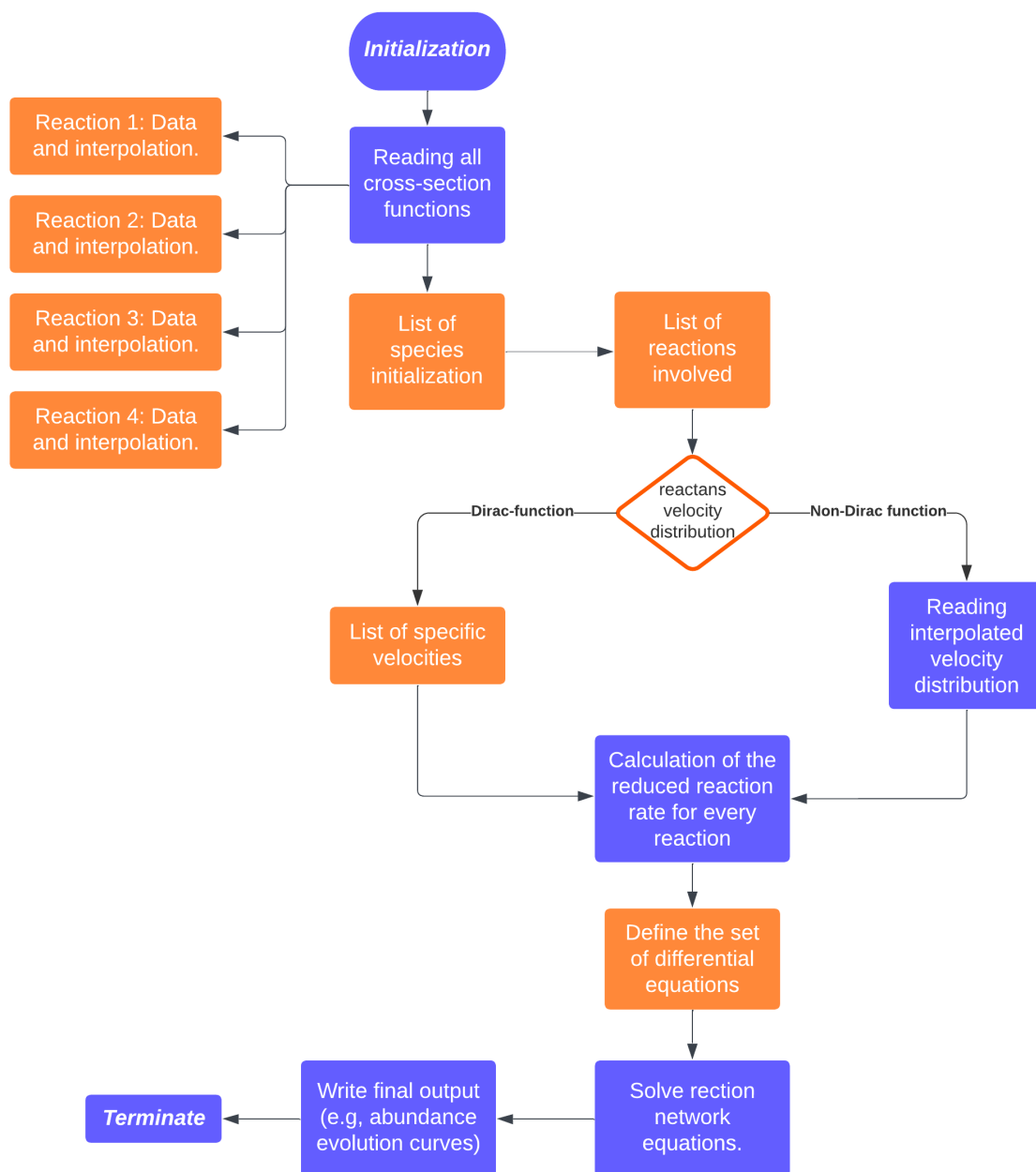


Figure B.1: Flow diagram of Reaction Network Calculator written in Mathematica and implemented in the present work.

Appendix C

C++ routine: Monte Carlo deuterium breakup.

A Monte Carlo simulation was proposed in order to obtain the energy distribution function for the three fragments. These were labeled in the code as: the neutron 1 was the one that inelastically scattered with the deuterium, whereas the neutron 2 is the fragment coming from the deuterium breakup.

The code starts asking the number of events and the neutron energy, in the laboratory system, that is impinging the deuterium. With this information the code calculates all kinematic information related with the inelastic scattering where the deuterium absorbs 0.1 MeV over its binding energy. At this point the first pair of angles are randomly generated (θ^{CM} , ϕ^{CM}). These angles give the information of how the energy is shared by these two particles.

After this, the kinematic information related with the deuterium breakup were calculated in the deuterium rest frame and the second pair of angles were randomly generated (θ^{Rest} , ϕ^{Rest}). Again, these angles give the information of how the energy is shared by these two fragments.

Finally, the velocity and momentum composition were performed for the three final particles in the laboratory reference frame guided by the energy and momentum conservation at every step. The flow diagram is shown in the figure [C.1](#).

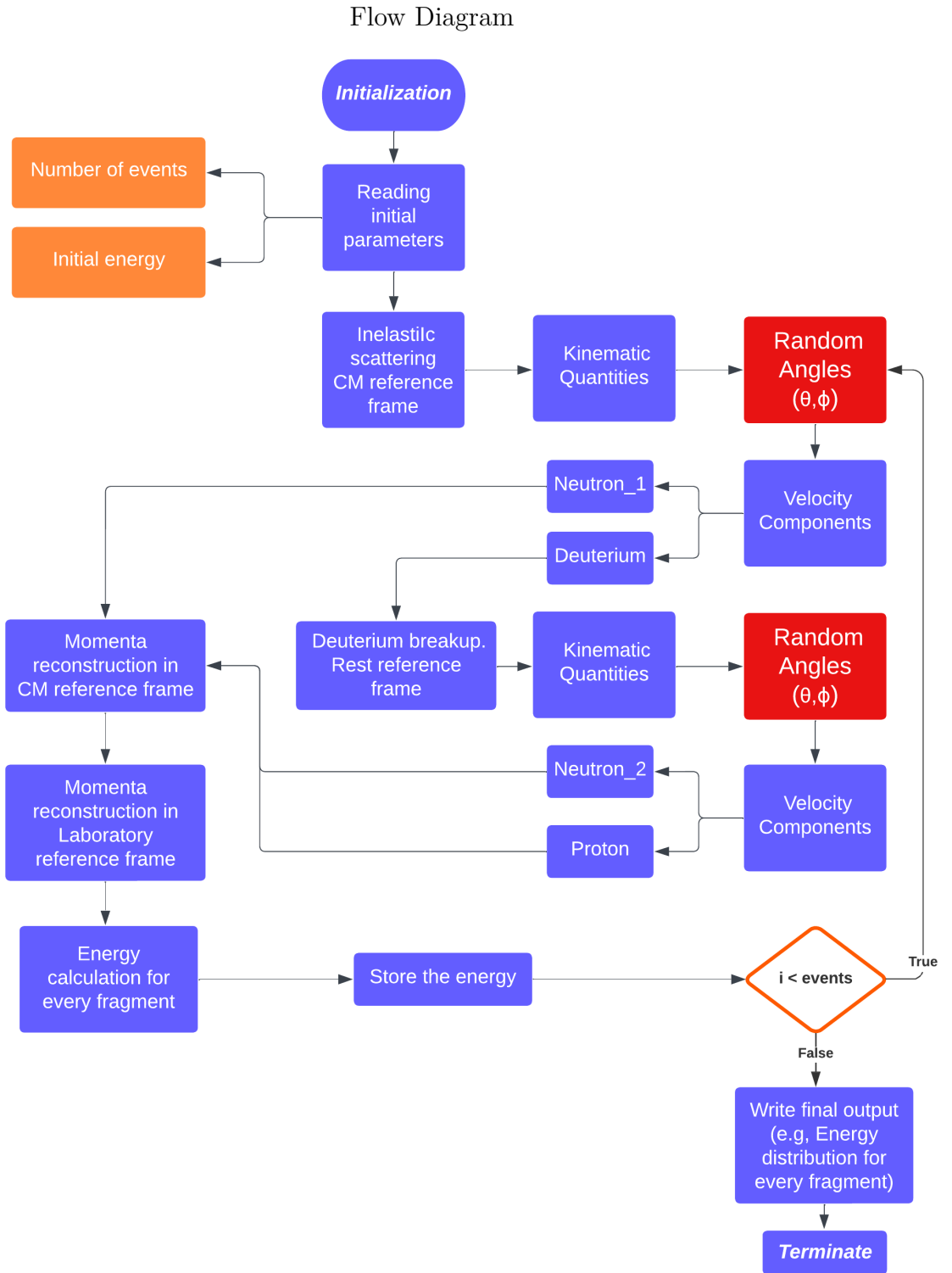


Figure C.1: Flow diagram of deuterium breakup Monte Carlo simulation written in C++ (39) and implemented in the present work.

Bibliography

- [1] FUSION PHYSICS. International Atomic Energy Agency. 2012.
- [2] TECHNOLOGY ROADMAP - NUCLEAR ENERGY, 2015 EDITION, INTERNATIONAL ENERGY AGENCY, FRANCE, AND IEA "ENERGY TECHNOLOGY" PERSPECTIVES. 2015, fig (1.9).
- [3] *R. Toschi*. NUCLEAR FUSION, AN ENERGY SOURCE. *Fusion Engineering and Design* 36 (1997) 1 - 8.
- [4] THE PHYSICS OF INERTIAL FUSION. BEAM PLASMA INTERACTION, HYDRODYNAMICS, HOT DENSE MATTER. *S. Azeni, J. Meyer-Ter-Vehn*. Oxford science publications.
- [5] THE HISTORY OF NUCLEAR ENERGY. U.S. Department of Energy Office of Nuclear Energy, Science and Technology.
- [6] STATISTICS REPORT: KEY WORLD ENERGY STATISTICS 2021. International Energy Agency. 2021.
- [7] *C. Rubbia. et al*. CONCEPTUAL DESIGN OF A FAST NEUTRON OPERATED HIGH POWER ENERGY AMPLIFIER. CERN/AT/95-44(ET).
- [8] EUROPEAN RESEARCH ROADMAP TO THE REALISATION OF FUSION ENERGY. EUROfusion. 2018.
- [9] *U. Jetter*. DIE SOGENANNTTE SUPERBOMBE. *Physicalische Blatter* 6, page 199, 1950.
- [10] TOKAMAKS. *J. Wesson*. Clarendon-press Oxford. third edition, 2004.
- [11] *A. B. Zylstra. et al*. BURNING PLASMA ACHIEVED IN INERTIAL FUSION. *Nature*. Vol 601, 27 of January 2022.

- [12] *B. Bishop*. LAWRENCE LIVERMORE NATIONAL LABORATORY ACHIEVES FUSION IGNITION. 2022.
- [13] DEUTERIDE MATERIALS. *J. Liu, X. Liu*. Springer Nature Singapore. 2019.
- [14] DATA BASE FOR MASSES AND BINDING ENERGIES. CONSULTED IN JUNE OF 2023. AVAILABLE IN: <https://www-nds.iaea.org/amdc/>
- [15] INTRODUCTORY NUCLEAR PHYSICS. *S. Krane*. Oregon State University. 1988.
- [16] NUCLEAR PHYSICS OF STARS. *C. Iliadis*. WILEY-VCH Verlag GmbH & Co. KGaA, Weinheim. 2007.
- [17] NUCLEAR PHYSICS. *A. Kamal*. Graduate text in physics Springer Series. 2014.
- [18] SUPERNOVAE AND NUCLEOSYNTHESIS. AN INVESTIGATION OF THE HISTORY OF MATTER, FROM THE BIG BANG TO THE PRESENT. *D. Arnett*. Princeton series in Astrophysics. 1996.
- [19] THERMONUCLEAR KINETICS IN ASTROPHYSICS. *W. Raphael Hix, Bradley S. Meyer*. Nuclear Physics A 777 188-207. 2006.
- [20] SOME THOUGHTS ON THE $P(^6\text{Li},\alpha)^3\text{He}(^6\text{Li},p)^8\text{Be}$ CHAIN REACTION. *J.R. McNally, JR. and K.E. Rothe*. IEEE International conference on plasma science Montreal, Canada. June 4-6 1979.
- [21] NUCLEAR FUSION CHAIN REACTION APPLICATIONS IN PHYSICS AND ASTROPHYSICS. *J.R. McNally and JR.* Symposium on applications of nuclear data in science and technology; Paris, France; 12 Mar 1973.
- [22] *Koning A, Bauge E, Dean C, Dupont E, Fischer U, Forrest R, Jacqmin R, Leeb H, Kellett M, Mills R, Nordborg C, Pescarini M, Rugama Y, Rullhusen P*. STATUS OF THE JEFF NUCLEAR DATA LIBRARY. IN: INTERNATIONAL CONFERENCE ON NUCLEAR DATA FOR SCIENCE AND TECHNOLOGY (ND2010); 26 April 2010; Jeju island (Korea). JOURNAL OF THE KOREAN PHYSICAL SOCIETY 59 (2); 2011.p. 1057-1062. JRC66451
- [23] *K. Shibata, O. Iwamoto, T. Nakagawa et al.* JENDL-4.0: A NEW LIBRARY FOR NUCLEAR SCIENCE AND ENGINEERING, J. Nucl. Sci. Technol. 48,1 (2011)

- [24] *G. Chiba, K. Okumura, K. Sugino, Y. Nagaya, K. Yokoyama, T. Kugo, M. Ishikawa and S. Okajima* JENDL-4.0 BENCHMARKING FOR FISSION REACTOR APPLICATIONS, *J. Nucl. Sci. Technol.* **48**,172 (2011)
- [25] *D.A. Brown, M.B. Chadwick, R. Capote, A.C. Kahler, A. Trkov, M.W. Herman et al.* ENDF/B-VIII.0: THE 8TH MAJOR RELEASE OF THE NUCLEAR REACTION DATA LIBRARY WITH CIELO-PROJECT CROSS SECTIONS, NEW STANDARDS AND THERMAL SCATTERING DATA. *Nuclear Data Sheets* **148** (2018) 1-142.
- [26] EXPERIMENTAL NUCLEAR REACTION DATA (EXFOR). CONSULTED IN JUNE OF 2023. AVAILABLE IN: <https://www-nds.iaea.org/exfor/exfor.htm>
- [27] EVALUATED NUCLEAR DATA FILE (ENDF). CONSULTED IN JUNE OF 2023. AVAILABLE IN: <https://www-nds.iaea.org/exfor/endlf.htm>
- [28] *G.M. Hale.* ${}^6\text{Li}(n,\alpha),T$ CROSS SECTION INTERPOLATED BY ENDF. CONSULTED IN JUNE OF 2023. AVAILABLE IN: <https://www-nds.iaea.org/exfor/servlet/E4sGetTabSect?SectID=8943076&req=7899&PenSectID=13590381>
- [29] *P.E. Koehler.* COMPARISON OF WHITE NEUTRON SOURCES FOR NUCLEAR ASTROPHYSICS EXPERIMENTS USING VERY SMALL SAMPLES. *Nucl. Instr. Meth.* **A460**, 352 (2001).
- [30] *H. Beer, F. Kappeler.* NEUTRON CAPTURE CROSS SECTION ON ${}^{138}\text{Ba}$, ${}^{140,142}\text{Ce}$, ${}^{175,176}\text{Lu}$ AND ${}^{181}\text{Ta}$ AT 30 KEV: PREREQUISITE FOR INVESTIGATION OF THE ${}^{176}\text{Lu}$ COSMIC CLOCK. *Physical Review C.* Volume 21, Number 2 (1980).
- [31] IAEA TECDOC SERIES. COMPENDIUM OF NEUTRON BEAM FACILITIES FOR HIGH PRECISION NUCLEAR DATA MEASUREMENTS. *Physical Review C.* 2014.
- [32] *E. Staritzky, D. Walker.* LITHIUM HYDRIDE, LiH , AND LITHIUM DEUTERIDE, LiD . University of California. Los Alamos scientific laboratory.
- [33] ${}^3\text{He}(D,p)\alpha$ CROSS SECTION INTERPOLATED BY ENDF. CONSULTED IN JUNE OF 2023. AVAILABLE IN: https://www-nds.iaea.org/exfor/servlet/X4sShowData?db=x4&op=get_plotdata&req=-1&ii=4249&File=E4R10086_e4.zvd.dat.txt

- [34] *W. Moller, F. Besenbacher.* A NOTE ON THE ${}^3\text{He}+\text{D}$ NUCLEAR-REACTION CROSS SECTION. *Nuclear instruments and methods* 168. (1980) 111-114.
- [35] $\text{T}(\text{D}, \alpha)n$ CROSS SECTION INTERPOLATED BY ENDF. CONSULTED IN JUNE OF 2023. AVAILABLE IN: <https://www-nds.iaea.org/exfor/servlet/E4sGetTabSect?SectID=88666&req=10385&PenSectID=7403356>
- [36] *Cheng, Hok-Chuen.* TWO-BODY DECAY KINEMATICS. University of Michigan, Ann Arbor. April 28, 2015.
- [37] *P.G. Young, G.M. Hale, M.B. Chadwick.* $n(\text{D}, 2n)^1\text{H}$ CROSS SECTION INTERPOLATED BY ENDF. CONSULTED IN AUGUST OF 2023. AVAILABLE IN: <https://www-nds.iaea.org/exfor/servlet/E4sGetIntSection?SectID=8943002&req=15378&e4up=0&PenSectID=13590307&pen=0>
- [38] NDSOLVE MATHEMATICA FUNCTION. CONSULTED IN AUGUST OF 2023. AVAILABLE IN: <https://reference.wolfram.com/language/ref/NDSolve.html>
- [39] *M. Mazzocco.* "BREAKUP-D". Private communication (2023).
- [40] *L. Fortunato, G. Albertin, A.F. Lopez-Loaiza.* "REACTION NETWORK CALCULATOR: RNC 2.2". Private communication (2023).

Signature.